Air-Cushion Tactile Sensor for Medical Applications

Zbyszewski, Dinusha

Awarding institution:
King's College London

Title: Air-Cushion Tactile Sensor for Medical Applications

Author: Dinusha Zbysewski

Air-Cushion Tactile Sensor for Medical Applications

Dinusha Zbyszewski

A thesis submitted in partial fulfilment of the requirements for the degree of

Doctor of Philosophy in Mechanical Engineering

King's College London, University of London

2012

Abstract

In the surgical field, the trend tends increasingly towards performing minimally invasive procedures as they offer improved aesthetics, a reduction in blood loss, tissue trauma and post operative complications. However, the limited accessibility of the surgical site due to the use of small incisions does generate a few drawbacks.

One of the main concerns is that surgeons cannot manually palpate the tissue they are operating on as they would in traditional open surgery. Manual palpation of the surgical site is performed to feel any tissue abnormalities such as tumours that may be present. This inability to feel the organs through minimally invasive surgery (MIS) is known as a lack of haptic feedback.

Over the last decade, there has been an extensive amount of research in tactile and force sensing for MIS in an effort to overcome this limitation. The air cushion sensor for MIS is one of those. This novel sensing concept employs a spherical component that is surrounded by a cushion of air, to roll over the surface under inspection. The proposed sensing concept employs optical sensing when it is rolled to determine the areas of increased stiffness in a tissue. Using this concept, three sensors were designed and built. Their ability to detect tissue abnormalities in ex vivo tissues was assessed and so was their capability at estimating the force distribution over that area. The results show that all of the sensors were capable of detecting the tissue abnormalities and that one sensor was able to generate a force distribution map of the area under investigation.

Acknowledgements

I would like to express my deepest gratitude to my supervisors, the Guy's Hospital Urology Department and their medical staff, my colleagues and my family. This thesis would not have been possible without their guidance and support.

I would first of all like to thank my supervisors, particularly Prof. Prokar Dasgupta without whom I would not have had the chance to embark on and conduct my PhD in the medical field and Dr. Apostolos Georgakis who despite not being my supervisor actively supported me, advised me and motivated me through hell and high water. I am grateful for their suggestions, encouragements and guidance.

I would also like to thank Mr. Benjamin Challacombe from the Urology Department at Guy's Hospital for his collaboration and his valuable input in sharing medical knowledge.

In addition, I am indebted to all my colleagues from the Centre of Robotics Research who supported me throughout my research, sharing their thoughts on various technical discussions. I would like to thank especially, Ramon Sargeant, Asghar Ataollahi, Panagiotis Polygerinos, Allen Jiang, Indika Wanninayake, Helge Wurdemann, and Vahid Aminzadeh.

I finish by thanking my family and friends for their incredible love and support.

Table of Contents

List of Figures and Tables

List of Figures

List of Tables

Nomenclature

The following descriptive list shows basic annotations between symbols and their meanings. Abbreviations used in this thesis and their descriptions are also provided.

2D	two dimensional
3D	three dimensional
ABS	Acrylonitrile Butadiene Styrene
AESOP	Automated Endoscopic System for Optimal Positioning
CABG	Coronary Artery Bypass Graft
CFD	Computational Fluids Dynamics
CT	Computer Tomography
DAQ	Data Acquisition
DARPA	Defence Advanced Research Project Agency
DoF	Degrees of Freedom
DVRT	Differential Variable Reluctance Transducer
EM	Electromagnetic
EMF	Electro-Magnetic field
ETO	Ethylene Oxide
F	Force
FBG	Fibre Bragg Gratings

LED	Light Emitting Diode
LESS	Laparo-Endoscopic Single Site
LIM	Light Intensity Modulation
LVDT	Linear Variable Differential Transformer
MASH	Mobile Advanced Surgical Hospital
MEDFAST	Medical Forward Area Surgical Team
MIS	Minimally Invasive Surgery
MR	Magnetic Resonance
MRI	Magnetic Resonance Imaging
MIRS	Minimally Invasive Robotic Surgery
NASA	National Air and Space Administration
NoR	Norm of Residual
NOTES	Natural orifice Translumenal Endoscopic Surgery
OPUS	One Port Umbilical Surgery
P_{inside}	Pressure measured inside the sensor
P_{comp}	Pressure measured at the outlet of the compressor
PAM	Pneumatic Artificial Muscle
PVDF, PVF2	Polyvinylidene Fluoride
RMI	Rolling Indentation Imaging

SARP	Surgical Assistant Robot for Prostatectomy
SILS	Single Incision Laparoscopic Surgery
SAP	Single Access Site
SPA	Single Port Access
SPL	Single Port Laparoscopy
SRI	Stanford Research Institute
TUES	Trans Umbilical Endoscopic Surgery
TURP	Trans Urethral Resection of the Prostate
US FDA	United States Food and Drug Administration

Chapter 1 - Introduction

The world of medicine has evolved dramatically in recent years. In the surgical field, the trend tends increasingly towards performing minimally invasive procedures. From laparoscopic to robot assisted surgery, these procedures offer tremendous benefits to the patient and the surgeon. However, currently, they also all have one major drawback in common – a reduced or total lack of haptic feedback during surgery.

This introductory chapter is aimed at providing the reader with an overview of the work presented in this thesis. Firstly, the aims and objectives of this research with respect to overcoming the lack of tactile feedback in minimally invasive surgery (MIS) are stated. The contributions to science and the main achievements are then summarised. Finally, the layout of the overall structure of the thesis is presented.

1.1 Overview

Minimally invasive surgery (MIS) including both laparoscopy and robot-assisted surgery can typically be described as a form of surgery that is performed through a number of small incisions. The incisions vary in size ranging from 3-12 mm in diameter (Bicchi, Canepa, De Rossi, Iacconi, & Scilingo, 1996). The incisions are

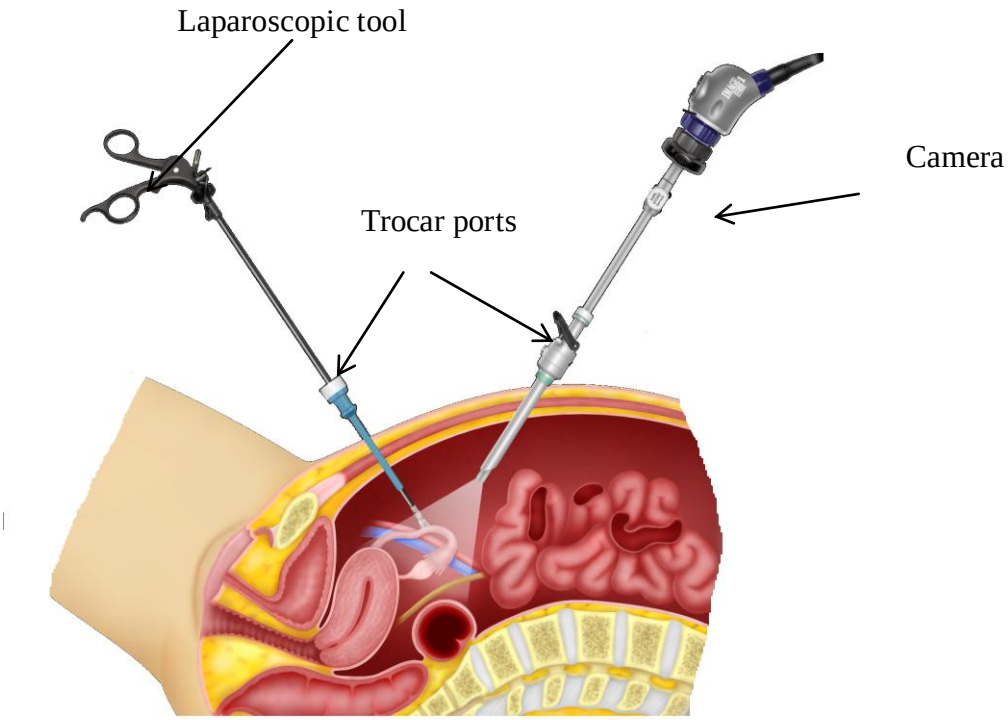

Figure 1.1: Traditional Minimally Invasive surgery, picture adapted from (Melkafertility website).

strategically located so as to offer access to the surgical site; they remain open with the help of trocar ports. A camera is initially inserted through one of the incisions to obtain a field of view of the surgical site. The laparoscopic tools are then inserted through the remaining incisions (as illustrated in Figure 1.1).

As an approach, MIS has many advantages over traditional surgery. One large incision is replaced with several smaller incisions reducing post-operative pain, scarring, and the immunological stress response of the tissue (Fuchs, 2002). Direct observation of the surgical site is replaced by a magnifying camera enabling an enhanced view of anatomical structures. Other advantages include potentially reduced tissue trauma and reduced length of hospital stay coupled with earlier post-operative return to normal duties, improved rehabilitation time and aesthetics to name but a few.

These advantages come at the cost of an increase in the technical skills required to perform MIS competently, often requiring dedicated periods of specialist and fellowship training for the surgeon.

MIS has a number of drawbacks according to (Treat, 1995). First of all, the lack of direct access to the surgical site makes it impossible for surgeons to palpate and feel organs with their hands. In traditional surgery, this technique is used to detect any tissue abnormalities that an organ may have, including tumours. Another problem is that the distal dexterity is reduced due to the friction between the laparoscopic tools and the trocar port. The torque required to rotate the tools also makes it very difficult to sense the actual contact forces between the tool and tissue. These drawbacks increase the possibility of accidental tissue trauma.

One more limitation is the lack of wide observation of the operative site due to the camera's limited field of vision. There is also the loss of direct hand-eye coordination due to the fact that tools have to move around a fixed point reducing the degrees of freedom (DoF) to four (excluding the tip's motion): pitch, yaw, roll and insertion (Tavakoli, Aziminejad, Patel, & Moallem, 2006). The directions are also reversed in-vivo (Tendick & Cavusoglu, 1997) which is one more reason for the need for extensive training.

This reduction of visual and haptic feedback, coupled with impaired dexterity in laparoscopy, can lead to accidental tissue damage (Tendick & Cavusoglu, 1997) and significantly reduces the surgeon's ability to feel the structures on which he or she is operating. During the surgery, there are several types of principle feedback that are usually required by the surgeon, which are visual feedback, force (kinaesthetic) feedback, and tactile (cutaneous) feedback. Force and tactile feedback information

known as haptics represent the sensation felt by the human hand (Okamura, Methods for haptic feedback in teleoperated robot-assisted surgery, 2004). Visual feedback alone is not always sufficient as tissue abnormalities or tumours that are embedded into an organ below the tissue surface are not always visible. This sense of feel is essential for performing tissue palpation, classification, manipulation, and suturing. It is therefore required in all types of surgery including traditional surgery, MIS, and MIRS.

Recently, a number of surgical robotic systems have been developed to attempt to overcome the problems of traditional MIS. These include two commercialised computer integrated systems such as the ZeusTM Surgical System from Computer Motion, Inc. (Uranues, et al., 2002) and the da VinciTM Surgical System from Intuitive Surgical, Inc. (Guthart & Salisbury Jr., 2000). Both are master-slave robotic systems which have three or four robotic arms to manipulate the surgical tools precisely in the surgical site under surgeon tele-operated control.

Since the distinct advantages of the robotic systems are the ability to scale down the hand movements, filter the tremor, and eliminate the problems due to the impairment of hand-eye coordination caused by the fulcrum effects, they provide a much better outcome for the surgery. In addition to these, improvements based on three dimensional (3D) vision and high distal dexterity tools also allow complex surgical procedures which are usually difficult to be conducted by conventional minimally invasive means, such as coronary artery bypass grafting (Tabaie, Reinbolt, Graper, Kelly, & Connor, 1999) and mitral valve repair (Murphy, Miller, Langford, & Snyder, 2006), to be effectively performed.

However, the lack of haptic feedback in the current robotic systems is still one of the major downsides of the surgical systems.

A number of sensors have been developed but their application for tactile and force feedback in an MIS/MIRS setting is limited due to their cost, accuracy, dimension, sensing range, sterilisability and ability to operate in specific surgical environments.

In this thesis a novel tactile sensor is presented that addresses these issues.

1.2 Aims and Objectives

The principal aim of this research is to design, build and test a sensor that can provide surgeons with some form of tactile information during MIS. The desired specifications of the tactile sensor for MIS are as follows:

- The sensing component of the sensing device should be located in close proximity of the area under inspection so that any tissue interaction can be effectively detected and not be affected by any surrounding forces.
- Due to the previous requirement, the sensing component and the sensing device must not exceed an outer diameter of 12 mm so that they can be inserted through a standard size of trocar port (Bicchi, Canepa, De Rossi, Iacconi, & Scilingo, 1996).
- The sensing device must provide the surgeon with tactile information of the tissue under inspection through a visual, auditory or haptic display.
- The sensing components of the sensing device should be sterilisable.
- The sensor should also be of an overall low manufacturing cost.
- It would be advantageous if the sensing components were Magnetic Resonance Imaging (MRI) compatible in order to be available for the

upcoming tendency of performing Minimally Invasive Robotic Surgery (MIRS) under an MRI scanner.

In this research, a novel tissue investigation approach is proposed that employs a rolling mechanical imaging (RMI) technique to rapidly acquire soft tissue tactile information such as embedded soft tissue abnormalities and tumours (Zbyszewski, et al., 2009) (Noonan, Liu, Zweiri, Althoefer, & Seneviratne, 2007). A novel optical sensing scheme is proposed that is used in conjunction with the RMI technique to acquire tactile information. In this research, a number of optical sensing prototypes were designed. These were subsequently built and tested. The sensors' designs were further improved, to achieve the main objective of having an MIS compatible tactile sensor with force capability estimation. The abovementioned research areas are summarised as the following objectives:

- To create a sensing device that is manoeuvrable when used with the RMI technique, in order to roll effectively in any direction over the surface under investigation.
- The sensing device should have the ability to generate the fast creation of mechanical images of the surface under investigation illustrating the stiffness and/or force distribution over that area.
- The sensing device should have the capability to acquire data of a large area with relative ease and at a reasonable speed.
- The sensor should be compatible to be used with robotic assisted minimally invasive surgery.
- The sensor should maintain its condition during its application.

- To maintain a low manufacturing cost so that it can be used in a disposable manner and thus maintain its sterility.
- To lead to a wide range of applications based on its purpose.
- To investigate the sensor's capabilities of force estimation.
- To evaluate and validate the sensing device for its intended use in MIS.

1.3 Summary of Contributions

The aim of this research is to create a system that would help surgeons overcome the known problem of the lack of haptic feedback during MIS. The design of this novel sensor has addressed this limiting issue. Below is a summary of the major contributions and achievements of this research.

- The proposal of three air cushion tactile sensor designs for tissue investigation and their feasibility for MIS applications. The first design with a spherical tip measures a change in tissue stiffness by interrupting a light beam generated by an optical sensing setup that consists of a light emitting diode (LED) and a light collecting diode (Zbyszewski, et al., 2009). The second design is a fully MRI-compatible tactile sensor with a spherical tip that measures the change in tissue stiffness by monitoring the position of the sphere through the use of a single emitting and collecting optical fibre coupler (Zbyszewski, Polygerinos, Seneviratne, & Althoefer, A Novel MRI Compatible Air-Cushion Tactile Sensor for Minimally Invasive Surgery, 2009). The third design measures the change in tissue stiffness in the same manner as the second design but it also has the capability to estimate the forces exerted by the spherical tip onto the tissue through the use of pressure sensors.

- The proposal of three low cost tactile sensors that are suitable for rolling mechanical imaging. These sensors can be used to determine variations on the surface of soft material as well as at levels at depth below the surface of the soft material (Zbyszewski, Polygerinos, Seneviratne, & Althoefer, A Novel MRI Compatible Air-Cushion Tactile Sensor for Minimally Invasive Surgery, 2009). A number of applications for such sensors exist. They could be used on human or animal tissue to investigate internal organs such as liver and kidneys or blood vessels such as arteries. The applications are not limited to the internal organs; it could be used on the outer body, such as on the skin, for example to aid in breast cancer diagnosis. Alternatively, similar sensors to theses have been used in the food industry for quality inspection, for instance to establish the firmness of a fruit (Hedrick, Hisada, & Mulloney, 2007)(McGlone & Jordan, 2000).
- The concept of the air cushion tactile sensors and the results and their future applications have been widely praised and embraced by the medical community with which and for which it was designed, developed and built. This has resulted in the sensors collecting a number of awards (see Awards section).
- The structure and design of the sensor enable it to be used for a wide range of applications. The stiffness of the tactile sensor can be altered depending on its application by simply changing the air pressure used. The air used in the sensor ensures that the sphere maintains its condition by clearing any transferred fluids or materials collected during the application of the sensor.
- The low manufacturing cost of the sensor lends itself to be used as a disposable sensor enabling a simpler sterilisation process.

- The second design of the tactile air cushion sensor can be used within an MR environment. This feature allows the sensor to be used as a tactile sensor during MRI-guided interventions which is considered an important step in the field of MRI guided surgery (Zbyszewski, Polygerinos, Seneviratne, & Althoefer, A Novel MRI Compatible Air-Cushion Tactile Sensor for Minimally Invasive Surgery, 2009).
- An international patent was successfully granted for the designs and applications of the air cushion tactile sensors. The patent further reinforces the individuality of theses sensors (see Patent publication section).

1.4 List of Author's Publications

The work presented in this thesis resulted in the following peer-reviewed publications, book chapters, awards and one patent. All entries are listed below:

1.4.1 Journal Publications

1. Zbyszewski Dinusha; Challacombe Benjamin; Liu Hongbin; Seneviratne Lakmal; Dasgupta Prokar; Murphy Declan; Althoefer Kaspar, "Air-cushion force-sensitive probe for soft tissue investigation during minimally invasive surgery", *Journal of Endourology*, 2009; vol. 23, no.9, pp.1421-1424.
2. Zbyszewski Dinusha, Challacombe Benjamin, Li Jichun, Seneviratne Lakmal, Althoefer Kaspar, Dasgupta Prokar, Murphy Declan; "A comparative study between an improved novel air-cushion sensor and a wheeled probe for minimally invasive surgery", *Journal of Endourology*, 2010; vol. 24, no.7, pp.1155-1159.

3. H. Liu, P. Puangmali, D. Zbyszewski, O. Elhage, P. Dasgupta, J. S. Dai, L. Seneviratne, and K. Althoefer, “An indentation depth−force sensing wheeled probe for abnormality identification during minimally invasive surgery”, *Proceedings of the IMechE Part H: Journal of Engineering in Medicine*, 2010, vol. 224, no. 6, pp. 751–763.
4. Panagiotis Polygerinos, *Student Member, IEEE,* Dinusha Zbyszewski, *Student Member, IEEE,* Tobias Schaeffter, Reza Razavi, Lakmal Seneviratne, *Member, IEEE,* and Kaspar Althoefer, *Member, IEEE*, “MRI-Compatible Fiber-Optic Force Sensors for Catheterization Procedures”, IEEE *Sensors Journal,* vol. 10, no. 10, pp.1598-1608, October 2010.

1.4.2 Conference Publications

1. D. Zbyszewski, K. Althoefer, “Distributed force sensing using rolling air-cushion sensor”, *BioEngineering 11,* London, United Kingdom, 2009
2. D. Zbyszewski, K. Althoefer, H. Liu, L. Seneviratne, B. Challacombe, P. Dasgupta, “A comparative study between an improved novel air cushion sensor and a wheeled probe for minimally invasive surgery”, *27th World Congress of Endourology & SWL WCE,* Munich, Germany, October, 2009.
3. D. Zbyszewski, P. Polygerinos, L. Seneviratne, K. Althoefer, “A Novel MRI Compatible Air-Cushion Tactile Sensor for Minimally Invasive Surgery”, *IEEE International Conference on Intelligent RObots and Systems (IROS),* St Louis, Missouri, USA, 2009, pp.2647-2652.
4. Dinusha Zbyszewski, Hongbin Liu,Oussama Elhage, Ben Challacombe, Prokar Dasgupta, Kaspar Althoefer, Lakmal Seneviratne, "A comparative study between novel air-cushion probe and wheeled probe for MIS",

Engineering and Urology Society, 24th Annual Meeting, Chicago, Illinois, 2009.

5. Zbyszewski, D., A., Althoefer, K., Seneviratne, L., "A Novel Air-Cushion Tactile Sensor for Minimally Invasive Surgery", *Human Adaptive Mechatronics (HAM),* 2008; and then presented at *2009 IEEE International Conference on Networking, Sensing and Control (ICNSC),* Okayama, Japan, 2009.
6. K. Althoefer, D. Zbyszewski, H. Liu, P. Puangmali, L. Seneviratne, B. Challacombe, P. Dasgupta, D. Murphy, "Air-Cushion Force Sensitive Probe for Soft Tissue Investigation during Minimally Invasive Surgery", *7th IEEE Conference on Sensors*, Lecce, Italy, 2008, pp. 827 – 830.
7. D. Zbyszewski, A. Bhaumik, K. Althoefer, L. D. Seneviratne, "Tactile Sensing using a Novel Air Cushion Sensor: A Feasibility Study", *IEEE International Conference on Intelligent Robots and Systems (IROS),* Nice, France, 2008, pp. 41 – 46.
8. D. Zbyszewski, H. Liu, P. Puangmali, K. Althoefer, C. S. Nunes, L. D. Seneviratne, B. Challacombe, D. Murphy, and P. Dasgupta, "Wheel/Tissue Force Interaction: A New Concept for Soft Tissue Diagnosis during MIS", *30th Annual International Conference of the IEEE Engineering in Medicine and Biology Society (EMBC08),* Vancouver, Canada, 2008, pp.5556-5559.
9. Kaspar Althoefer, Dinusha Zbyszewski, Hongbin Liu, Pinyo Puangmali, Ben Challacombe, Declan Murphy, ProkarDasgupta, Lakmal Seneviratne, "Air-cushion force sensitive probe for soft tissue investigation during minimally invasive surgery", *26th World Congress of Endourology & SWL WCE*, Shangai, China, 2008.

1.4.3 Awards

The work carried out during this research degree also received the following international awards.

1. Winner of **Session Highlights Category** at the 27th World Congress of Endourology & SWL WCE, Munich, Germany, October, 2009
2. Winner of the **Outstanding Paper Award** at the Engineering and Urology Society, 24th Annual Meeting, Chicago, Illinois, 2009.
3. Winner of **Session Highlights Category** at the 26th World Congress of Endourology & SWL WCE, Shangai, China, 2008.
4. Winner of the **Best Research Paper in recognition of excellence in endourological research** at the 26th World Congress of Endourology & SWL WCE, Shangai, China, 2008.

1.4.4 Book Chapters

1. K. Althoefer, H. Liu, P. Puangmali, D. Zbyszewski, D. Noonan, and L. D. Seneviratne, "Force sensing in medical robotics", *in Mechatronics in Action, 1st ed., D. Bradley and D. W. Russell, Eds. London: Springer-Verlag*, 2010, pp. 157–172.
2. Ben Challacombe, Kaspar Althoefer and Dan Stoianovici, "Emerging robotics", Chapter in *New Technologies in Urology, New Techniques in Surgery Series, 2010,* Volume 7, Part I, pp. 49-56. Acknowledgement: the authors would like to acknowledge the contributions from Mr Hong bin Liu, Mr Dinusha Zbyszewski, Mr David Noonan, Professor Lakmal Seneviratne and Dr. Adriano Cavalcanti.

1.4.5 Patent Publication

1. K. Althoefer, D. Zbyszewski, P. Puangmali, and L. Seneviratne, “Air cushion sensor for tactile sensing during minimally invasive surgery”, International Patent WO2009147399 (A1), Dec. 2009.

1.5 Thesis Outline

Chapter 1: This chapter is used as a brief introduction to MIS; it explores some of the benefits and drawbacks that surround the technique and technology. The specific area of research is described followed by the aims and objectives of this PhD. Additionally, the overall contributions to sciences are outlined. Later, the author’s publications, including, journals, conference proceedings, book chapters and patent are listed. Finally, the chapter concludes with a brief summary of each chapter and an outline of the thesis structure.

Chapter 2: This chapter contains a literature review on the topic providing the reader with a range of background information that is needed to understand the problem that the researcher is trying to overcome. The chapter starts with a brief description of the history of endoscopy, followed by explaining the concept of minimally invasive surgery. This is followed by discussing the advances in robotic assisted surgery and the need for sensory substitution. A range of the different types of force and tactile sensors used for minimally invasive surgery are discussed followed by explaining the use of magnetic resonance imaging. The process of rolling indentation as a mean to acquire tactile information is explained and some related work to the proposed sensor is also presented.

Chapter 3: This chapter is dedicated to describing and explaining the conceptual idea and structure of the proposed sensor. The reason for using an optical sensing scheme for this concept is explained. The three designs of the sensors that incorporate the concept are described with their sensing principle and their limitations.

Chapter 4: This chapter is dedicated to establishing the characteristics of Sensor 3 by estimating the force generated by the sensor. The experimental test rig is presented with the experimental procedures explained. The experimental results are presented. An experimental model for the force estimation is subsequently derived from the experimental results.

Chapter 5: This chapter presents the applications of Sensor 1, Sensor 2 and Sensor 3. The experimental procedures used for all three sensors are explained. The experimental results are then presented and discussed.

Chapter 6: A summary of the achievements of the sensors is presented and future work is also suggested.

Chapter 2 - Literature Review

2.1 History of Endoscopy

Endoscopy is the process of looking inside the body for medical reasons .The first signs of medical endoscopy can be traced back to Hippocrates (460 BC -375 BC) lifetime, during which he used a speculum to carry out a rectal examination (Jones, Wu, & Sopper, 2004). However, due to the technical limitations of guiding light into the body orifices, such procedures were restricted.

The first successful attempt to guide light into a human body cavity was achieved by Philipp Bozzini (1773-1809) (Berci & Forde, 2000) with his 'Lichleiter' (German for light conductor) which was designed to hold a candle with a metal casing to which a range of metal tubes were attached in order to guide the light into the relevant body cavities (Prevedello, Doglietto, Jane, Jagannathan, Han, & Laws, 2007). This invention was then further improved by Antoine Jean Desormeaux (1815-1882) (Verger-Kuhnke, Reuter, & Beccaria, 2007). He added a system of mirrors and replaced the candle with a lamp flame burning a mixture of turpentine and alcohol to increase the luminosity of the light, allowing direct vision of the internal organs. By calling his instrument an 'endoscope' Desormeaux coined the term (Verger-Kuhnke,

Reuter, & Beccaria, 2007). Maximilliam Nitze (1848-1906) later placed the light source at the tip of the endoscope by miniaturising Thomas Edison's filament globe, thus creating the first electrically illuminated cystoscope (Gross & Kollenbrandt, 2009). So far these inventions have focused on rigid endoscopy. The first recorded form of flexible endoscopy came from Kelling (1866-1945) in 1898, who invented a flexible esophagoscope with a maximum flexing angle of 45 degrees (Berci & Forde, 2000). In 1901 Kelling performed the first laparoscopic surgery on a dog using Nitze's cystocope, calling it a 'celioscopy' (Hatzinger, Badawi, Langbein, & Hacker, 2005). That same year, Dimitri Oskarovich Ott (1859-1929) performed the first documented laparoscopy using an external light source, a speculum and a gynaecological head mirror; describing it as a 'ventroscopy' (Ott, 1901). It was not until 1910 when Hans Christen Jacobaeus (1879-1937) used the term 'laparoscopy' that it became accepted as the terminology to be used to describe these types of interventions (Jacobaeus, 1910). In 1987, Phillipe Mouret removed a patient's gallbladder laparoscopically making it the first time laparoscopy entered the world of general surgery (Litynski, 1999), although it had been common place in the specialised field of gynaecology since 1941 (Rock & Warshaw, 1994). In recent years, the term 'minimally invasive surgery' has replaced the term 'laparoscopy', especially when referring to the wide therapeutic application of the procedure (Modlin, Kidd, & Lye, 2004).

2.2 Minimally Invasive Surgery

Minimally invasive surgery (MIS) is a branch of Medical Endoscopy, which includes but is not limited to laparoscopic surgery and robot-assisted surgery. It can be defined simply as major or minor surgery that is performed through very small incisions,

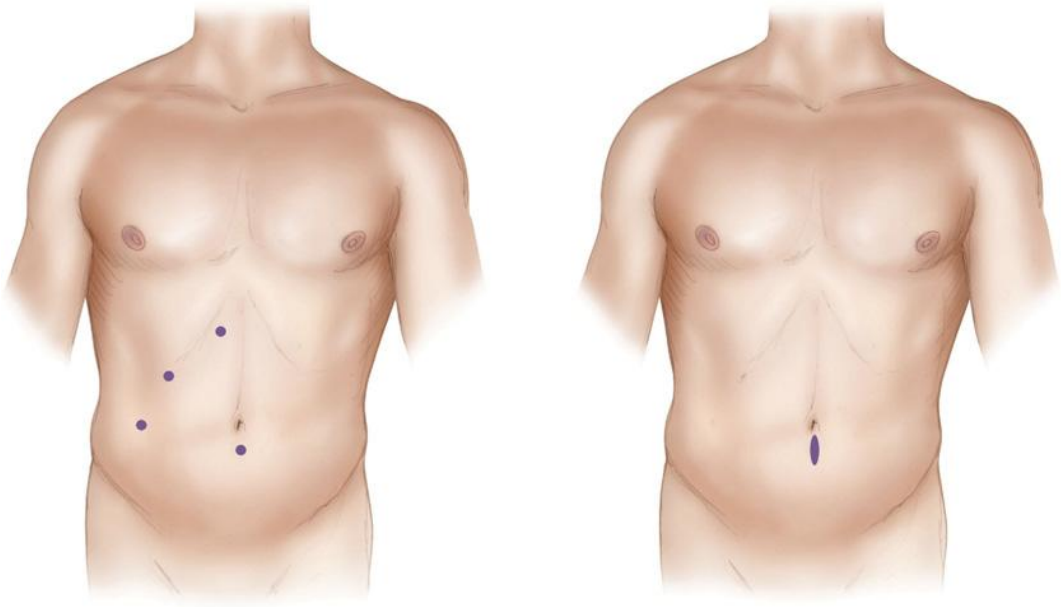

Figure 2.1: On the left, the multiple incisions of traditional laparoscopy port sites and on the right, the single-incision laparoscopy port site (Ulmer, 2010).

varying from 3 mm to 12 mm in diameter (Bicchi, Canepa, De Rossi, Iacconi, & Scilingo, 1996). The incisions are strategically located so as to offer the optimum access to the surgical site. These remain open with the help of trocar ports which also act as gas tight valves as the surgical site is insufflated with carbon dioxide, so as to separate internal organs from each other and gain access to specific tissue structures (Schreiber, Steichen, & Kraas, 2001). The insufflation is also used to create a better and bigger working environment for an improved ease of movement and better access with the endoscopic tools. An endoscopic magnifying camera is inserted through one of the incisions to transmit an enhanced view of the anatomy and pathology to the surgeon, and endoscopic instruments are inserted through the other incisions (Zbyszewski, et al., 2008).

The trend of minimally invasive surgery is towards LESS and NOTES. LESS (Laparo-Endoscopic Single-Site surgery) is also known as SILS (Single incision

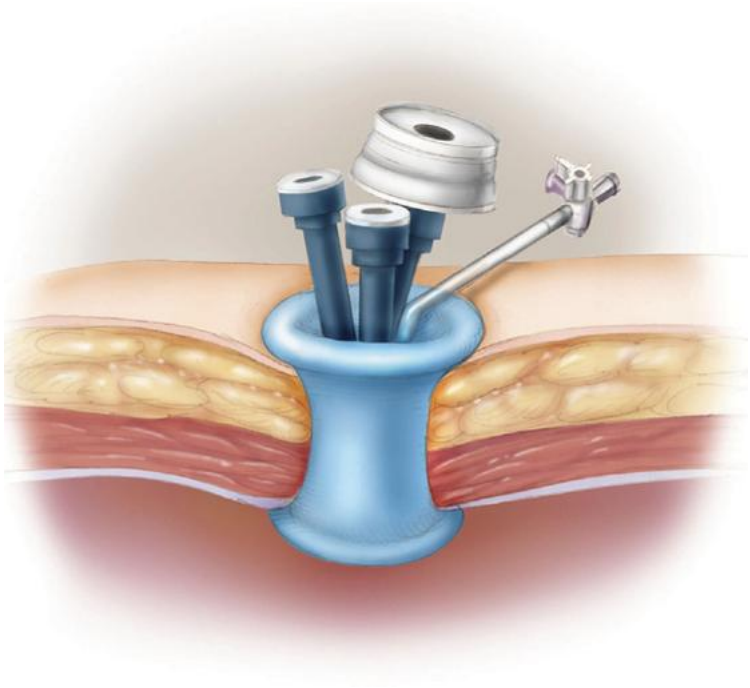

Figure 2.2: A single incision laparoscopic surgery trocar port (Ulmer, 2010)

Laparoscopic Surgery). This advanced minimally invasive surgery techniques consists of a single entry point, usually at the umbilicus, through which all endoscopic instruments enter. Other acronyms are SPA (Single Port Access), OPUS (One-Port Umbilical Surgery), SAS (Single Access Site), SPL (Single Port Laparoscopy) and TUES (Trans-Umbilical Endoscopic Surgery) (Michalik, Orłowski, Frask, Bobowicz, Adamczewska, & Lech, 2009)(Zhu, 2009).

The locations of the single incision for LESS, in contrast to multiple incisions in traditional laparoscopy are illustrated in Figure 2.1. For illustration purposes a single incision laparoscopic trocar port is shown in Figure 2.2.

The benefits of LESS are that it can be achieved with standard laparoscopic instruments (Bucher, Pugin, Buchs, Ostermann, Charara, & Morel, 2009). According to (Mintz, Talamini, & Cullen, 2008) NOTES (Natural Orifice Translumenal

Endoscopic Surgery) is the next frontier in MIS procedures. The natural orifices that can be used for NOTES through which a flexible endoscope is inserted are the anus, the vagina, the urethra and the mouth by respectively puncturing the rectum, the vagina, the urinary bladder and the stomach (Pearl & Ponsky, 2008). The first NOTES of its kind was the removal of a healthy kidney through the donor's vagina performed at Johns Hopkins (JHM, 2009).

Minimally Invasive surgery has been credited with the following benefits in comparison to open surgery: quicker recovery of the patient, shorter hospital stays, less narcotic requirement (Gill, et al., 2003), reduced blood loss, wound complications are less frequent (Franklin, et al., 1996), quicker return to daily activities, improved immunologic response and improved cosmesis (Kim, et al., 2001). Minimally invasive surgery has also made some surgeries possible which carried a too high risk factor if performed through open surgery (Kobiela, Stefaniak, Mackowiak, Lachinski, & Sledzinski, 2008). Another advantage of minimally invasive surgery is that it is a full-fledged technology, thus making it affordable and ubiquitous (Lanfranco, Castellanos, & Desai, 2004).

2.2.1 Drawbacks of Minimally Invasive Surgery

There are several drawbacks to minimally invasive surgery. During traditional open surgical procedures, surgeons use their hands and fingers as tools to locate and detect palpable abnormalities such as tumours (Zbyszewski, et al., 2008) and have a direct view of the surgical site (Schostek, Schurr, & Buess, 2009). During minimally invasive surgery, direct access to the surgical site is impossible, thereby preventing direct surgical palpation (Schostek, Schurr, & Buess, 2009). According to (Eltaib & Hewit, 2003), this is one of the fundamental drawbacks of minimally invasive

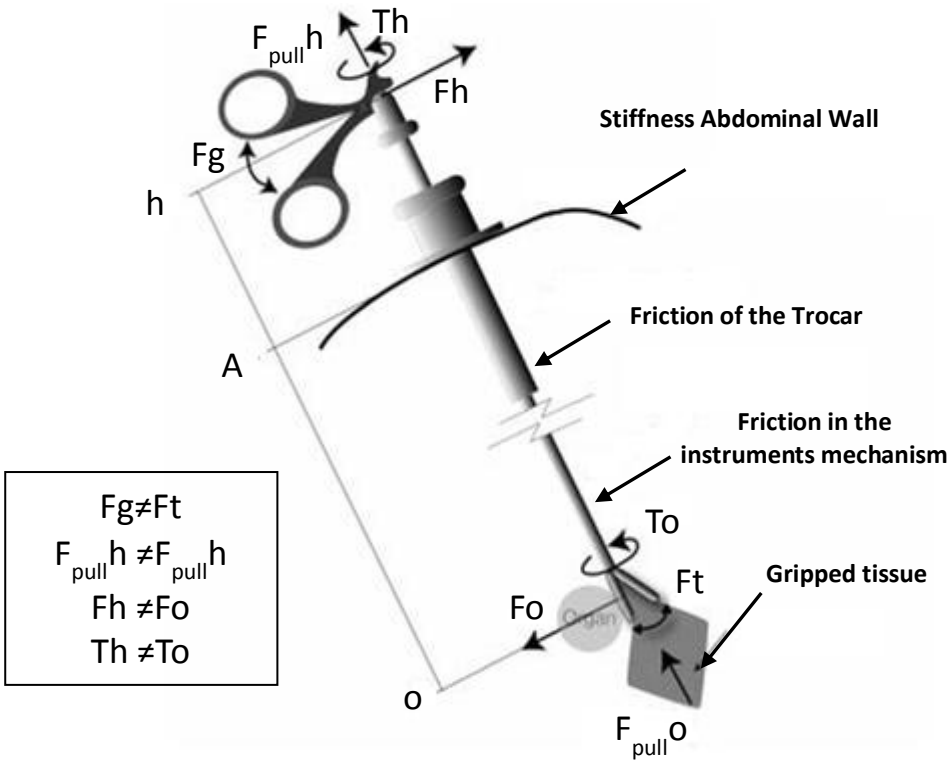

Figure 2.3: Interference factors in traditional minimally invasive surgery (Westebring-Van der Putten, Goossens, Jakimowicz, & Dankelman, 2008).

surgery. Some contact force between the laparoscopic tools and the tissue contact can be felt by the surgeon through the laparoscopic tools but these are limited (Schostek, Schurr, & Buess, 2009). The friction between the trocar ports and the laparoscopic instruments skews the actual contact forces with the tissue, making the sensing of any tissue reaction forces through the instrument's shaft extremely difficult (Puangmali P. , Althoefer, Seneviratne, Murphy, & Dasgupta, 2008).

This issue is clearly explained and is illustrated in Figure 2.3 where the Fg is the grip force, Ft is the tip force, Fh is the hand force, Fo the organ force, $F_{pull}h$ is the pull force at the handle, $F_{pull}o$ is the pull force at the organ, Th is the torque applied at the

handle and To is the torque force exerted at the organ (Westebring-Van der Putten, Goossens, Jakimowicz, & Dankelman, 2008).

This problem is known as a lack of or reduced haptic feedback. Haptics illustrate both cutaneous (tactile) and kinaesthetic (force) information, both of these are required to mimic the sensation felt by a human hand (Okamura, Methods for haptic feedback in teleoperated robot-assisted surgery, 2004). Kinaesthetic feedback is affected by the special surgical instruments (Schostek, Schurr, & Buess, 2009) and the abdominal wall resistance (Picod, Jambon, Vinatier, & Dubois, 2005). It is also affected by the instrument's mechanism (Westebring-Van der Putten, Goossens, Jakimowicz, & Dankelman, 2008) and the friction forces that are generated when the instrument is rotated, pulled or pushed through the trocar port (Van den Dobbelsteen, Schooleman, & Dankelman, 2007) (Tirabassi, Wadie, Tashjian, & Moriarty, 2007). Despite this, kinaesthetic feedback is still provided to some extent through minimally invasive instruments (Bholat, Haluck, Murray, Gorman, & Krummel, 1999).

Additionally, there is a loss of wrist articulation (Camarillo, Krummel, & Salisbury Jr., 2004) due to surgical tools' movements being constrained at the insertion point, meaning that the tools' degrees of freedom (DOF) are limited to only four: insertion, roll, yaw, and pitch (Tavakoli, Aziminejad, Patel, & Moallem, 2006) as illustrated in Figure 2.4.

In contrast the human hand and wrist have a total of seven degrees of freedom (Lanfranco, Castellanos, & Desai, 2004), providing a wider range of movements. During the procedure the surgeon monitors the movement of the tools on a two dimensional monitor (Breedveld, Stassen, Meijer, & Jakimowicz, 2000) which can be counter intuitive as there is no depth perception (Lanfranco, Castellanos, & Desai,

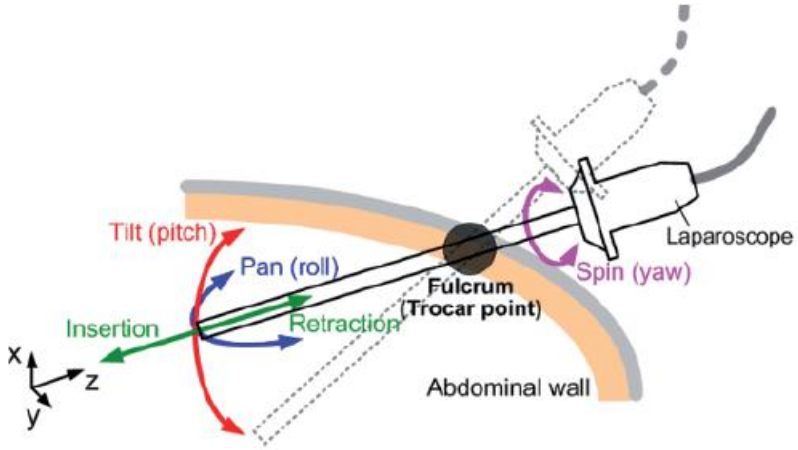

Figure 2.4: Movement of an instrument around the insertion point (Kuo & Dai, 2009)

2004). The tools have to be moved in the opposite physical direction to reach a target on the screen, this is also known as the fulcrum effect (Gallagher, McClure, McGuigan, Ritchie, & Shechy, 1998).

Another disadvantage is that any physiological tremors from the surgeon are amplified through the laparoscopic tools (Lanfranco, Castellanos, & Desai, 2004). In contrast to visual feedback and kinaesthetic feedback, which can be perceived to some extent, tactile feedback is entirely lost with traditional laparoscopic instruments (Schostek, Schurr, & Buess, 2009). This type of surgery is also more technically demanding with an increase of surgeon fatigue (Cuschieri, 1995) due to poor ergonomics (Reyes, Tang, & Cuschieri, 2006) (Berguer, Forkey, & Smith, 1999) and crowding of the operating theatre (Alarcon & Berguer, 1996). In short, reduced visual, haptic, and tactile feedback, along with issues of lack of dexterity can lead to accidental tissue damage (Tendick & Cavusoglu, 1997). Some of these drawbacks were later overcome by robot assisted Minimally Invasive Surgery (Lanfranco, Castellanos, & Desai, 2004).

2.3 Robotic Assisted Minimally Invasive surgery

The first robotic assisted surgery took place on 11th April 1985: it consisted of a CT (computer tomography) guided brain tumour biopsies using a Unimation Puma 200 robot, which resulted in a faster procedure and more importantly in greater accuracy (Kwoh, Hou, Jockheere, & Hayati, 1988). In 1988, (Davies, 2000) used a Puma 560 industrial robot to perform a feasibility study for a transurethral resection of the prostate. Unfortunately safety concerns arose from the use of such an industrial robot in close proximity of people, resulting in the termination of any future works (Cleary & Nguyen, 2001) (Davies, 2000).

Around the mid to late 1980's (Lanfranco, Castellanos, & Desai, 2004) a group of scientists, including Scott Fisher PhD (Francis, 2006) at the National Air and Space Administration (NASA) Ames research centre wanted to develop telepresence surgery by using virtual reality. Virtual reality is defined as "the use of computer modeling and simulation that enables a person to interact with an artificial three-dimensional (3-D) visual or other sensory environment. Virtual reality applications immerse the user in a computer-generated environment that simulates reality through the use of interactive devices, which send and receive information and are worn as goggles, headsets, gloves, or body suits" (Encyclopædia Britannica, Science & Technology: Virtual Reality). Concurrently, at the Stanford Research Institute (SRI) Joseph Rosen MD and his team were working on robotic technology and telemanipulation (Satava, 2003). Dr Fisher and his team joined forces with Dr Rosen's team in the early 1990's (Lanfranco, Castellanos, & Desai, 2004), with a vision of telepresence surgery by integrating surgical robotics with interactive virtual reality (Albani, 2007). This work got Richard Satava MD's attention, a general surgeon from the US army (Satava, 2003). He saw the potential in decreasing fatalities in war by allowing a surgeon to

Figure 2.5: The Automated Endoscopic System for Optimal Positioning (AESOP) in action (Sim, Yip, & Cheng, 2006)

diagnose and treat soldiers through telepresensce (Satava, 2003). The soldier would be placed into a vehicle with robotic surgical equipment known as Medical Forward Area Surgical Team (MEDFAST) and would be operated on remotely from a Mobile Advanced Surgical Hospital (MASH) (Satava, 2003). This vision enabled Dr Satava to get funding from the US army to collaborate with Dr Fischer and Dr Rosen's team of the SRI Green Telepresence System (Satava, 2003). This was achieved on animal models such as performing a suture and a knot on ex-vivo porcine intestine (Satava, 2003) but has yet to be implemented for battle field casualty care (Albani, 2007).

Following this development, Frederik Moll MD saw the commercial potential that such a system would have with patients undergoing MIS procedures (Francis, 2006).

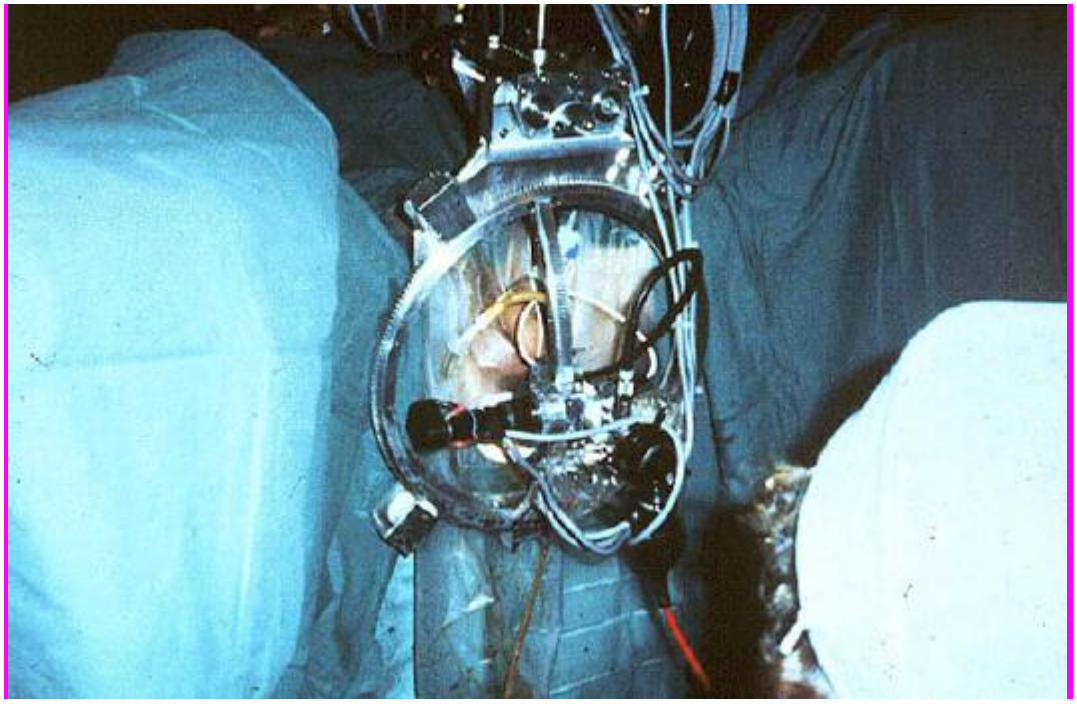

Figure 2.6: The ProBot is the first prostate resection robot (Sim, Yip, & Cheng, 2006).

In 1985, this led to Robert Younge, John Freund and Frederik Moll (Francis, 2006) starting up the company Integrated Surgical Systems (now Intuitive Surgical Inc) (Lanfranco, Castellanos, & Desai, 2004) by acquiring the license for the SRI Green Telepresence System. In 1989, with funding from the Defense Advanced Research Projects Agency (DARPA) and NASA (Francis, 2006), Yulun Wang PhD created his own company, Computer Motion Inc, which developed the Automated Endoscopic System for Optimal Positioning (AESOP), as illustrated in Figure 2.5, which was a table mounted system to control an endoscopic camera (Albani, 2007).

On the 25th March 1991, Davies et al used the world's first active robot for surgery under computer planning and control on a patient (Ng, Davies, Hibberd, & Timoney, 1993). The robot, known as "SARP" (Surgical Assistant Robot for Prostatectomy), was the first prostate robot to be used to remove substantial amounts of prostatic

tissue from a live patient, during a transurethral resection of the prostate (TURP) (Ng, Davies, Hibberd, & Timoney, 1993). SARP was later improved into the PROBOT (as illustrated in Figure 2.6) so as to commence full clinical trials (Harris, Mei, Hibberd, & Davies, 1997).

Around the same time Integrated Surgical Systems, Inc. of Sacramento, California, developed the Robodoc, a robotic system to core out the femur with greater precision for hip replacements (Bargar, Bauer, & Börner, 1998). In 1992, the Robodoc underwent clinical trials under US FDA (United States Food and Drug Administration) for total hip replacement procedures in humans (Mantwil, Schulz, Hollstein, Kammal, Fay, & Jurgens, 2005). The Robodoc can be seen in operation in Figure 2.7.

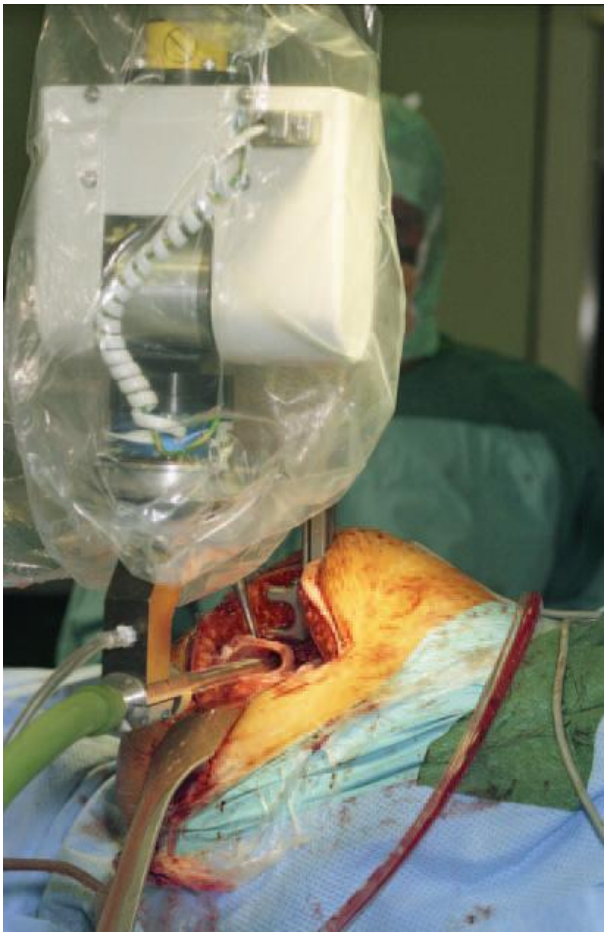

Figure 2.7: The Robodoc during femoral canal milling operation (Mantwil, Schulz, Hollstein, Kammal, Fay, & Jurgens, 2005).

In 1993, AESOP 1000 was the first endoscopic manipulator to be granted US Food and Drug Administration (FDA) approval for use in humans (Sim, Yip, & Cheng, 2006). In creating AESOP, Yulun successfully attracted the attention of the business community and thus secured funding through the commercial sector for a complete robotic surgery system independently of DARPA (Satava, 2003).

In the mean time Intuitive Surgical Inc were completely redesigning the SRI Green Telepresence System and eventually marketed it as the da Vinci Surgical System(Satava, 2003). The da Vinci robotic system is based on a master slave design,

Figure 2.8: The da Vinci Surgical System layout (Intuitive Surgical Product Images, 2005).

where the slave is a tele-operated cart with three or four robotic arms and the master is a surgical console controlled by the surgeon (Noonan, Liu, Zweiri, Althoefer, & Seneviratne, 2007). The layout of the surgical system is clearly illustrated in Figure 2.8.

Following the success of the da Vinci Surgical System, Computer Motion Inc introduced the Zeus system (Albani, 2007) which also was a master slave design. The Zeus surgical system is shown in Figure 2.9.

The master slave robot is also known as an online robot which relies on continuous input from the surgeon, who controls its every movement in real-time (Sim, Yip, & Cheng, 2006). In 2003, Computer Motion Inc and Intuitive Surgical Systems merged resulting in the manufacturing of the Zeus platform being discontinued (Albani, 2007).

Figure 2.9: The Zeus surgical system in action (Sim, Yip, & Cheng, 2006)

Robotic surgery has brought many additional benefits to the field of minimally invasive surgery, without suppressing those already existing. For the surgeon such systems offer a more ergonomic position to perform surgery, a three dimensional vision with depth perception (Francis, 2006), improved dexterity with adjustable motion scaling and physiological tremor filtering. Additionally the use of a robot also enables surgery on morbidly obese patient (Jacobsen, Berger, & Horgan, 2003). Other benefits include restored hand eye coordination compared to laparoscopic surgery and tissue magnification of up to 12 times (Albani, 2007). According to (Davies, 2000) well designed robotic systems also offer the ability:

- To move with accuracy and predictability in a reprogrammable and predefined complex three dimensional path.
- To perform repetitive motion for extended periods of time without tiring.

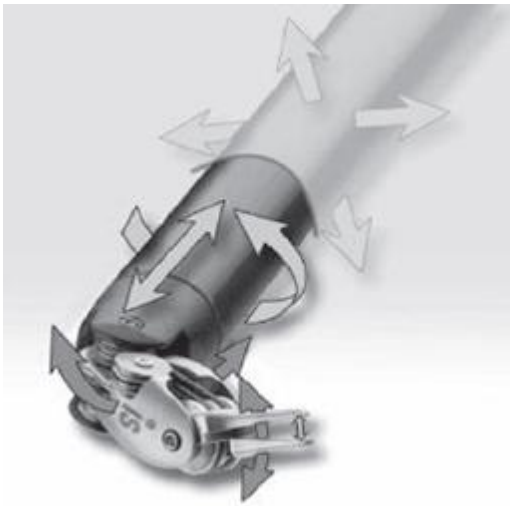

Figure 2.10: The Endowrist technology illustrated with its 7 degrees of freedom (Albani, 2007).

- To actively limit tools to a specific path or location to prevent any injury to vital regions.
- To move, hold and locate tools within a hazardous environment without endangering the surgeon.

The concept of tele-surgery has even become a reality (Pirisi, 2003). The da Vinci Surgical system also offers an increased range of motion with 7 degrees of freedom with its Endowrist Technology (Figure 2.10), which includes the following motions: insertion and roll of the shaft, yaw and pitch and grip at the tip of the instrument and pitch and yaw at the port site (Jacobsen, Berger, & Horgan, 2003). In addition to these, improvements based on 3D vision and high distal dexterity tools enables the effective performance of complex surgical procedures usually difficult to conduct by conventional minimally invasive means, such as coronary artery bypass grafting (Tabaie, Reinbolt, Graper, Kelly, & Connor, 1999) and mitral valve repair (Murphy, Miller, Langford, & Snyder, 2006).

Benefits to patients associated with robotic surgery include reduced post-operative pain, faster recovery, shorter hospital stay, better cosmesis resulting from smaller incisions (Wilson, 2009), reduction in blood loss and tissue loss and a faster return to work (Ulmer, 2010).

2.3.1 Drawbacks of Minimally Invasive Robotic Surgery

Despite the many improvements that robotics assisted minimally invasive surgery offers over laparoscopic surgery; it still suffers from some significant drawbacks. First of all, the purchase costs of robotic systems are elevated, for example, the four arm da Vinci system and a da Vinci S system priced at $1.33 million and $1.53million, respectively and with an annual service of $130 thousand dollars (Albani, 2007). The reduced or lack of haptic feedback that is a major concern in laparoscopic surgery is unfortunately also present in MIRS forcing the surgeon to rely heavily on visual cues rather than tactile cues (Wilson, 2009).

During the surgery, there are several types of principle feedback that are usually required by the surgeon, which are visual feedback, force (kinaesthetic) feedback, and tactile (cutaneous) feedback. This sense of feel is essential for performing tissue palpation, manipulation, and suturing. It is therefore required in all types of surgery including traditional surgery, MIS, and MIRS.

2.4 Sensory substitution

To overcome this lack of haptic feedback during MIS and MIRS, a number of sensors have been built to relay information back to the surgeon; this is known as sensory substitution. Sensory substitution is defined by (Kaczmarek, Webster, Bach-y-Rita, & Tompkins, 1991) as the use of one human sense to receive information normally

received by another sense, or in the case of the sense of touch it could be the use of one area of the skin to perceive tactile information from another area of the skin. These sensors are designed to measure force applied to a tissue and/or tactile information of a tissue and to reflect them electronically to the surgeon through a visual, auditory or haptic display (Westebring-Van der Putten, Goossens, Jakimowicz, & Dankelman, 2008). The visual display illustrates the force and/or tactile information through a graphical illustration and the auditory display represents these information through an auditory signal (Westebring-Van der Putten, Goossens, Jakimowicz, & Dankelman, 2008).

The main visual display system in an operating theatre is the endoscopic monitor, on which the surgeon is focused while carrying out tissue palpation (Schostek, Schurr, & Buess, 2009). Any gaze away from the monitor would force the surgeon to readjust and refocus to a new visual field (Bitterman, 2006). It is therefore important to limit such a visual strain by placing tactile visualisation data as close as possible to the main field of view (Schostek, Schurr, & Buess, 2009). The tactile visualisation data can be displayed in many forms, ranging from a separate monitor, to LED devices (Dargahi & Najarian, 2003) and to overlaid video feed on the endoscopic monitor (Schostek, Schurr, & Buess, 2009). Tactile information can encompass a number of parameters, for this reason visual display system have been developed explicitly to reflect those parameters with respect to the tactile instrument (Schostek, Schurr, & Buess, 2009). This is illustrated by (Dargahi, Najarian, & Ramezanifard, 2007), with a visual display that shows colour coding to depict a change in the hardness distribution within a cross section of a tactile grasper. A study by (Tavakoli, Patel, & Moallem, Haptic Feedback and Sensory Substitution during Telemanipulated Suturing, 2005) showed that visual feedback is beneficiary in controlling the force exerted during

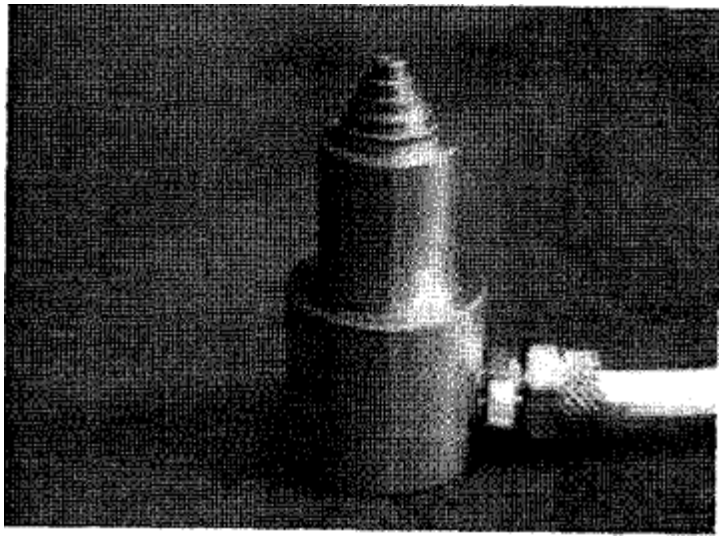

Figure 2.11: The setup of the haptic display (Scilingo, Bicchi, De Rossi, & Iacconi, 1998).

surgical procedures such as stitching and can also improve the outcome of more skilful tasks such as knot tying (Kitagawa, Dokko, Okamura, & Yuh, 2005). However it must be noted that the effectiveness of visual feedback is dependent on the nature of the surgical task at hand (Schostek, Schurr, & Buess, 2009).

In the operating theatre during surgery, the only machine to produce a real auditory display is the pulse oximeter (Schostek, Schurr, & Buess, 2009) which associates the pitch of the pulse tone to the level of the oxygen saturation (Santamore & Cleaver, 2004). A tactile enhancement instrument for minimally invasive surgery designed by (Yao & Hayward, 2005) which used haptic display and auditory display showed during a study that auditory feedback was superior in detecting one small cut and two cuts and performed equally well at detecting no cut and a deep cut to haptic feedback. Unfortunately compared to visual and tactile displays, auditory displays offer only a limited range of information as the acoustic dimensions of auditory signals are limited to semantic content, tone, pitch, location and loudness (Schostek, Schurr, & Buess, 2009).

As opposed to visual and auditory displays, tactile displays require physical contact with the surgeon's hand, meaning that they require more stringent requirements with regards to the ergonomics so as not to interrupt the surgeon's workflow (Schostek, Schurr, & Buess, 2009). The tactile display would need to be incorporated into the handle of a laparoscopic tool that is fitted with the corresponding tactile sensor, or in the case of telerobotic surgery the tactile display would be fitted onto the surgeon's console (Schostek, Schurr, & Buess, 2009). Tactile data display seems to be the most natural way of relaying information, as it makes use of the original perception channel, the surgeon's sense of touch (Schostek, Schurr, & Buess, 2009). The tactile display of the tactile features of the tissue under investigation is achieved through the use of actuators (Schostek, Schurr, & Buess, 2009). There are several types of haptic display, these include but are not limited to; kinaesthetic, which uses an array of forces and positions to counter the user's forces and positions, a vibro-tactile display which utilises an array of vibrating pins which display the change in force as a change in amplitude or frequency of vibrations, a relief-tactile display which employs an array of movable pins in contact with the skin that vary the deflection of the pin in relation to the force, a stretch-tactile display which relays information through spatio-temporal patterns of mechanical skin stretch (Westebring-Van der Putten, Goossens, Jakimowicz, & Dankelman, 2008) and an electro-tactile display employs electrodes located onto the skin to generate the sense of touch (Lundborg, Rosen, Lindstrom, & Lindberg, 1998). A couple of haptic displays are mentioned below. A haptic display (shown in Figure 2.11) created by (Scilingo, Bicchi, De Rossi, & Iacconi, 1998) was able to replicate the rheological behaviour of surgical tissues. This was achieved by increasing the contact area with the finger as the contact force increased; this was controlled pneumatically.

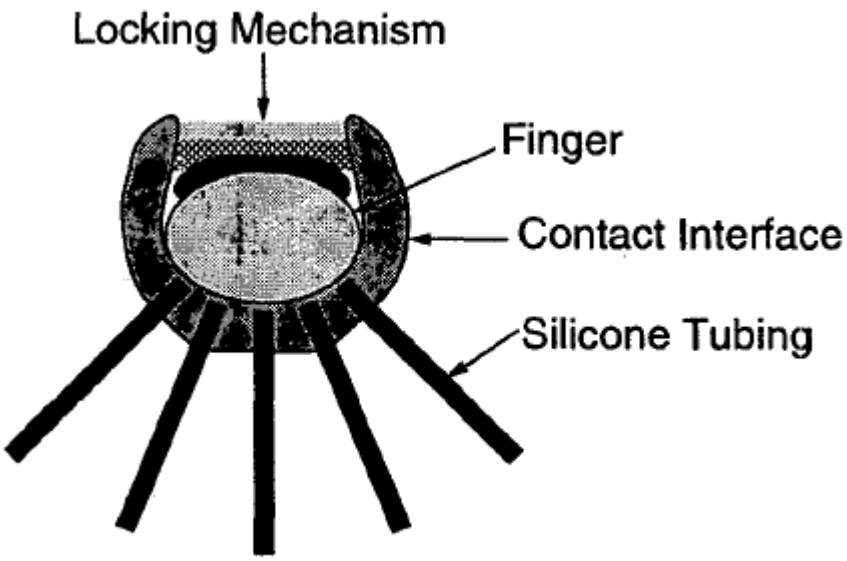

Figure 2.12: The contact interface with the locking mechanism (Moy, Wagner, & Fearing, 2000).

Some tactile displays make use of pneumatically actuated silicone rubber (Moy, Wagner, & Fearing, 2000) where the finger is in constant contact with the silicone pad as it is wrapped around the finger (displayed in Figure 2.12).

Having briefly discussed the various types of displays in sensory substitution, it is time to look at the various types of tactile sensors that provide the information in sensory substitution.

2.5 Force and tactile sensors for Minimally Invasive Surgery

Having discussed earlier the need for tactile feedback in MIS, we now focus our attention on various types of force and tactile sensors and their location on the laparoscopic tool.

The sensing element on a laparoscopic tool of a tactile and force sensor can be positioned outside the patient's body in an extracorporeal position, or inside the patient's body in an intracorporeal position.

Using extracorporeal sensing elements on the laparoscopic tool can be advantageous for a number of factors. The constraints with regards to the size and the material used for the sensing element are relatively lenient, as it does not have to fit through the trocar port and thus does not need to be sterilisable (Rausch & Werthschuetzky, 2009). However, any extracorporeal sensing element will be affected by the friction generated between the trocar port and the shaft of the laparoscopic tool (Salle, Gosselin, Bidaud, & Gravez, 2001). The sensing element can also be affected by the resistance of the abdominal wall depending on the angle and direction of tilt of the laparoscopic tool (Picod, Jambon, Vinatier, & Dubois, 2005). The mechanism used by certain laparoscopic tools also needs to be taken into account, as some of them have a mechanical efficiency that is inferior to 50% due to the friction in the mechanisms that is used (Sjoerdsma, Herder, Horward, Jansen, Bannenberg, & Grimbergen, 1997).

The main benefit of using intracorporeal sensing elements is that they are not affected by the surrounding forces that hinder extracorporeal sensing elements. However, due to the nature of their placement intracorporeal sensing elements on laparoscopic tools have to follow stringent requirements. Their size must conform to MIS standards so as to fit through trocar ports and their design and materials have to be sterilisable. This means the sensor and its sensing element must be designed to withstand the challenging sterilisation processes. The two processes capable of sterilising surgical equipment are steam sterilisation, also known as autoclave and chemical sterilisation. Steam sterilisation is widely used. It consists of heating up the surgical tool to 121°C or 134°C for a period of time of 15 minutes or 3 minutes, respectively (Babb & Bradley, 1995). Chemical sterilisation, as its name states, uses chemical agents such as Ethylene oxide gas (ETO) to achieve the same goal. However, this process is costly

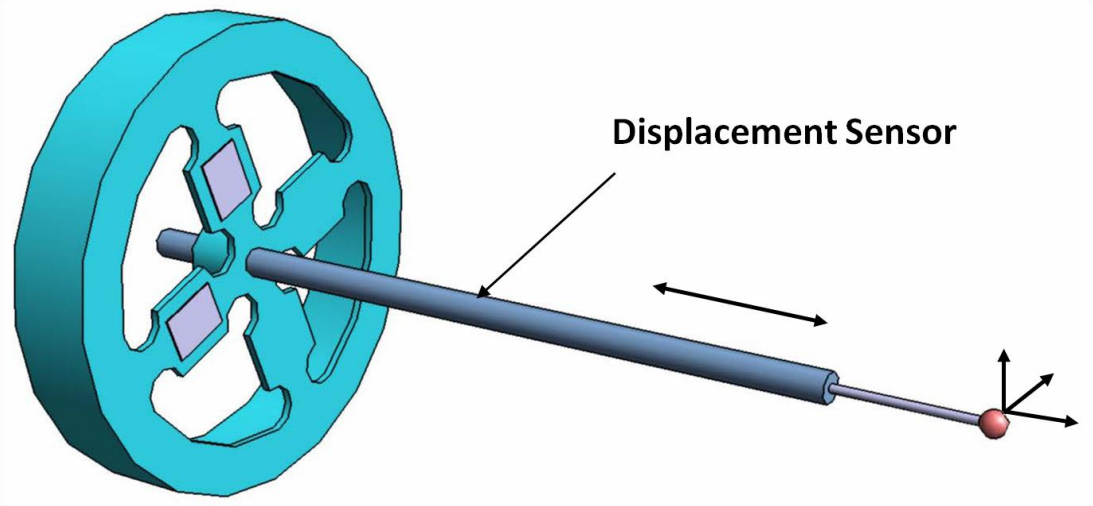

Figure 2.13: The whisker sensor with the DVRT used to measure the normal displacement of the sensor (Bebek & Cavusoglu, 2007).

and requires a sterilisation period of 20 hours (Spaun, Goers, Pierce, Cassera, Scovil, & Swanstrom, 2010).

Puangmali et al. (Puangmali P. , Althoefer, Seneviratne, Murphy, & Dasgupta, 2008) have extensively described the various types of sensing methods that exit for MIS, below is a brief description of their work.

2.5.1 Displacement-Based sensing

This type of sensing is based on the principle of detecting the change in displacement of an elastic component such as a spring. There are a number of displacement sensors that can be used to attain accurate displacement measurements, such as digital encoders, potentiometers and linear variable differential transformers (LVDT). This type of sensing has been used in the work of (Bebek & Cavusoglu, 2007), where a whisker sensor is designed to monitor the motion of a heart during Coronary Artery Bypass Graft (CABG). The displacement of the sensor in the normal direction was

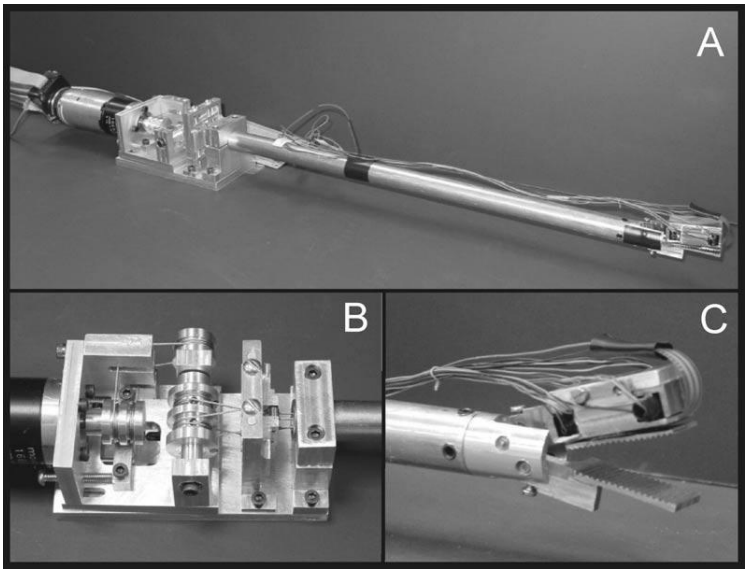

Figure 2.14: Laparoscopic grasper (Tholey, Pillarisetti, Green, & Desai, 2004).

monitored by using a Differential Variable Reluctance Transducer (DVRT). This is shown on Figure 2.13.

2.5.2 Current-Based sensing

This sensing method measures the current of electric motors actuating certain joints. In the case of servo controlled mechanism joints, the value of the generated torques or forces is proportional to the armature current of the motors (Klafter, Chmielewski, & Negin, 1989). This sensing method led to the design of a laparoscopic grasper (Tholey, Pillarisetti, Green, & Desai, 2004) actuated by a DC motor with cable driven jaw mechanism which is illustrated in Figure 2.14. The force of the graspers was derived by the current applied to the motor but unfortunately this method did not yield accurate results (Tholey, Pillarisetti, Green, & Desai, 2004). This method does not measure the force directly, it is just an estimation based on the current of the motors.

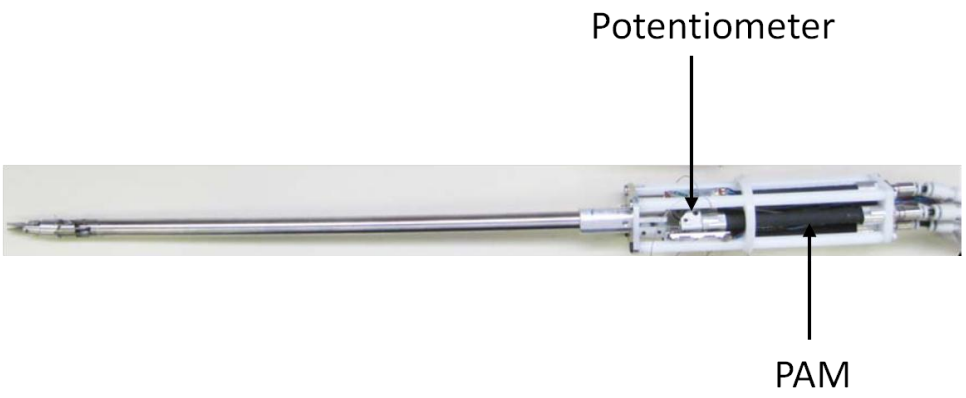

Figure 2.15: The forceps' manipulator with the potentiometer used to monitor the contraction of the PAM (Li, Kawashima, Tadano, Ganguly, & Nakano, 2011).

2.5.3 Pressure-Based Sensing

This type of sensing is an actuator based approach that can use current, as mentioned above, just as well as it can make use of pneumatic equipment. Pneumatic actuators are used to measure forces through pneumatic pressure. An example of this is the work carried out by (Li, Kawashima, Tadano, Ganguly, & Nakano, 2011) where the forces of a forceps' tip are measured without a force sensor but by analysing the contraction of artificial pneumatic muscles (PAM). The forceps' manipulator is illustrated in Figure 2.15.

2.5.4 Resistive-Based Sensing

A strain gauge is a common sensing element in force sensors as it provides an accurate measurement. The gauge is bonded to a flexible structure so that when force is applied to the structure, the electrical resistance of the strain gauge changes which in turn yields an electrical measurement of the applied force. An illustration of this is seen in the second design of the whisker sensor by (Bebek & Cavusoglu, 2007) where

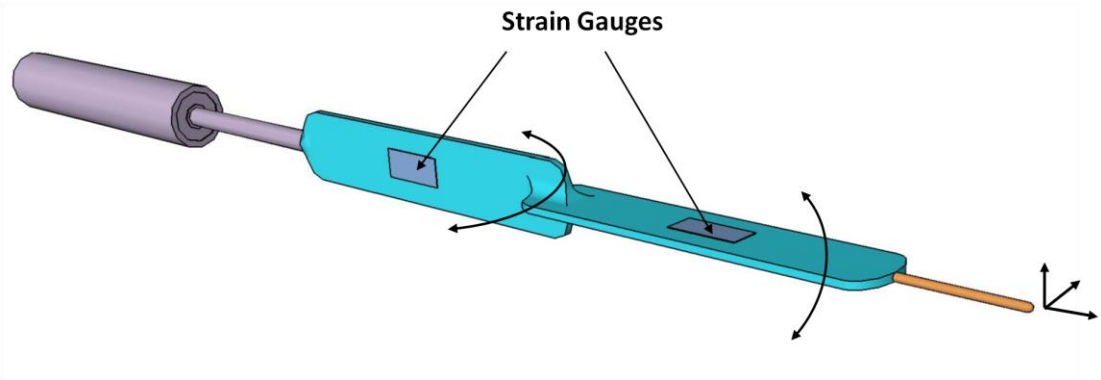

Figure 2.16: The strain gauges are setup in an orthogonal position to each other to measure the deflection of the tip in 2D (Bebek & Cavusoglu, 2007).

two strain gauges are used in an orthogonal setup so as to measure the two dimensional (2D) lateral movements of the tip of the instrument as seen in Figure 2.16

The disadvantage of a strain gauge is the trade off between the stiffness of the structure and the sensitivity of the measurement; the stiffer the structure, the lower the sensitivity (Craig, 2003).

2.5.5 Capacity-Based Sensing

This type of sensing method is used for measuring very small deflections which cannot be measured using strain gauges. Capacity based sensing benefits from the fact that the deflection is not directly temperature dependant. A miniaturised tactile sensor has been developed by (Peng, Sezen, Rajamani, & Erdman, 2009) which uses MEMS capacitive sensing membranes with different stiffness' to estimate tissue stiffness. A diagram of the conceptual structure of the sensor is displayed in Figure 2.17.

The range of sensitivity of this array is achieved by varying the stiffness of the membrane. Despite the fact that the thickness and gap height of numerous membranes

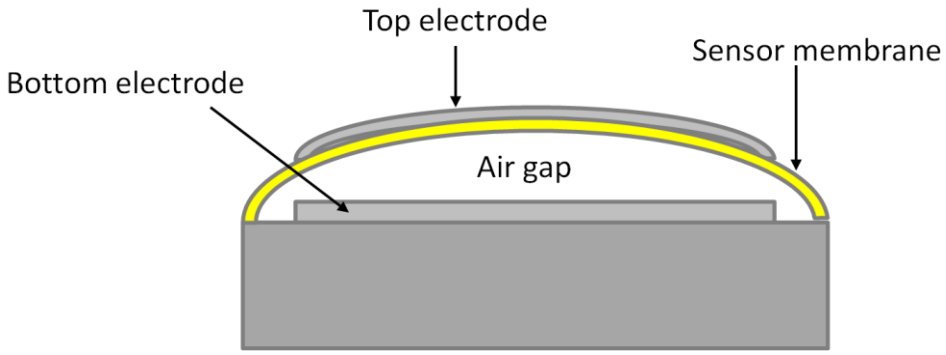

Figure 2.17: A conceptual diagram of the capacitive sensing membrane (Peng, Sezen, Rajamani, & Erdman, 2009).

will be identical, their stiffness will be defined by the diameter of the membrane, thus they will have different compliances under the same load (Peng, Sezen, Rajamani, & Erdman, 2009). Such sensors tend to be limited to applications that require accurate measurement over a small range.

2.5.6 Piezoelectric-Based Sensing

Piezoelectric materials can proportionally produce voltage when their structure is compressed, resulting in deformation. A small compression generates a large output voltage which is optimal for detecting small forces. A popular piezoelectric material used for tactile sensors is polyvinylidene fluoride (also known as PVDF or PVF2) (Klafter, Chmielewski, & Negin, 1989). An MIS tactile sensor with force position and measurement capabilities is put forward by (Qasaimeh, Sokhanvar, Dargahi, & Kahrizi, 2009). The sensor comprises of sensor units that each are teeth shaped with layers of micromachines silicon, a PVDF layer and a plexiglass layer with a gap in the middle to allow for deflection as illustrated in Figure 2.18 (Qasaimeh, Sokhanvar, Dargahi, & Kahrizi, 2009).

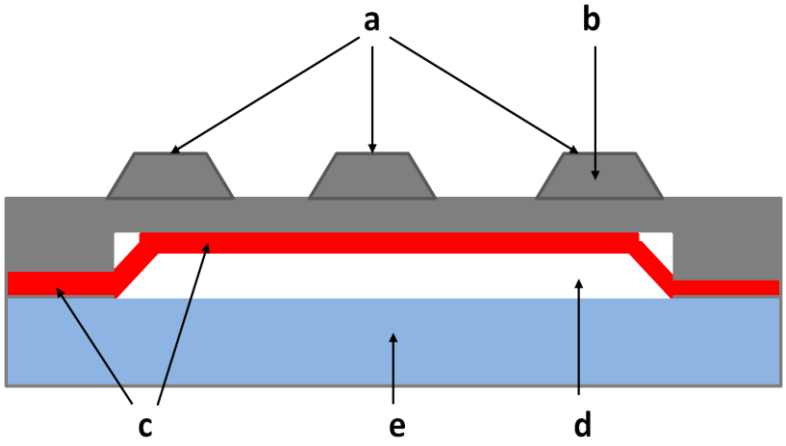

Figure 2.18: Cross sectional schematic configuration of the tactile sensor. Where a) is the teeth shape, b) is the first layer of micromachined silicone, c) is the PVDF layer, d) is the channel for deflection, and e) is the Plexiglas layer (Qasaimeh, Sokhanvar, Dargahi, & Kahrizi, 2009).

Piezoelectric tactile sensors are unfortunately very sensitive to changes in temperature and so require insulation or compensation to acquire accurate tactile data.

2.5.7 Vibration-Based Sensing

Vibro-tactile sensors use a dynamic approach as opposed to a passive response when measuring dynamic mechanical properties. The resonance frequency, amplitude and phase are altered when the sensor makes contact with the soft tissue. This is due to the viscoelastic properties of the tissue that dampens the harmonic oscillation. This method can be used to measure the stiffness of a tissue. Such a device was developed at the Fraunhofer Institut Biomedizinische Technik, St Ingebert, Germany (Baumann, Plinkert, Kunert, & Buess, 2001) and consists of a cylindrical permanent magnet of 3 mm diameter and a 1 mm thickness set in motion by an AC coil and attached to a ferrite tube with a glass rod. Vibrations are transmitted through the stimulating pestle through a latex membrane (shown in Figure 2.19) onto the tissue under investigation

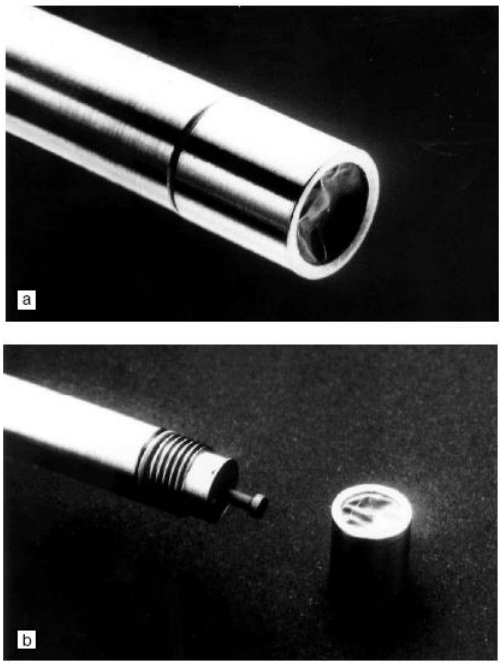

Figure 2.19: Vibrotactile sensor prototype (Baumann, Plinkert, Kunert, & Buess, 2001).

and the resulting resonance frequency of the system is measured (Baumann, Plinkert, Kunert, & Buess, 2001). A similar design was also used in 1996 by (Petter, Biehl, & Meyer, 1996).

2.5.8 Optical-Based Sensing

The main components of an optical fibre force sensor are a light source, a modulator and an optical detector. Light is initially generated by the light source and is transmitted to the modulator (also known as a transduction element) through an optical fibre. This light is then modulated in proportion to the force values measured and the light then travels to the optical detector through another optical fibre. This layout is illustrated in Figure 2.20.

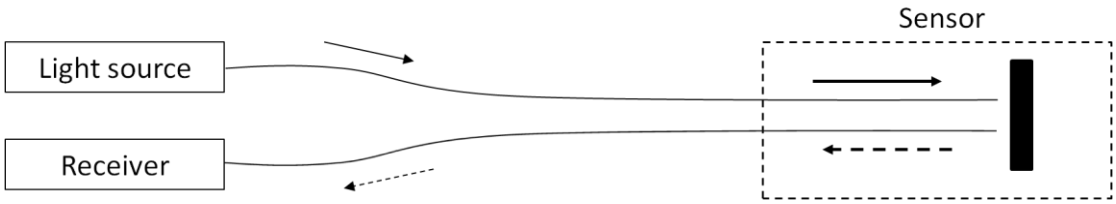

Figure 2.20: A setup using two optical fibres to transmit and receive light (Peirs, et al., 2004).

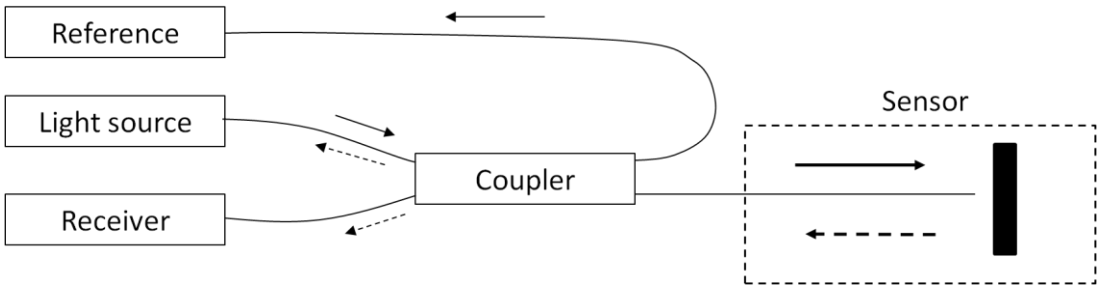

Figure 2.21: A setup that uses a coupler to couple transmitted and received light into a single fibre (Peirs, et al., 2004).

An alternative setup is also used that employs a coupler to couple transmitted and received light into a single fibre (shown is Figure 2.21).

Then the light is converted into an electrical signal and processed by electronic equipment. An important benefit of an optical fibre sensor is that it can be used in conjunction with Magnetic Resonance Imaging (MRI).

2.6 Fibre optics

The first documented scientific record of light guiding dates back to 1841. It was Daniel Colladon who showed his students at the University of Geneva an experiment where light was focused by a lens through a water tank and along a hole on the opposite side of the tank through which a water jet was spurting (Hecht, 1999). As the

light rays hit the jet at an angle, they become trapped in the liquid due to the total internal reflection and thus followed the curvature of the water jet (Hecht, 1999). This became known as “La fontaine Colladon” which translates as the Colladon fountain (an illustration of this can be found in Figure 2.22. Since then, the field of guiding light has evolved dramatically with the apparition of fibre optics.

An optical fibre behaves in a similar manner to the Colladon fountain. It can be considered to be a coaxial cylindrical transparent medium with a central core and an outer cladding (Jackson, 1985). The central core of the optical waveguide is used to channel the light by employing the process of total internal reflection and the outer cladding which has a lower refractive index than the core is used to keep the light inside the core (Gloge, 1971). The guiding nature of an optical fibre is defined by the diameter of its core and its numerical aperture (Jackson, 1985). The numerical aperture defines the maximum angle at which the fibre can accept light and retain it inside its core.

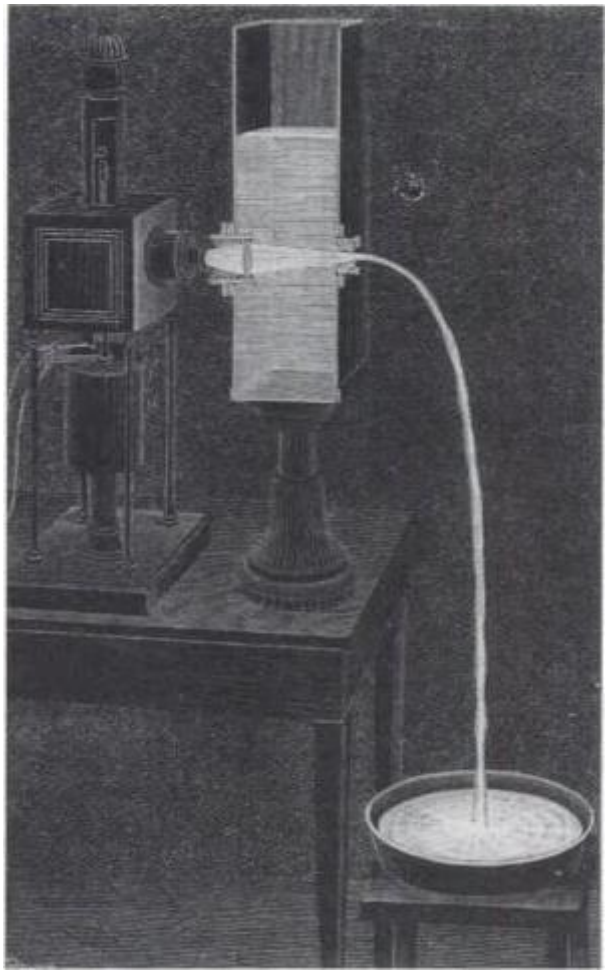

Figure 2.22: The Colladon fountain displaying the light trapped inside the curvature of the water jet (Hecht, 1999).

Although the main drive for the development of the fibre optic was the telecommunication industry, since the start of the 1970's it has been used for sensing purposes (Grattan & Sun, 1999). The success of optical fibre sensor technology has been noted in the fields of hydrophones, pressure, strain and temperature measurement and in chemical and biomedical markets (Grattan & Sun, 1999). Optical sensors can either be intrinsic or extrinsic devices. The intrinsic devices refer to the sensors where the interaction arises within the optical fibre and extrinsic devices refer

to the sensors that use optical fibres to couple light to and from the sensing area (Grattan & Sun, 1999).

There are a number of sensing principles for optic fibre sensing which use the modulation and demodulation of light. These include the phase shift sensors, polarization sensors, frequency sensors and intensity sensors. The detection of frequency, polarization and phase in optics require the use of interferometric techniques which label them as interferometric sensors (Selvarajan & Asundi, 1995) (Grattan & Sun, 1999). Interferometric sensors offer a very high level of sensitivity and resolution compare to intensity sensors but suffer from complex designs (Grattan & Sun, 1999)(Selvarajan & Asundi, 1995). There are three principle fibre optic sensing schemes that are used for displacement sensors. These are the Fabry-Perot interferometer, the Fibre Bragg Gratings (FBG) and the light intensity modulation (LIM).

2.6.1 Fabry-Perot Interferometer

The Fabry-Perot interferometer is a well known fibre optic sensing scheme that modulates the phase of the light. An illustration of a Fabry-Perot interferometer is displayed in Figure 2.23 where light beams are shone through an optical fibre on a set of two parallel mirrors allowing multiple reflections. Mirror 1 permits some parts of the light beams to pass through it and some other parts to be reflected back. The light beams that pass through mirror 1 are then reflected back by mirror 2, thus generating multiple offset beams. This resulting interference produces a high resolution interferometer. Similar types of interferometers also exist, such as the Mach-Zehnder (Zhao, Zhang, Yao, Jiang, & Chen, 2007) and the Michelson (Lawall & Kessler, 2000) interferometers that also operate by modulating the phase of light shift.

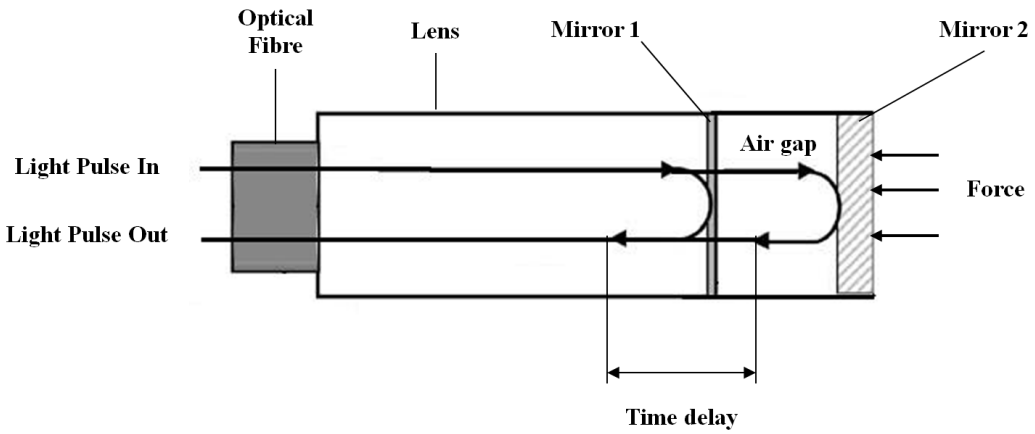

Figure 2.23: An illustration of a Fabry-Perot interferometer sensor that monitors force change. The phase shift of the light generated by the parallel mirrors measure the force applied on mirror 2. This illustration is an adaptation of (Gangopadhyay, 2004).

2.6.2 Fibre Bragg Gratings (FBG)

Bragg Gratings, which are written inside the core of an optical fibre, are a scheme that employs light wavelength modulation. The gratings enable the fibre to reflect specific wave lengths of light and transmit the others. Fibre Bragg Grating based sensors benefit from an inherent self-referencing capability (Grattan & Sun, 1999). FBG sensors can be used for a range of application including displacement and pressure sensing. The working principle of a FBG sensor is that as light from a spectral broadband source enters the fibre optic; a specific spectral component at Bragg wavelength is reflected or in transmission is omitted from the observed spectrum (Grattan & Sun, 1999). A schematic of this is shown in Figure 2.24a) and a graphical illustration is shown in Figure 2.24b).

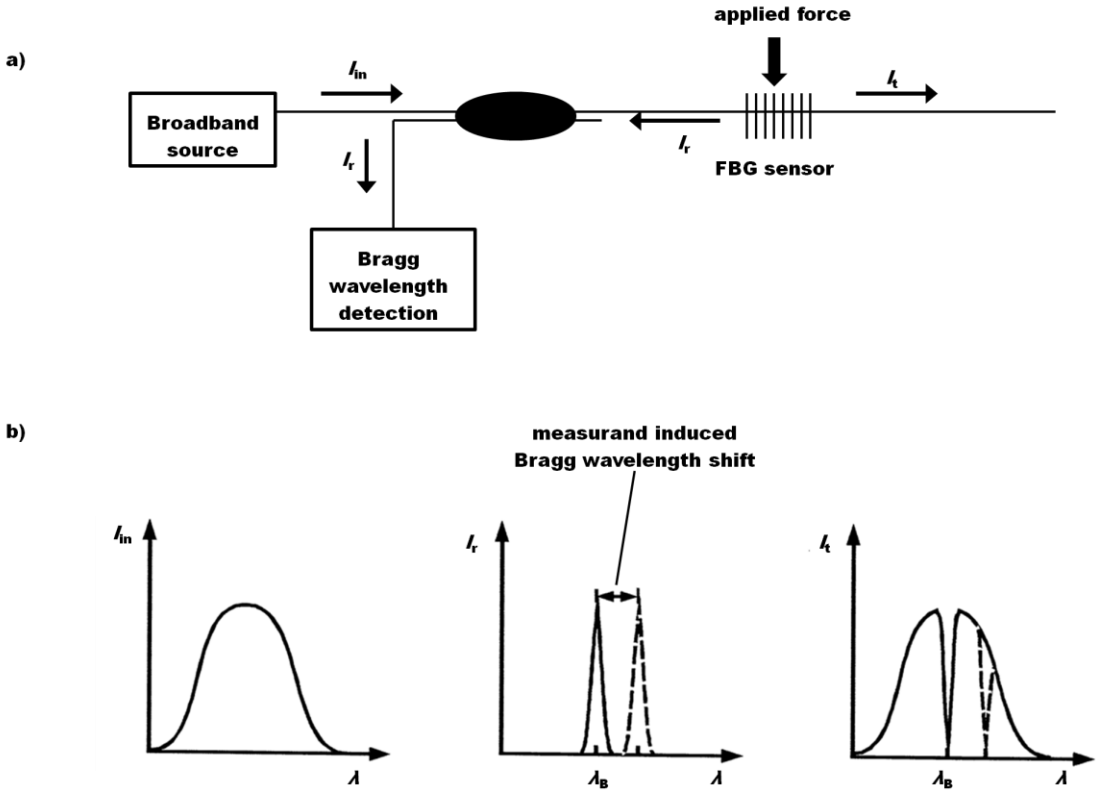

Figure 2.24: a) a simple schematic of a Bragg grating sensor based system illustrating the light input as I_{in}, the transmitted light as I_t and the reflected light as I_r. b) The graphical representation of the light input, reflected and transmitted and the corresponding wavelengths. The figures are adapted from (Grattan & Sun, 1999).

2.6.3 Light Intensity Modulation (LIM)

Light Intensity Modulation is a fibre optic sensing scheme where light is transmitted through one optical fibre (known as the transmitting fibre) to another optical fibre (known as the collecting fibre) via a reflector, by altering the medium through which the light is transmitted or by fibre bending. Any change in the position of the reflector, in the medium the light is being transmitted or in the bending of the fibre affects the intensity of the light travelling to the optical detector. A number of optical

fibre sensing schemes have been suggested using light intensity modulation by means of reflectance. These are:

1. Parallel fibres, which use an emitting and receiving fibre in a parallel structure. Altering the position of the reflector will affect the amount of light that is collected. The closer the fibres are to the reflector the more light is collected (Chaudharia & Shaligram, 2002).
2. Inclined fibres, which use the same setup as parallel fibres expect that the fibres are positioned at a relative angle from one another, the variation of that angle affects the sensitivity of the fibres (Buchade & Shaligram, 2006).
3. Bent-tip fibres, which use a similar concept to the inclined fibre but are more space efficient (Puangmali, Althoefer, & Seneviratne, 2009).
4. Single fibre, which uses the same fibre to transmit light and collected any reflected light; this is performed using a fibre optic coupler (Kulkarni, Lalasangi, Pattanashetti, & Raikar, 2006).

Light intensity modulation was chosen for this research as the optical scheme for the detection of the spherical component of the sensor as described earlier. The main benefits of light intensity modulation are its low cost and its simplicity.

2.7 Magnetic Resonance Imaging

Magnetic Resonance Imaging (MRI) is defined as a form of imaging that can offer high resolution, digitized three dimensional images of human tissue with a precise coordinate system; thus producing accurate and updated spatial information of the target tissue (Elhawary, Tse, Hamed, Rea, Davies, & Lamperth, 2008). The main advantage of MRI over Computed Tomography (CT) is the non-exposure of the patient to ionising radiation, making it suitable for real time image guided

interventions (Elhawary, Tse, Hamed, Rea, Davies, & Lamperth, 2008). Despite the advantages of MRI there are a number of constraints that need to be addressed when developing equipment for a Magnetic Resonance (MR) environment. The intense static magnetic fields, the spatial and temporal field gradients, the radio frequency (RF) pulses and the sensitive signal detection coils (Elhawary, Tse, Hamed, Rea, Davies, & Lamperth, 2008) are all constraints that need to be overcome when designing a mechatronic device.

The static magnetic fields are used to magnetise the hydrogen protons in the patient's body (Elhawary, Tse, Hamed, Rea, Davies, & Lamperth, 2008). The range of the magnetic fields in MR systems used for clinical and research environments range from 0.064-8.0 Tesla (Shellock, 2002). The static field and its related spatial gradient can affect ferromagnetic and very paramagnetic materials (Elhawary, Tse, Hamed, Rea, Davies, & Lamperth, 2008). Time-varying magnetic field gradients are used to achieve position dependent variations of magnetic field strength and are pulsed during and between RF excitation pulses (Ng, Ahmad, Nizam, & Abdullah, 2003).

RF pulses are used in MRI for excitation of the magnetised protons (Elhawary, Tse, Hamed, Rea, Davies, & Lamperth, 2008). Any conductive material inside the MRI scanner bore is affected by these RF pulses as they produce currents in them which can generate intense heating (Elhawary, Tse, Hamed, Rea, Davies, & Lamperth, 2008).

The RF sensitive signal detection coils are used to collect the signal from the excited protons as they return to their state of equilibrium (Elhawary, Tse, Hamed, Rea, Davies, & Lamperth, 2008). This RF probe can be affected by materials that are dielectric or conductive (Chinzei, Kikinis, & Jolesz, 1999) or influenced by any

circuit inside the scanner room as it can generate electromagnetic (EM) noise (Elhawary, Tse, Hamed, Rea, Davies, & Lamperth, 2008).

These potential constraints and interaction between an MR environment and a device create the need to differentiate between MR safety and MR compatibility.

A device is said to be MR safe when it has been used in an MR environment and presented no risk to the patient or any other individual but its presence may influence the quality of the diagnostic information (Shellock, 2002).

A device is said to be MR compatible when it is MR safe and its use in an MR environment does not significantly affect the quality of the diagnostic information and its functionality is not affected by the MR device (Shellock, 2002).

These requirements make most traditional tactile and force sensors unsuitable for an MR environment with the exception of optical fibre force sensing as shown by the work of (Tada, Sasaki, & Ogasawara, 2002), who developed an optical 2-axis force sensor usable in MRI environments.

2.8 Rolling Indentation

Another way to assess the "feel" of the tissue interaction of a surgeon during surgery is to use intelligent instruments that were designed to measure the mechanical soft tissue properties (i.e. the areas of increased stiffness or softness in tissue) and relay this information back to the surgeon to help him/her in tissue diagnosis (Challacombe, Althoefer, & Stoianovici, 2010). This can be achieved through the extension and static indentation of the tissue under investigation as described by (Brouwer, Ustin, Bentley, Sherman, Dhruv, & Tendick, 2001). Wellman et al. (Wellman & Howe,

1997) have also developed a device for the investigation of embedded tumours in soft tissue with a static indentation probe.

A novel tissue investigation approach that employs a rolling mechanical imaging (RMI) technique to rapidly acquire soft tissue tactile information such as embedded soft tissue abnormalities and tumours shows promising results (Noonan, Liu, Zweiri, Althoefer, & Seneviratne, 2007). This approach differs from static indentations as the wheel probe enables the assessment of a larger area of soft tissue in a relatively short time (Noonan, Liu, Zweiri, Althoefer, & Seneviratne, 2007).

The wheeled probe which is illustrated in Figure 2.25 is a sensor made of a wheel and force/torque sensor. The wheel of the sensor is made of aluminium and has a width of 10 mm and a diameter of 5 mm which is within the accepted MIS standards. The wheel is used during the process of rolling indentation and acts an end effector for the sensor. The wheel is mounted to a force/torque sensor (ATI NANO17 SI-12-0.12 with NI PCI 6034E 16-bit DAQ). This sensor provides the measurement of three force components (x, y, and z direction) which are acting on the wheel during the process of rolling indentation.

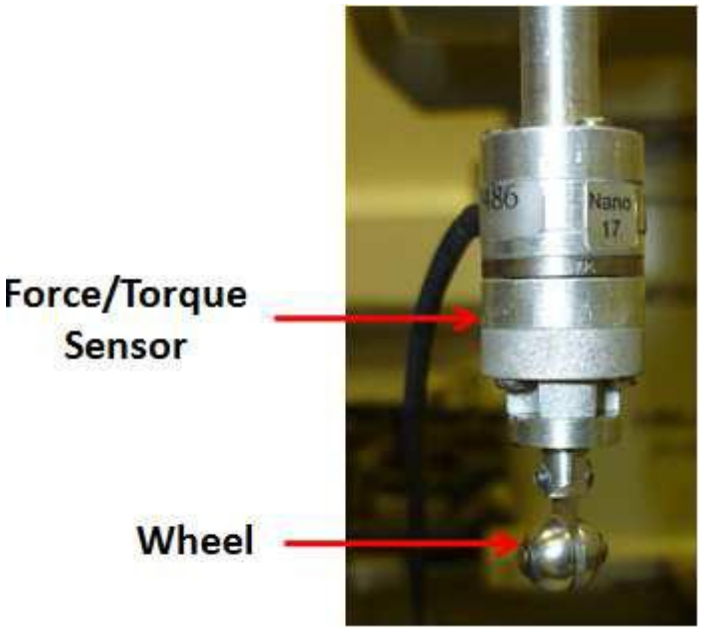

Figure 2.25: The structure of the wheeled probe sensor illustrating the relative position of the force/torque sensor to the wheel.

The process of rolling indentation requires the wheeled probe sensor to be rolled in parallel paths over the soft surface that is under investigation. Each roll of the wheeled sensor acquires information regarding the forces measured by the force torque sensor. Once the process of rolling indentation with this wheeled probe is completed, a pseudo-colour map (see Figure 2.26) is generated using the data acquired by the force/torque sensor. The pseudo-colour map is used to display the spatial variations of tissue stiffness caused by the differences of the internal tissue structure (Liu H. , Noonan, Challacombe, Dasgupta, Seneviratne, & Althoefer, Rolling mechanical imaging for tissue abnormality localization during minimally invasive surgery, 2010). The reaction forces of the soft surface with the wheeled probe are also available from this pseudo-colour map.

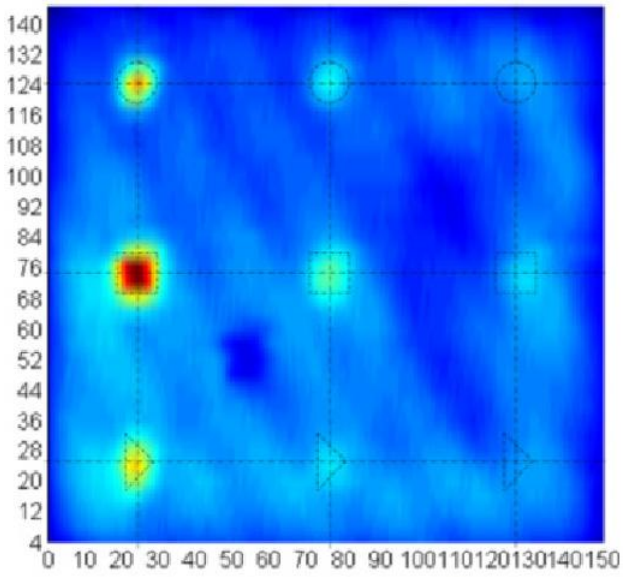

Figure 2.26: The Rolling Mechanical Imaging (RMI) map of a silicone phantom with embeded nodules detected by the wheeled probe (Liu H. , Noonan, Challacombe, Dasgupta, Seneviratne, & Althoefer, Rolling mechanical imaging for tissue abnormality localization during minimally invasive surgery, 2010)

Despite the many benefits of the wheeled probe sensor, it does have some drawbacks. The cost of the force/torque sensor (ATI NANO17 SI-12-0.12) is in excess of 5000 GBP, making it a very expensive design. The force measurements of the wheel probe are only possible if the wheel probe is rigidly connected to the force/torque sensor, prohibiting the attachment of the wheeled probe to a flexible manipulator. This design limitation also greatly reduces the surgical environment in which the wheeled probe can be used. The use of a wheel also limits the manoeuvrability of the sensor, reducing the number of trajectories that can be taken to straight line path, as the wheeled sensor would have to be constantly repositioned to perform curved paths and other trajectories.

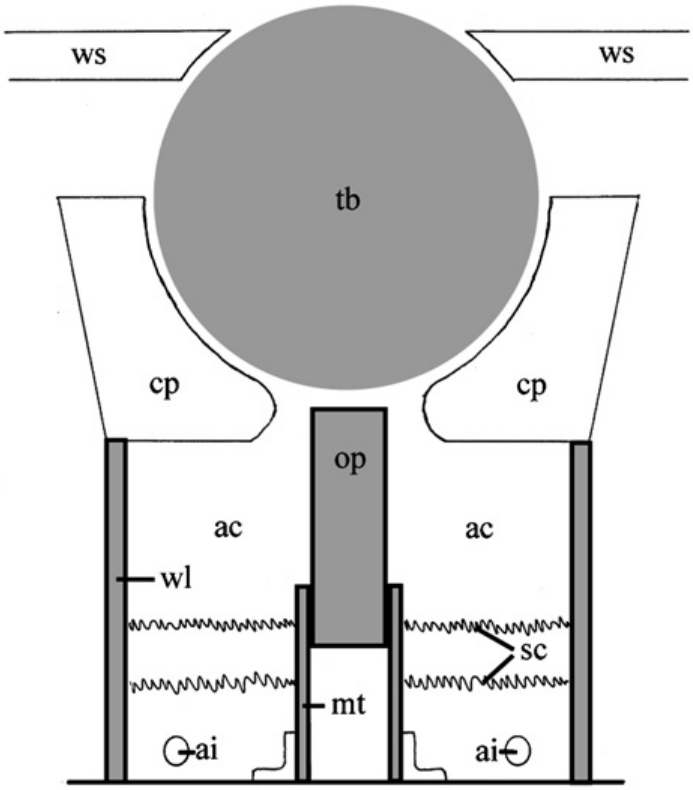

Figure 2.27: "Diagram of the mechanical device, viewed from the side. (ac: air chamber; ai: air inlets; tb: ball on which the animal stands; cp: plaster cup in which ball floats; op: optical encoder that signals movement of the ball; mt: central mount that supports the encoder; sc: screens that smooth airflow; wl: wall of air chamber; ws: work surface covering the device). The floating ball is exposed through a 2 inch hole in the work surface." (Hedrick, Hisada, & Mulloney, 2007).

2.9 Related airflow work

With the discussion of the benefits and the limitations of the wheeled probe rolling indentation, new tactile sensors were designed. These sensors, known as air-cushion tactile sensors are the main topic of discussion of this PhD thesis. These sensors employ the rolling mechanical indentation technique but look at addressing some of the aforementioned drawbacks of the wheeled probe sensor.

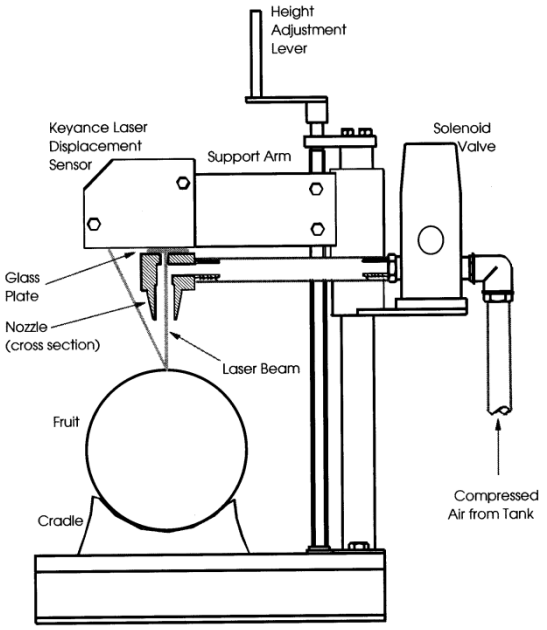

Figure 2.28: "A schematic diagram (not to scale) of the laser air-puff instrument. The nozzle is shown in cross-section with a shaded line following the vertical laser beam path to the fruit and then the imaging line (off-angle) back to the sensor." (McGlone & Jordan, 2000).

The proposed sensors have also drawn inspiration from the works of (Hedrick, Hisada, & Mulloney, 2007) and (McGlone & Jordan, 2000). In (Hedrick, Hisada, & Mulloney, 2007), the researchers investigated the walking behaviour of insects by employing a sphere that is floating on an air-cushion. This cushion is generated by a constant flow of air. The overall setup is illustrated in Figure 2.27.

The use of the air cushion was designed to minimise the level of friction during the rotation of the sphere, thus enabling the construction of an instrument sensitive enough to be rotated by the legs of an insect in a harness. The movements of the sphere was measured and used to interpret the walking behaviour of the insect. Inspiration was also taken from an application in the food industry. In (McGlone & Jordan, 2000), an approach is proposed to measure the firmness of fruits (apricots and kiwis in this particular case) by applying a sharp puff of air onto the fruit and

simultaneously measuring the tissue deformation using a laser displacement sensor (see Figure 2.28).

The novel sensors presented in this PhD thesis employ a combination of both of the above described concepts.

2.10 Conclusion

The field of Minimally Invasive Surgery has been presented with its advantages and drawbacks. The well documented concern of reduced or total lack of haptic feedback during laparoscopic and robotic assisted surgery has been explained. The range of the proposed sensing schemes designed in an attempt to address this drawback has been presented and their functioning explained. Despite all of these suggested systems none have completely overcome this issue. This PhD will attempt to offer another solution at addressing the issue at hand.

Chapter 3 – Sensor Designs

3.1 Introduction

The importance and requirement for tactile feedback during MIS are now clear following the extensive discussion in Chapter 2. The proposed system will aim to address the lack of haptic feedback by:

- Creating a sensing device that is manoeuvrable, in order to roll effectively in any direction over the surface under investigation.
- Designing a sensor that employs a concept that lends itself to miniaturisation such as MIS.
- Having a sensing device that has the ability to generate the fast creation of mechanical images of the surface under investigation and by illustrating the stiffness and/or force distribution over that area.
- Having a sensor that is compatible to be used with robotic assisted minimally invasive surgery.

This chapter discuss and illustrate the concept and structure of the proposed sensor. The various prototypes of this concept will be explained with their designs and

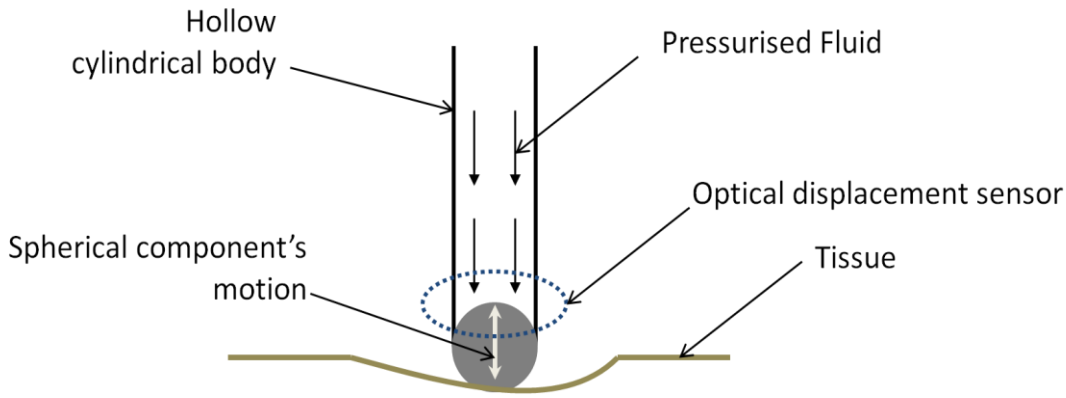

Figure 3.1: A schematic diagram of the conceptual idea and structure of the proposed sensor. The dimensions of the sensor should be within MIS standards and the resolution should be of at least 0.5 mm

associated drawbacks and limitation. The sensors' specifications will also be provided.

3.2 Conceptual idea and structure of proposed sensor

The proposed concept is to create a sensor that is manoeuvrable and that can be used to provide haptic feedback. This sensor could enable the creation of mechanical images displaying the tactile and force information of a soft material through the rapid acquisition of data, for example to identify tissue abnormalities in soft tissue. The sensor could also lend itself to miniaturisation to be placed at the tip of a surgical instrument for MIS.

The sensor's structure is to comprise of a hollow cylindrical body into which a fluid under pressure is supplied. The pressurised fluid can be either air or carbon dioxide as is used in MIS. The sensor is to have a component that is positioned in such a way that it is projected from the sensor's body under the pressure of the pressurised fluid. The component is to be of a spherical shape and to move relative to the sensor's body.

A displacement detection system for the projected spherical component is used; it is to be optically driven to allow the spherical component to move freely with respect to the body. The projected spherical component is to be illuminated and the light received from it is to be modulated to measure its displacement as it is moved by the pressure of the pressurised fluid. The measured displacement, in conjunction with the pressure of the fluid can then be used to estimate the force being applied by the sensor's spherical component. A schematic diagram of the conceptual idea and structure of the sensor is illustrated in Figure 3.1.

The benefit of this design is that while it is in use, the sensor's spherical component can effectively "float" on a cushion of pressurised fluid since it can move relative to the sensor's hollow body. The use of a "floating" spherical component relative to the hollow body of the sensor enables the sensor to be employed with soft materials that do not generate a large reaction force. As the "floating" component is to be freely movable with respect to the sensor body; the friction experienced by this component is moderately low enabling it to be moved smoothly across the surface of the soft material that is under investigation. The sensor would be used to measure the tactile distribution and estimate the force distribution of a soft material. This fluid under pressure is used to exert a specific force on the spherical component. As the sensor is rolled over soft material it exerts this force onto it. This specific force is countered by the reaction force of the soft material which is of opposite direction and causes the spherical component to be displaced against the pressure of the fluid. The displacement of the spherical component is proportional to the stiffness of the soft material. Thus areas of greater stiffness in a soft material will displace the spherical component by a bigger distance than areas of weaker stiffness that will generate a

smaller displacement of the spherical component. This can be used to determine areas of varying stiffness on the surface as well as below the surface of a soft material.

The diameter of the spherical component should only be slightly smaller than the diameter of the hollow cylindrical body. This is to maximise the area of the sphere; this is beneficial for a number of reason. A larger diameter of the spherical component allows for a greater surface area of the soft material to be covered per rolling motion. The spherical component is limited to be projected to a maximum of 49.9% of its size outside the hollow cylindrical body of the sensor. This projection of the spherical component may be substantially smaller depending on the design of the mechanism used to stop the sphere from completely exiting the hollow cylindrical body of the sensor. A greater surface area of the spherical component would also maximise the amount of pressure that can be applied onto it by the fluid and by the soft material under investigation.

As explained, one of the important requirements of the sensor is that its design lends itself to great manoeuvrability when it is rolled over a surface under investigation. This could only be achieved by using a spherical component as a wheel would struggle to acquire such a freedom of movement. As the spherical component of the sensor is its focal element of the sensor, its design revolves around it. As opposed to the approach of using a cylindrical wheel that is attached to a rigid axle (Liu H. , Noonan, Challacombe, Dasgupta, Seneviratne, & Althoefer, Rolling mechanical imaging for tissue abnormality localization during minimally invasive surgery, 2010), a sphere cannot rotate freely in any direction if it is attached to any component. Therefore, the only feasible way to monitor any movement of this spherical component was to use an optical sensing scheme. A number of optical sensing

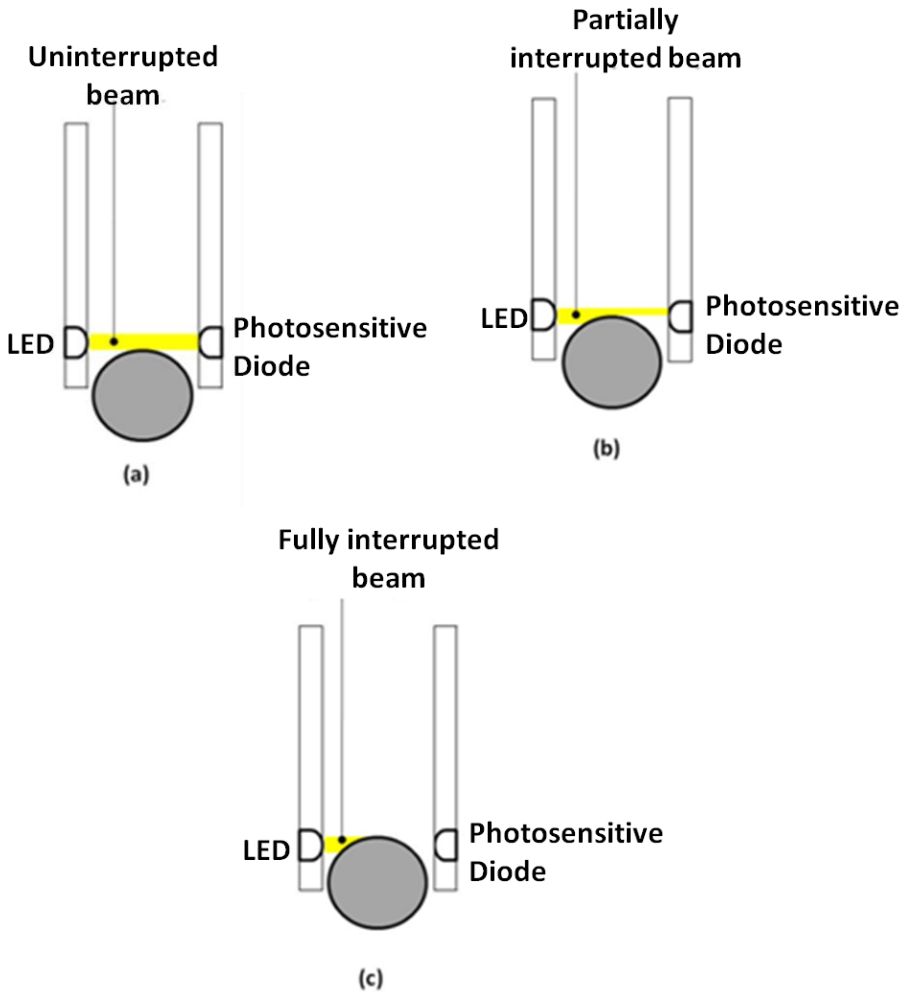

Figure 3.2: The optical scheme of the sensor illustrating the role of the LED and the photodetector (a) The position of the sphere is such that the beam of light is uninterrupted. (b) The position of the sphere partially interrupts the beam of light. (c) The position of the sphere fully interrupts the beam of light.

schemes exist; these are briefly explained in the previous chapter by looking at the optical fibre and the various forms of light modulation.

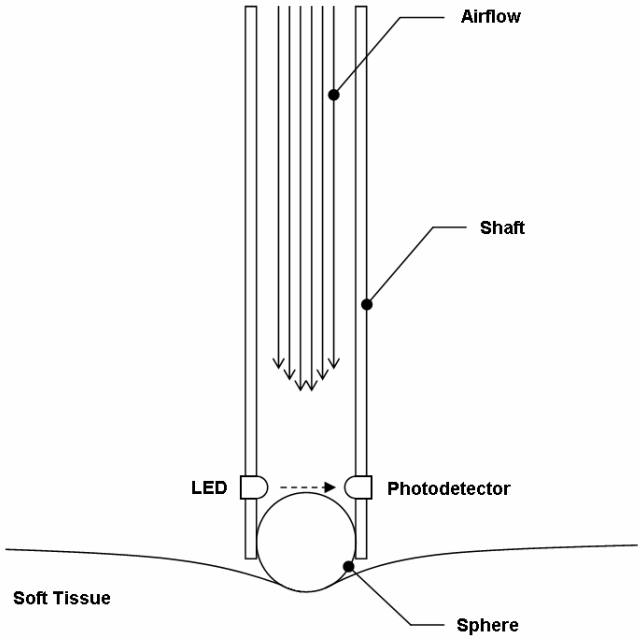

Figure 3.3: A schematic of the sensor illustrating the role of the optical scheme and the influx of air during the process of rolling indentation.

3.3 Sensor 1 – Principle and Structure

The first design that incorporated the conceptual idea of the proposed sensor was named Sensor 1. Sensor 1 was composed of four components. These were the sensor body, the spherical component and the two components used for the optical scheme. The sensor body which was made of a hollow cylindrical component, the spherical component which was used was a sphere and the two components employed for the optical scheme were an LED (Light Emitting Diode) and a photosensitive detector.

An optical scheme using light intensity modulation was employed to detect the displacement of the sphere when the sensor was in use. A beam was shone inside the hollow cylindrical body across the path of the spherical component. Any motion of the spherical component was detected by measuring the amount of light that was

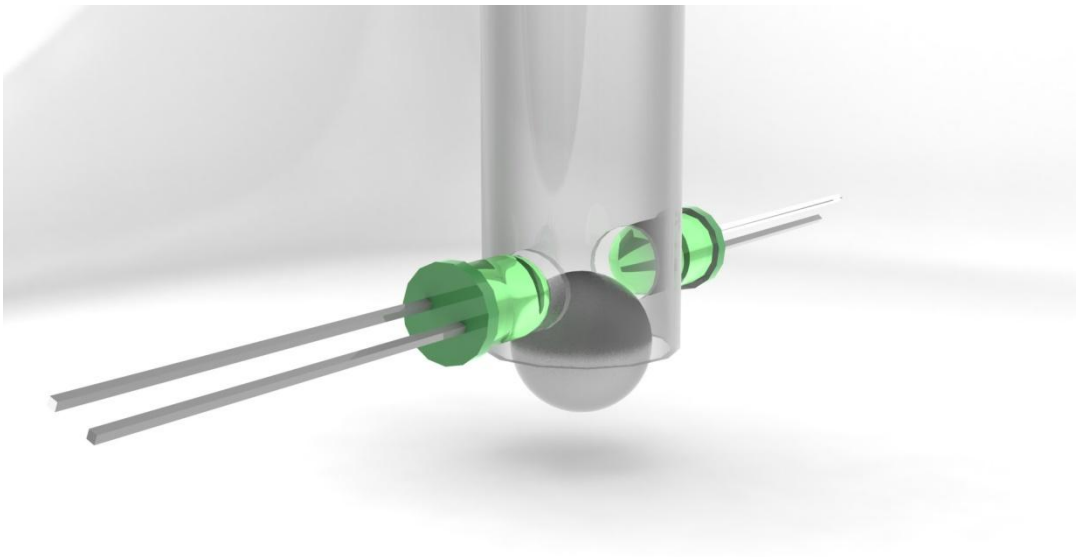

Figure 3.4: Two three-dimensional drawing of the sensor and its optical scheme. The LED and photosensitive diode are positioned opposite each other so as to monitor the light beam that is shone across the diameter of the hollow cylindrical body. As it can be noted from the drawings the LED and photosensitive diode are built into the wall of the hollow cylindrical body but do not obstruct any displacement of the sphere.

collected across the path of the sphere. This sensing principle is schematically explained in Figure 3.2. The projected spherical component of the sensor is located at the distal end of the hollow cylindrical body. When the sensor is in use, a pressurised fluid is supplied to the near end of the hollow cylindrical component; this is schematically illustrated in Figure 3.3.

The pressurised fluid enters the near end of the hollow body of the sensor and exerts a pressure onto the spherical component. This pressure onto the sphere increases the reaction force of the surface under investigation. This is reflected by the displacement of the sphere which is monitored by the optical sensing scheme. A three dimensional

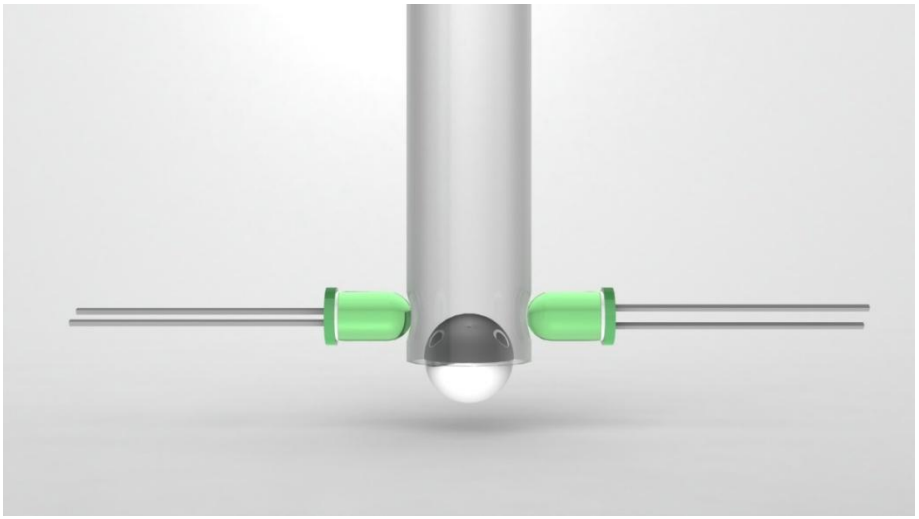

Figure 3.5: The tips of the LED and photosensitive diode are positioned inside the wall of the hollow cylindrical body and do not obstruct any movement of the spherical component.

representation of the sensor's optical scheme is illustrated in Figure 3.4 showing the position of the LED and the photosensitive diode relative to the sphere and the hollow cylindrical body.

The proposed air cushion sensor, Sensor 1 was composed of four components: a hollow cylindrical body, a spherical component, an LED and a photosensitive diode. The hollow cylindrical body had a height of 10 cm. The inner and outer diameters of the body were 11.5 mm and 12.5 mm, respectively. The material used for this component was plastic. At the distal end of this component, two cylindrical holes of 5 mm in diameter were drilled through the wall of the body. These holes which were normal to the body of the sensor were also positioned at opposite sides of one another. The holes were located 5 mm from the distal end of the hollow cylindrical body. The spherical component employed was a metal sphere with a mirrored surface of diameter 9 mm which was located partially within and partially protruding the distal end of the hollow cylindrical body. The location of the aforementioned cylindrical

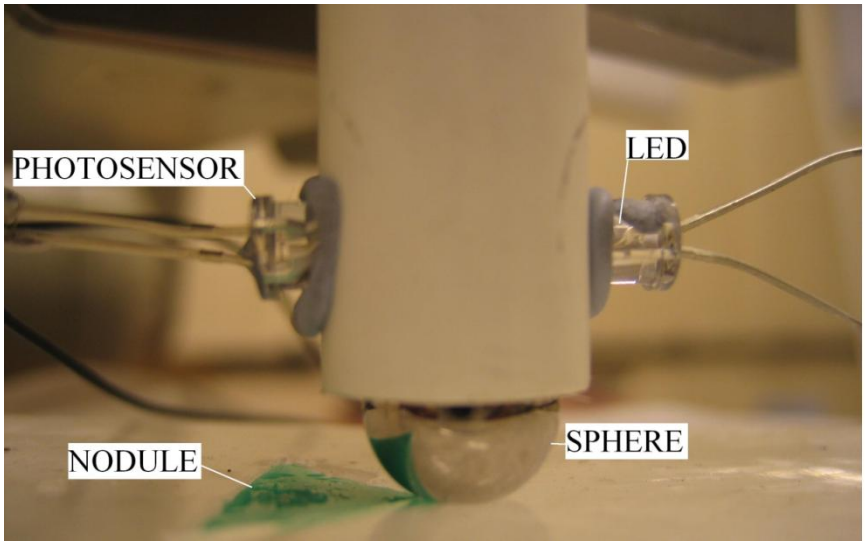

Figure 3.6: This structure of the sensor is shown, illustrating the relative position of the LED and photosensitive diode to the hollow cylindrical body of the sensor.

holes where based on the dimensions of the spherical component. If the diameter of the spherical component had been smaller, their location would have been nearer the distal end of the hollow cylindrical body and further away if the diameter of the spherical component was bigger. The cylindrical holes were designed to position an LED and a photosensitive diode for the optical sensing scheme. The LED and photo sensitive diode were inserted inside the walls of the hollow cylindrical body by 1 mm, this positioned their respective tips on the border of the inner diameter of the hollow cylindrical body; thus ensuring an unobstructed hollow cylindrical body for the spherical component to move along as shown in Figure 3.5.

A paste was used to fasten the LED and photosensitive diode to the hollow cylindrical body; this was also applied ensured an air tight seal. A picture of Sensor 1 is shown in Figure 3.6 illustrating the location of the LED and the photosensitive diode, on the body of the sensor.

a)

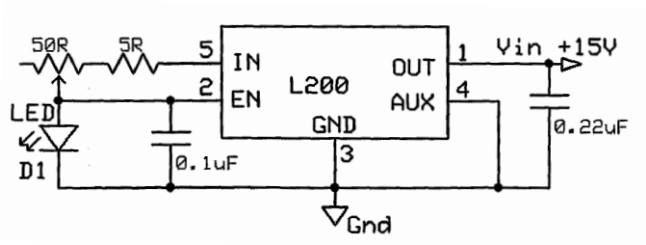

b)

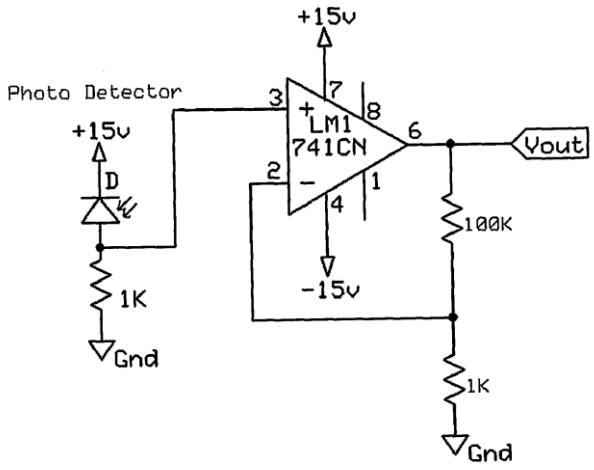

Figure 3.7: a) The electrical circuit used for the LED, b) the electrical circuit used for the photosensitive diode with the 741 op amp.

The LED used was a 5 mm super bright white light LED and a 5 mm photosensitive diode of spectral range 400 nm to 1100 nm. The electrical circuits used to power the LED and the photosensitive diode are displayed in Figure 3.7a and Figure 3.7b, respectively. The LED circuit was powered by 15 V, the intensity of the light was proportional to the voltage used. A decrease in the voltage applied reduced the intensity of the light source. The photosensitive diode was connected to a ±15V circuit which used a 741 operational amplifier to amplify the output signal. The photosensitive diode had a saturation voltage of 10 V. A variation in the light intensity was monitored by the photosensitive diode which was reflected by a change in the output voltage. The output voltage was read to a computer using a DAQ card (NI PCI−6034E).

The near end of the hollow cylindrical body was connected to a compressor via a hose. This was to allow the entry of a pressurised fluid into the hollow cylindrical body. The hose used had an internal diameter of 7 mm and was 3 m long. The hose was sealed to the near end of the hollow cylindrical body with plumbing tape to ensure an air tight connection.

3.3.1 Limitations of Sensor 1 design

Despite this sensor's ability to acquire tactile information of the surface that it is under investigation (as demonstrated in the Chapter 5), this design does not lend itself to miniaturisation for MIS. The dimensions of the hollow cylindrical body with the embedded LED and photosensitive diode far exceed the diameter of a standard laparoscopic trocar port of 12 mm. The components used for the optical detection scheme cannot be easily sterilised and could not be used in an MRI environment. Another drawback of this design is that the projected spherical component can completely exit the hollow cylindrical body as there are no restrictions to stop this from happening. This could be very dangerous for the patient in an MIS environment.

In order to overcome the design drawbacks of Sensor 1, a number of alternatives were suggested. These are described in the following section.

3.3.2 Alternative designs to Sensor 1

In order to miniaturise Sensor 1 to MIS standards and to achieve MRI compatibility the sensor needed to be redesigned. The LED and the photosensitive diode that were located in the side wall of the hollow cylindrical body of the sensor needed to be replaced. These components could be replaced with optical fibres as they are

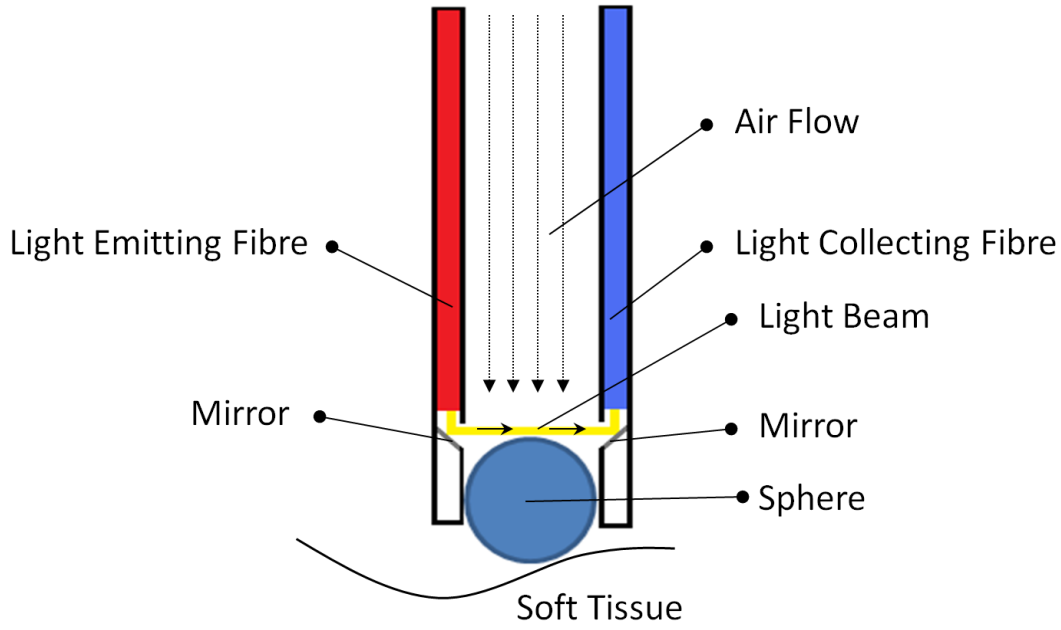

Figure 3.8: The air cushion sensor with the optical fibres embedded within the shaft walls. The mirrors are located at the tip of the fibres so as to generate a light beam across the shaft.

compatible with an MRI environment as no electronics would be used inside the patient's body. Another advantage of fibre optics is that they can be easily sterilised.

The proposed redesign of Sensor 1 is shown in Figure 3.8. The two optical fibres that replaced the LED and photosensitive diode run along the hollow cylindrical body within its walls, at opposite sides. One optical fibre performs as a light emitting fibre and the other optical fibre performs as a light collecting fibre. Two openings in the inner hollow cylindrical component's wall are made; these are located at the tip of the light emitting and light collecting fibres, respectively. In these openings, two mirrors are placed in the wall at an angle of 45° so that they deflect and collect the light, respectively, in a normal direction across the hollow cylindrical body of the sensor. Once again the same principle of monitoring the amount of light that is collected

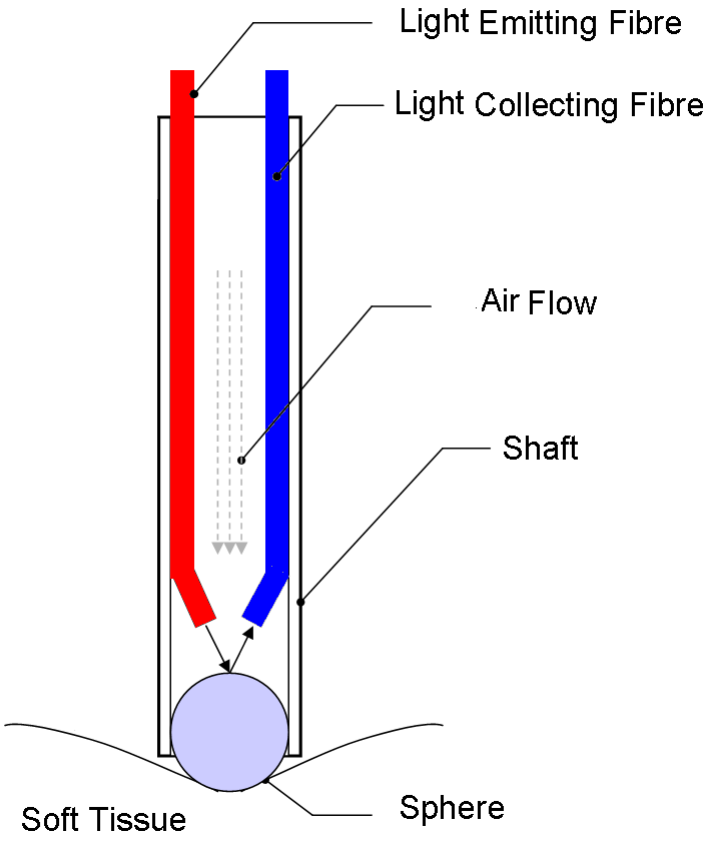

Figure 3.9: Proposed design and structure of the miniaturised air cushion sensor with the light being reflected of the sphere.

across the path of the spherical component would be used to establish the position of the sphere.

The main problem encountered when building this sensor was the difficulty in placing the mirrors accurately within the walls of the hollow cylindrical component so that they would face each other at the correct angle. The other drawback was the difficulty in keeping the surface of the mirrors perfectly clean to ensure adequate reflectivity. Due to these difficulties this design was abandoned and another design was sought after.

In this alternative design of Sensor 1, which is illustrated in Figure 3.9, the two optical fibres that replaced the LED and photosensitive diode run along the inner walls of the hollow cylindrical component at opposite sides of each other and act as a light emitting fibre and a light collecting fibre, respectively. As light is shone onto the sphere from the light emitting fibre it is reflected back off the sphere and collected by the light collecting fibre. A change in the position of sphere along the longitudinal axis of the hollow cylindrical component would result in a change of reflection of the angle of the light which is reflected as a change in light intensity which will be detected by the light collecting fibre. The reflectivity properties of the sphere would be preserved by the cleaning action of the flow of air onto the sphere by dispersing any fluids that might have contaminated the sphere during the process of rolling indentation. The main drawback with such a design was the difficulty in bending the optical fibres without damaging them and ensuring the correct angle of the fibres was obtained. For these reasons this redesign alternative was also discarded.

For the sensor to meet the requirements needed to operate in an MIS and MRI environment, its working principle and design necessitated a number of changes. These are explained and implemented in following section where Sensor 2 is described and its operating principle is explained.

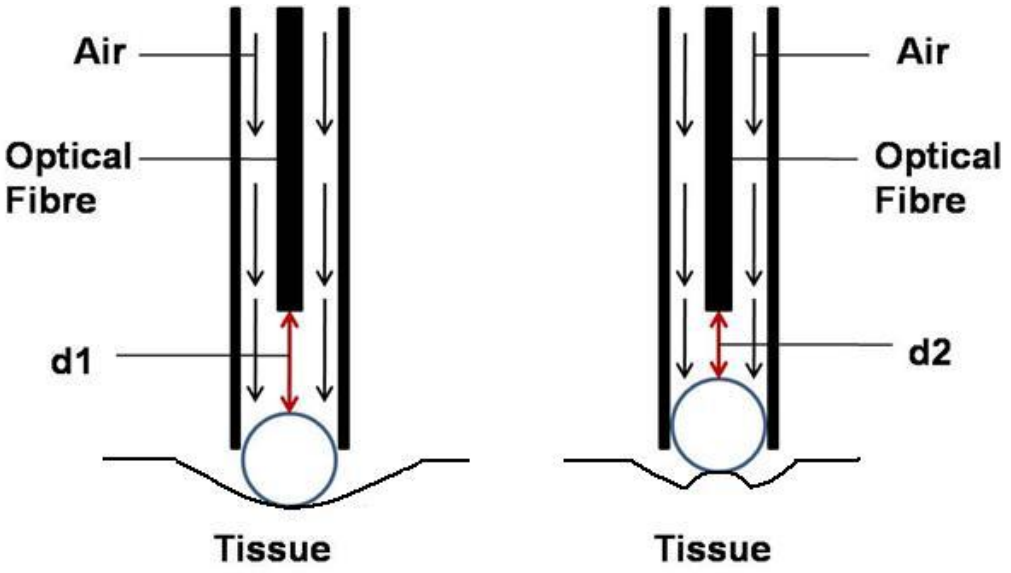

Figure 3.10: Schematic diagram of the novel sensor. The optical fibre shines a light onto the sphere and collects any reflections. The position of the sphere from the tip of the optical fibre is determined by the intensity of the reflected light.

3.4 Sensor 2 – Principle and Structure

The second design that incorporated the conceptual idea of the proposed sensor was named Sensor 2. Sensor 2 was composed of three components. These were the sensor body, the spherical component and single component used for the optical scheme. The sensor body was made of a hollow cylindrical component, the spherical component which was used was a sphere and the single optical component was an optical fibre. The LED and photosensitive diode of Sensor 1 design were replaced with an optical coupler. An optical coupler enables the sensor to use a single optical fibre to emit and to collect light. Once again a light intensity modulation scheme was employed to monitor and measure any displacement of the sphere when the sensor was in use. The optical fibre was suspended along the central axis of the hollow cylindrical

component with the help of brackets in a manner that permitted it to be placed right above the highest point of the spherical component. A beam of light was shone onto the top of the spherical component and reflected back, to and from the optical fibre, respectively. Any displacement of the spherical component was measured by the change in the light intensity that was reflected off the sphere. This sensing principle is schematically explained in Figure 3.10. The spherical component of the sensor is once more placed at the distal end of the hollow cylindrical component. The pressurised fluid and the optical fibre are both supplied from the near end of the hollow cylindrical component. To overcome the drawback of allowing the projected spherical component to exit entirely the body of the sensor, the distal end of the hollow cylindrical component has been tapered. A three dimensional drawing of the sensor's structure is illustrated in Figure 3.11(a) where the tapered end of the sensor's body is visibly refraining the spherical component from exiting the body of the sensor. The overall dimensions of the sensor are shown in millimetres in Figure 3.11(b). The material used for both the sensor body and the spherical component was ABS plastic. The fibre optic used was a plastic fibre optic. These three components ensure that the design of the sensor is MRI safe. The optical fibre was used as it is shielded from electromagnetic fields (EMF). All three components can be sterilised and their manufacturing cost is low; making them available for one use applications.

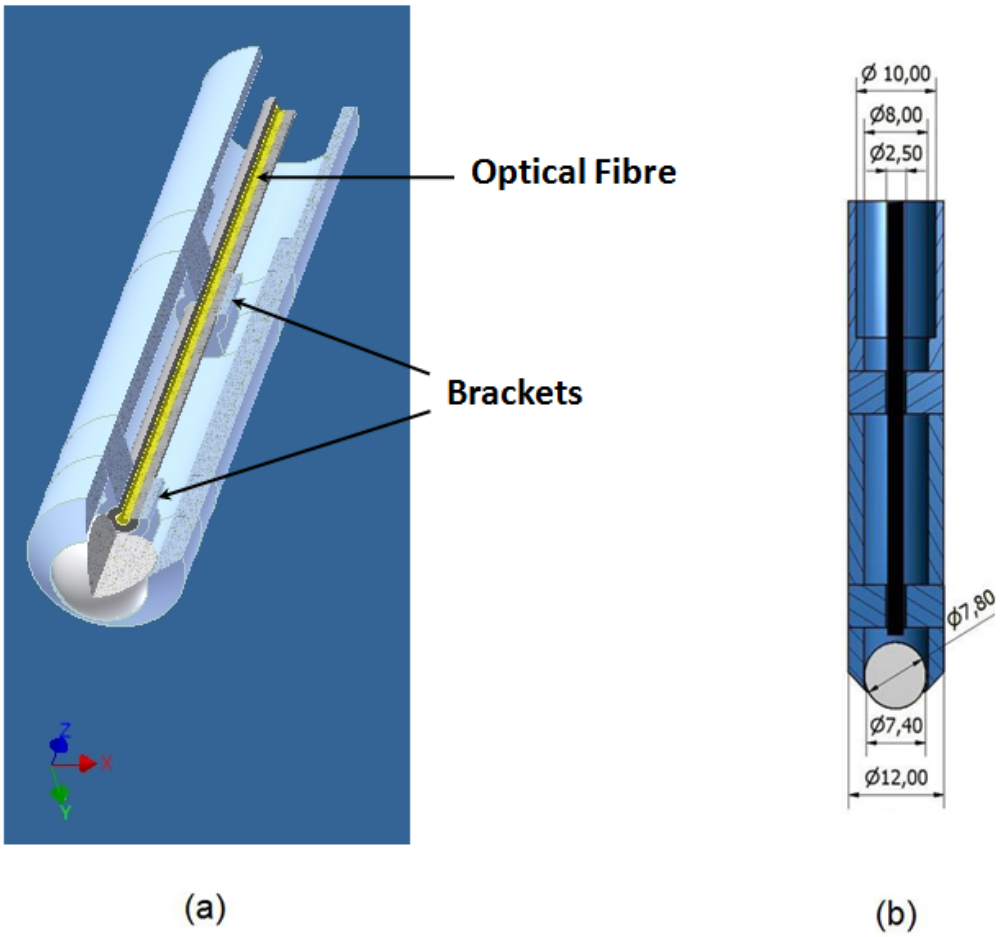

Figure 3.11: A three dimensional cross-sectional drawing of the proposed air-cushion tactile probe with the supporting brackets is shown in (a). The dimensions of the sensor are illustrated in (b) with all the measurements in millimetres.

The air cushion sensor, Sensor 2, was composed of three components, a hollow cylindrical body, a spherical component and an optical coupler. The hollow cylindrical body had a height of 60 mm and an outer diameter of 12 mm. The inner walls of the hollow cylindrical body had a diameter of 8 mm which increased to 10 mm at the near end and tapered down to 7.4 mm at the distal end. The increase in diameter at the near end was to accommodate the hose that was used to supply the hollow cylindrical body with a pressurised fluid. A 7.8 mm sphere in diameter was located at the tip (distal end) of the hollow cylindrical body. The taper down to 7.4

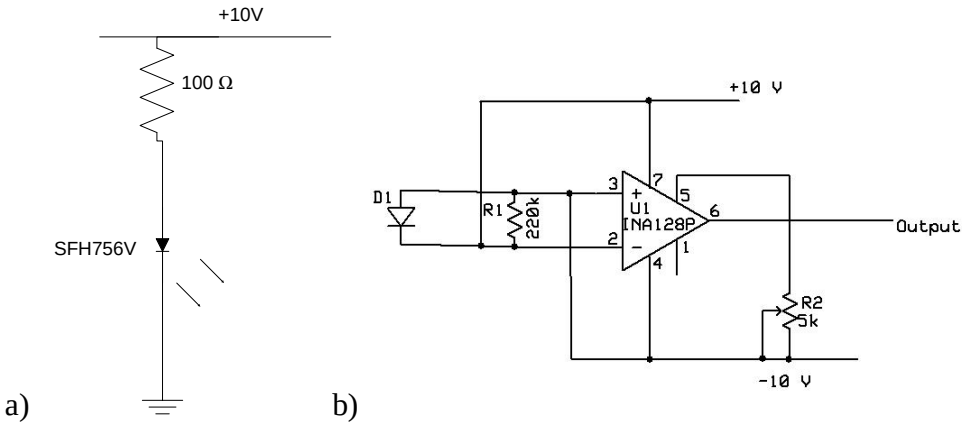

Figure 3.12: a) the electrical circuit used to power the LED b) the electrical circuit used for the photosensitive diode.

mm at the tip of the sensor's body was to prevent the 7.8 mm sphere from completely exiting the hollow cylindrical body when it was projected by the pressurised fluid. Two brackets were built inside and onto the walls of the hollow cylindrical body. They were separated by a distance of 25 mm. They had an inner diameter of 2.5 mm and were designed to support an optical fibre that was positioned just above the spherical component. The structure of the sensor with its dimensions is displayed in Figure 3.11. The entire body and sphere of the sensor were made out of acrylonitrile butadiene styrene (ABS) plastic which were built using a three dimensional rapid prototyping machine (Dimension 768). A picture of the sensor is displayed in Figure 3.13(b). The optical fibre used had an outer jacket of 2.2 mm and a core of 1 mm. The optical fibre used was the one end of a 1 x 2 optical coupler with 50:50 ratios (Industrial Fiber Optics, Inc.).

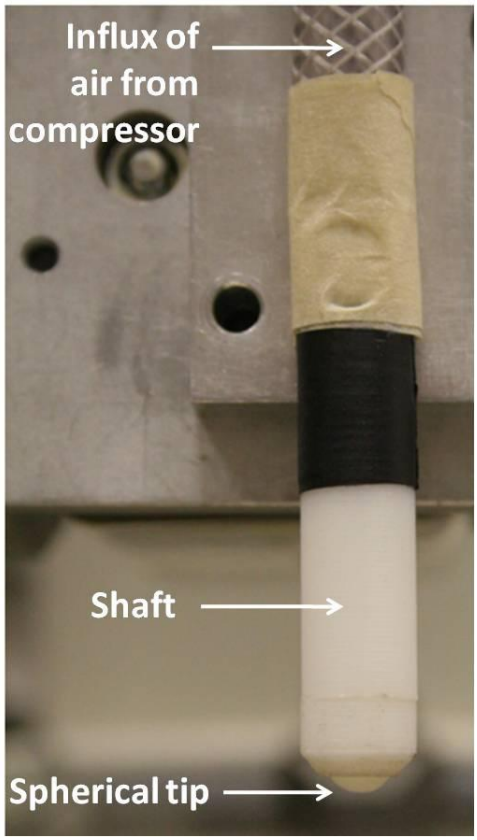

Figure 3.13: A picture of Sensor 2 illustrating its spherical component and the near end of the hollow cylindrical body connected to a hose supplying pressurised air to the sensor.

The optical coupler was connected to an optical scheme comprising of an LED and a photosensitive diode. The LED which was used as the light transmitter was an SF756V (Avago) of peak wavelength 660 nm. The photosensitive diode was an SFH250 (Avago) with a spectral range of 400 nm to 1100 nm. The electrical circuits used for the LED and photosensitive diode are illustrated in Figure 3.12a and Figure 3.12b, respectively.

The data acquisition card used was the National Instrument card NI USB-6211 and the output signal of the photosensitive diode was connected to it using a differential setup.

The near end of the hollow cylindrical body was connected via a hose to a compressor which was used to generate a pressurised fluid. The connection between the hose and the near end of the hollow cylindrical body was sealed with plumbing tape to ensure its air tightness.

The software used to interface with the data acquisition card and the output signals of the photosensitive was Labview 2012.

3.4.1 Limitations of Sensor 2 design

Despite this sensor's ability to acquire tactile information of the surface that it is under investigation (as demonstrated in the Chapter 5) and to be fully MRI compatible the sensor does suffer from one major drawback. Due to the tapered end of the hollow cylindrical component, when the spherical component is not sufficiently displaced by a reaction force, it prevents any pressurised fluid from leaving the sensor's body at an adequate rate. This generates a build up of pressure inside the hollow cylindrical component which can have two damaging consequences. The pressure exerted by the spherical component onto the surface under investigation is greater than what it should be which can in the context of MIS have damaging consequences on the soft tissue under inspection. There is also the possibility that the pressure build up becomes greater than what the sensor's structure can withstand which can result in a catastrophic failure of the sensor. To overcome this important limitation, the sensor structure was redesigned. The steps taken to address this drawback are implemented and explained in the following section where Sensor 3 is described and its operating principle explained.

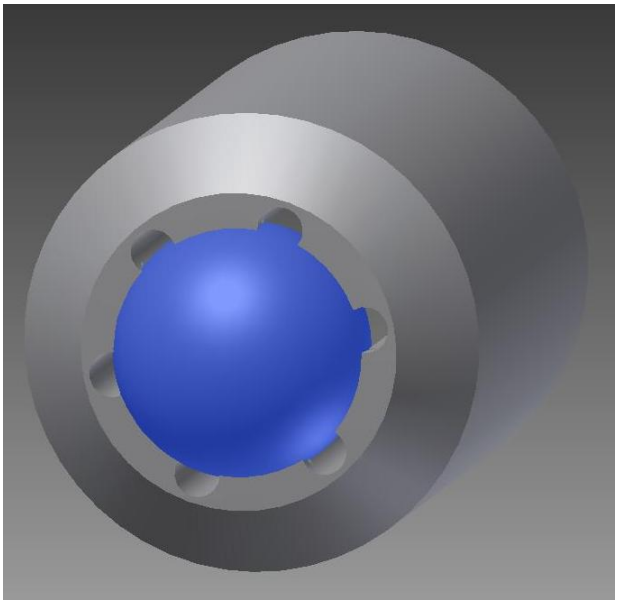

Figure 3.14: The distal end of the hollow cylindrical component is illustrated in this three dimensional drawing. The semi cylindrical openings around the tapered end enable a flow of air and retain the spherical component.

3.5 Sensor 3 – Principle and Structure

The third design that integrated the conceptual idea of the proposed sensor was named Sensor 3. Sensor 3 was design and built to address the limitations of Sensor 2. Sensor 3 used the exact same sensing principle as its predecessor by monitoring the light intensity that is reflected off the spherical component by means of a single optical fibre. The distal end of the hollow cylindrical component was altered to ensure that it performed two roles; the first was that it prevented the projected spherical component from completely exiting the hollow cylindrical body and the second was to address the issue of pressure build up behind the spherical component. This was achieved by creating semi cylindrical opening along the tapered end of the cylindrical component. These semi cylindrical opening allowed the pressurised fluid to exist the hollow cylindrical body when the spherical component was not sufficiently displaced by the

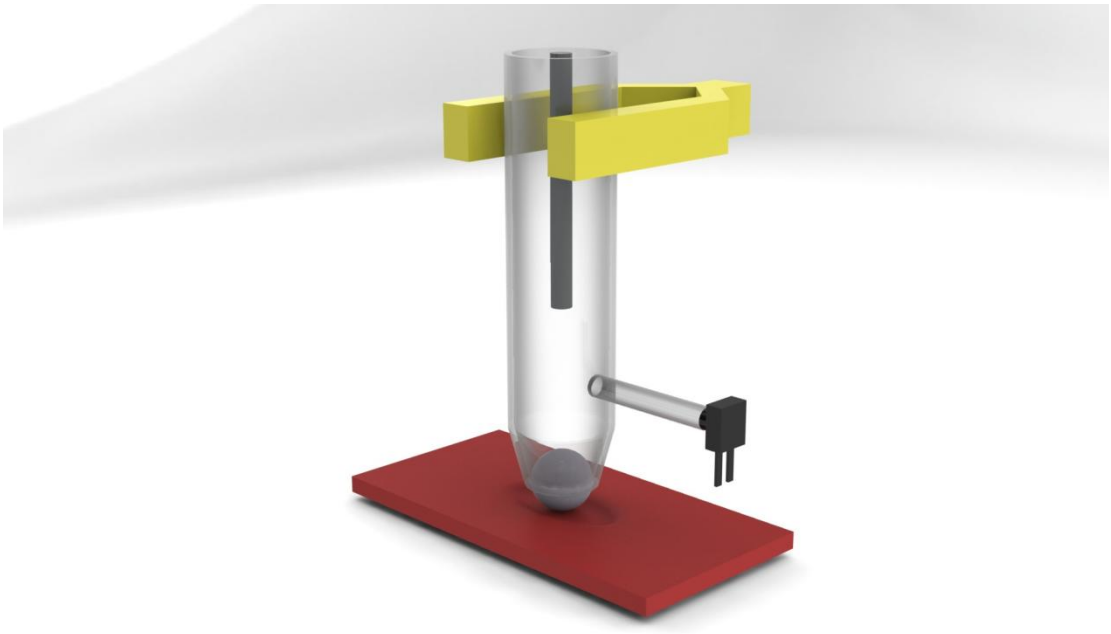

Figure 3.15: The pressure sensor is connected via a small tube to measure the pressure generated by the fluid inside the hollow cylindrical body of the sensor.

reaction force of the surface under inspection while retaining it within the hollow cylindrical body of the sensor. This is illustrated in the three dimensional drawing in Figure 3.14. In order to monitor the pressure build up in the body of the sensor, two pressure sensors were fitted to the design. A small opening was created through the wall of the hollow cylindrical body to allow a pressure sensor to be connected via a small tube. This is illustrated in Figure 3.15. The second pressure sensor was connected at the outlet of the compressor. The use of pressure measurements enable the estimation of the force exerted by the spherical component of the sensor onto the soft surface under investigation.

Finally, the plastic spherical component that was used in Sensor 2 was replaced by a metal mirrored sphere. This was done to increase the range of motion that could be measured by the optical sensing scheme.

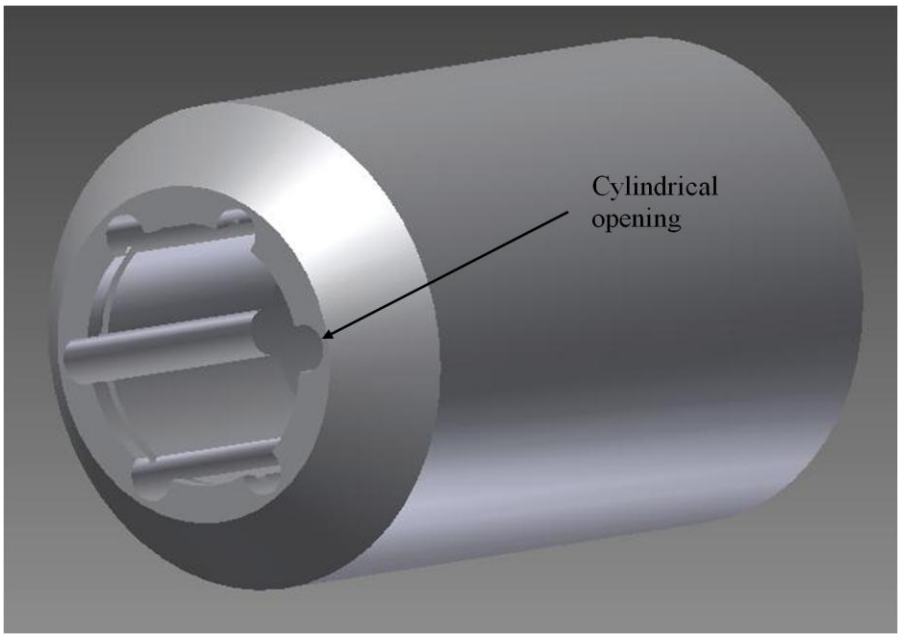

Figure 3.16: The slide on component fitted its 6 semi cylindrical openings around the tip.

The air cushion sensor, Sensor 3, is composed of four components, a hollow cylindrical body, a slide on component (for the distal end), a spherical component and an optical coupler. The hollow cylindrical body had a height of 50 mm and an outer diameter of 11 mm. The inner walls of the hollow cylindrical body had a diameter of 8 mm which increased to 10 mm at the near end. Two brackets were built inside and onto the walls of the hollow cylindrical body. They were separated by a distance of 25 mm. They had an inner diameter of 2.5 mm and were designed to support an optical fibre that was positioned just above the spherical component.

The slide on component had an outer diameter of 12 mm and an inner diameter of 11.1 mm with a taper down to 7.75 mm at its distal end. The slide on tip component was designed to slide onto the hollow cylindrical body. The tapered end of the slide on component was fitted with 6 semi cylindrical openings around the tip. The radius

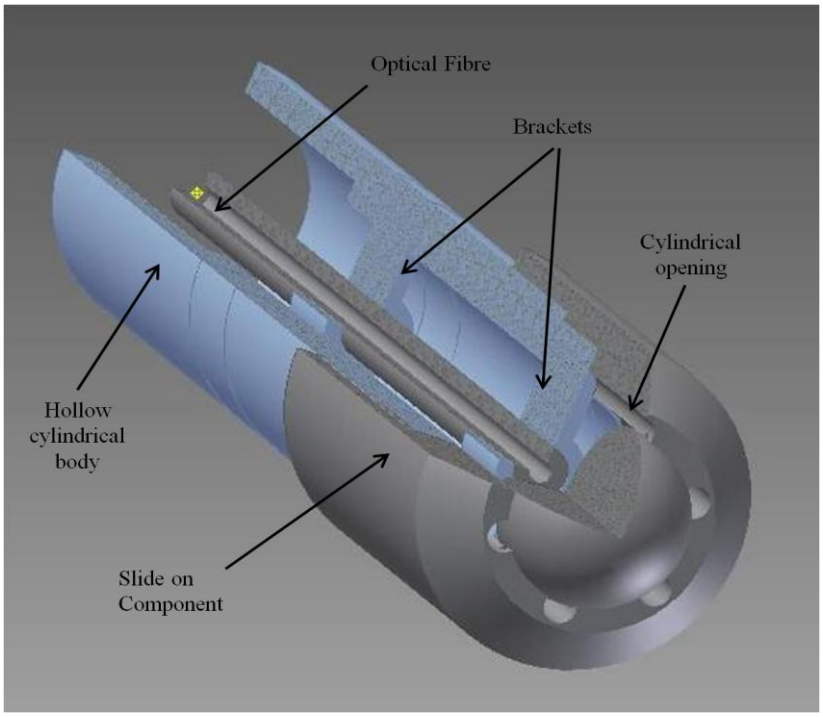

Figure 3.17: A CAD drawing of Sensor 3 illustrating the location of the hollow cylindrical body, the slide on component, the brackets, the cylindrical openings and the sphere.

of these semi cylindrical opening was 0.75 mm. A CAD drawing of the slide on component with its cylindrical openings is shown in Figure 3.16. The use of a slide on component was to enable easy access to the optical fibre and the spherical component.

The spherical component was a mirrored metal sphere of diameter 7.9 mm. A CAD drawing showing a sliced view of the sensor is displayed in Figure 3.17. The entire structure of the sensor with the exception of the spherical component was made using acrylonitrile butadiene styrene (ABS) plastic which was built using a three dimensional rapid prototyping machine (Dimension 768).

The optical fibre used had an outer jacket of 2.2 mm and a core of 1 mm. The optical fibre was the one end of a 1 x 2 optical coupler with 50:50 ratios (Industrial Fiber

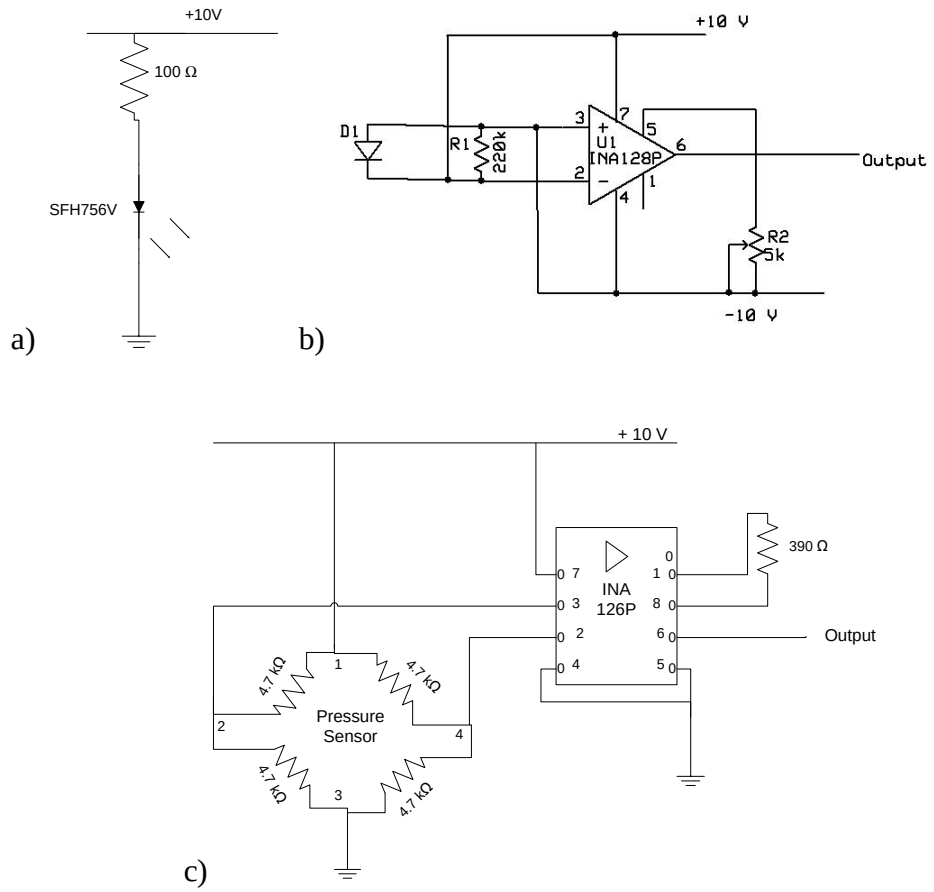

Figure 3.18: a) the electrical circuit used to power the LED b) the electrical circuit used for the photosensitive diode c) the electrical circuit used to power the pressure sensor, an operational amplifier INA 126P was used to amplify the signal received.

Optics, Inc.). The optical coupler was connected to an optical scheme comprising an LED and a photosensitive diode. The LED which was used as the light transmitter, was an SF756V (Avago) of peak wavelength 660 nm. The photosensitive diode was an SFH250 (Avago) with a spectral range of 400 nm to 1100 nm. The electrical circuits used for the LED and photosensitive diode are illustrated in Figure 3.18a and Figure 3.18b.

The pressure sensors used to measure the pressure inside the hollow cylindrical component and the pressure at the compressor's outlet were piezo pressure sensors of

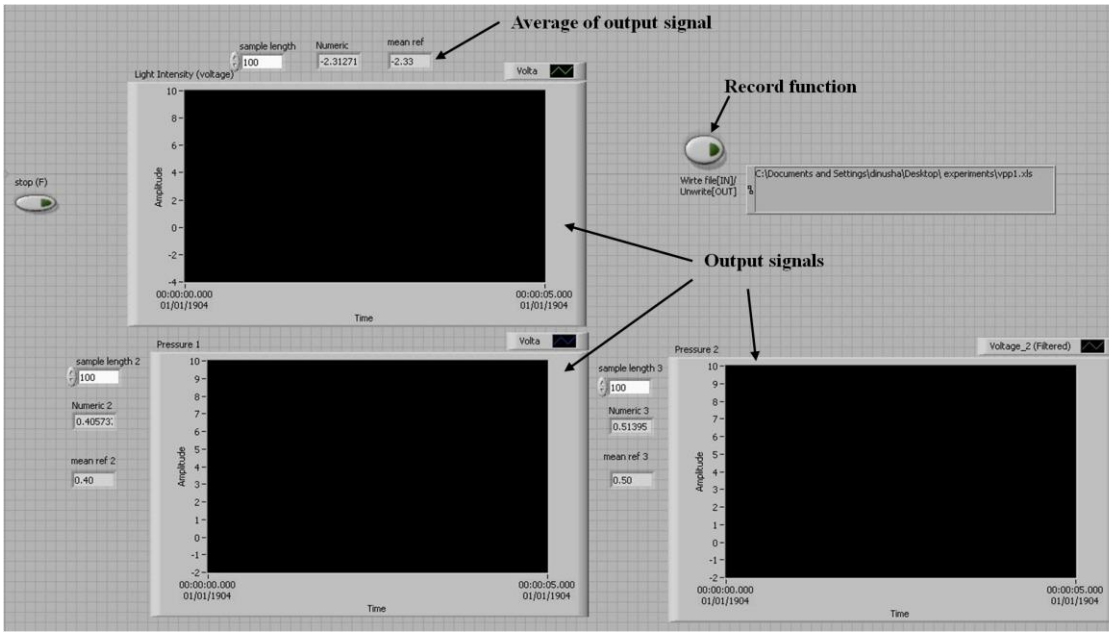

Figure 3.19: The GUI of the Labview program showing the light intensity output signal in the top left graph, P_{inside} output signal in the bottom left graph and P_{comp} output signal in the bottom right graph.

range 0-0.5psi (RS). The electrical circuit used to amplify the output signal for each pressure sensor is illustrated in Figure 3.18c.

The data acquisition card used was the National Instrument card NI USB-6211 and the output signals of the photosensitive diode and of the pressure sensors were connected to it using a differential setup.

The near end of the hollow cylindrical body was connected via a hose to a compressor which is used to generate pressurised air. The connection between the hose and the near end of the hollow cylindrical body was sealed with plumbing tape to ensure its air tightness.

The software used to interface with the data acquisition card and the output signals of the photosensitive diode and the pressure sensors signal outputs was Labview 2012.

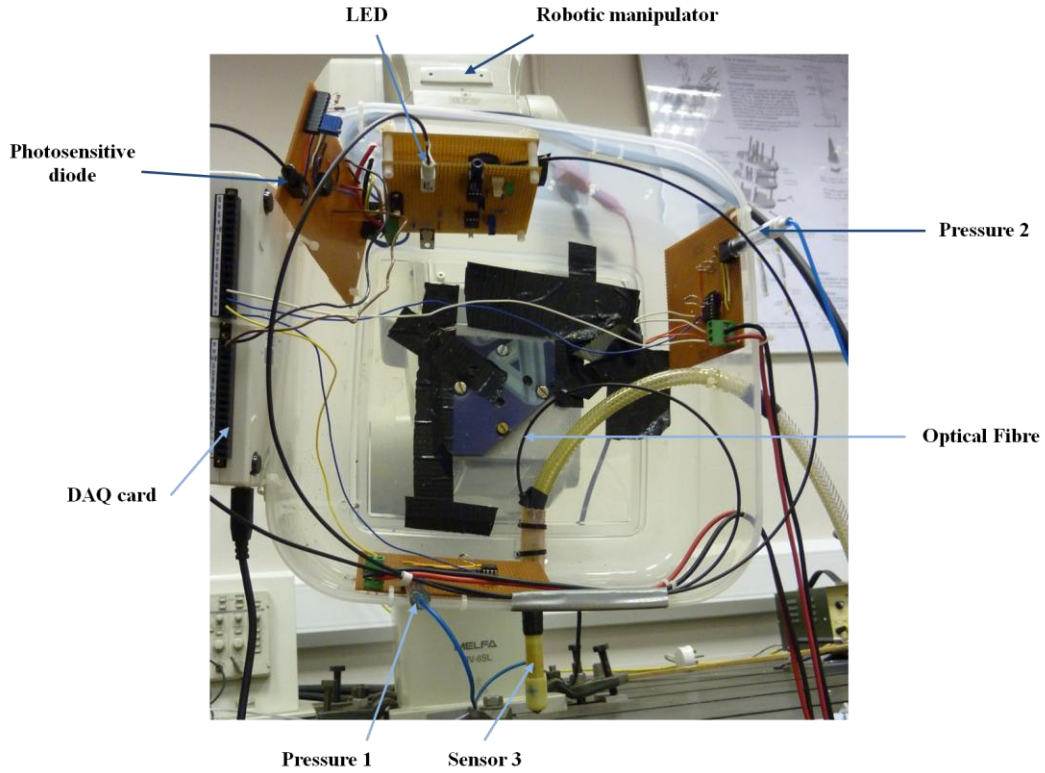

Figure 3.20: Sensor 3 and all of its sensing components are mounted onto the robotic manipulator.

The Graphical User Interface (GUI) of the program created can be seen in Figure 3.19. The program shows the data streaming in three graphs; one graph displays the signal output of the photosensitive diode and the others two show the signal output for each pressure sensor, respectively. The average output of each plot is also shown with the possibility of changing the sample size. A record function was also built in to permit the recording of data at the push of a button. The selection of the sampling rate and the wavelengths used were based on experimental results.

Sensor 3 and all of its components were attached to a casing to facilitate their experimental setup. They were also mounted onto the distal tip of a Mitsubishi RV-6SL 6-DOF robotic manipulator to achieve controlled movements of the sensor. A

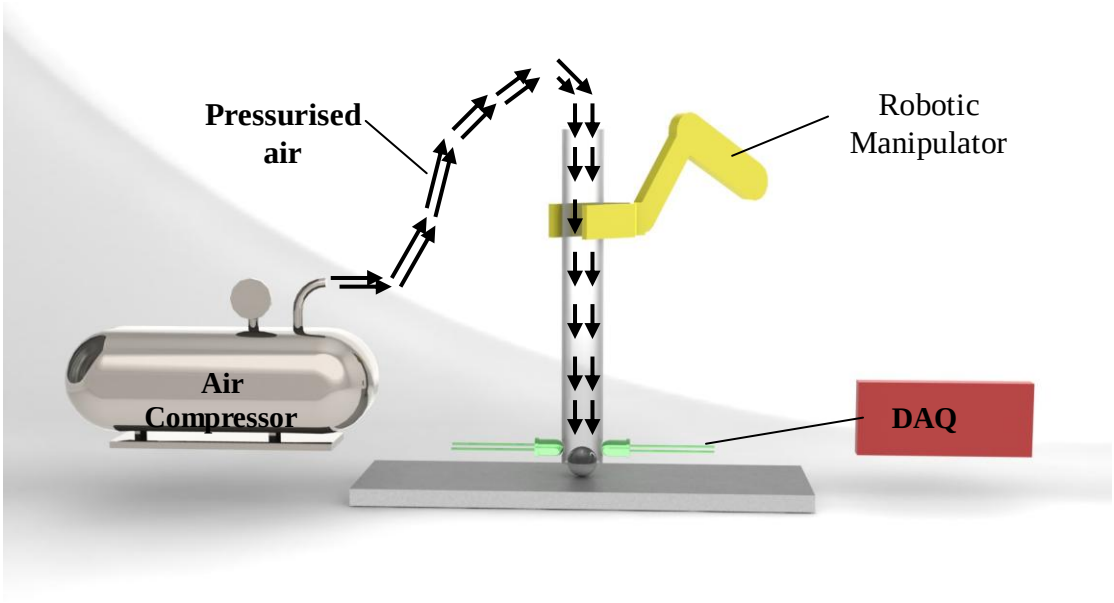

Figure 3.21: A schematic of the experimental setup used to control the sensor.

picture of this setup is shown in Figure 3.20. A schematic drawing of the experimental setup used for all three sensors is shown in Figure 3.21. Once setup, the optical sensing scheme of the sensor and its pressure sensors were calibrated as detailed in Chapter 4.

The sensor's ability to estimate force by using the pressure and displacement measurements from the pressure sensor and the light intensity modulation, respectively, is also detailed in Chapter 4.

3.6 Conclusion

The novel concept of the air cushion sensor has been presented in depth. The optical sensing scheme required to monitor the spherical component of the concept has been explained and three designs that embrace this concept have been presented. The

limitations of the designs are also described. In the next chapter the capability of Sensor 3 as a force sensor is examined experimentally.

Chapter 4 – Sensor Characteristics

4.1 Introduction

The importance of haptic feedback during Minimally Invasive Surgery has been explained in depth in Chapter 2. Haptic feedback is composed of two components; a cutaneous component which is a reflection of the tactile information and a kinaesthetic component which is an expression of the force information. Both these components are required to mimic the sensation felt by the human hand (Okamura, Methods for haptic feedback in teleoperated robot-assisted surgery, 2004). The acquisition of the force distribution by the proposed sensors would be advantageous. This would permit an air cushion tactile sensor to not only generate maps of areas of varying stiffness but it would also permit it to create force maps of the area under investigation. Another important reason in MIS of knowing the amount of force that is exerted by the sensor onto the surface under inspection is to ensure that no tissue damage occurs. The range of force that a sensor can apply onto a tissue is dependent on the organ/structure that it is investigating.

4.2 Force Estimation

The operating principle of the proposed sensors is to employ a pressurised fluid to enable a spherical component to "float" relative to the hollow body of the sensor when it is employed onto soft materials that do not generate a large reaction force. The force exerted by the spherical component onto the soft material under investigation is proportional to the pressure exerted by the pressurised fluid onto the spherical component. A difficulty existed in establishing a relationship between the pressure of the pressurised fluid and the force exerted by the spherical component onto the soft material. This was due to a number of factors. The system employed to circulate the pressurised fluid onto the spherical component was an open system in which it was inherently difficult to measure the pressure. The length of the components used to transport the pressurised fluid to the spherical component also needed to be taken into account for pressure variations. The pressurised fluid did not only exert pressure onto the spherical component but it is also streamed along its sides. The tapered end of the hollow cylindrical component in Sensor 2 and Sensor 3 compelled the pressurised fluid to be funnelled towards its distal end and the spherical component. These factors also generated turbulent flow within this open system. A Computational Fluids Dynamics (CFD) approach was considered but due to the complex range of constantly changing parameters which required extensive modelling when just an approximation was required it was deemed unnecessary to follow that route. Due to the complexity of these parameters, a relationship between the pressure of the pressurised fluid and the force exerted by the spherical component was established experimentally.

The sensor used to establish this relationship was Sensor 3 as it was designed to monitor the change in pressure in the system with its pressure sensors measuring the pressure at the outlet of the compressor and inside its hollow cylindrical body.

In Chapter 3, the conceptual structure and principle of the proposed sensor was introduced with its design and sensing principle. The implementation of Sensor 3's design, the components that were used to build it, the sensing scheme and its components and the experimental setup which was employed to operate the sensor were also discussed in detail.

In the next section the optical sensing scheme and pressure sensors of Sensor 3 were calibrated.

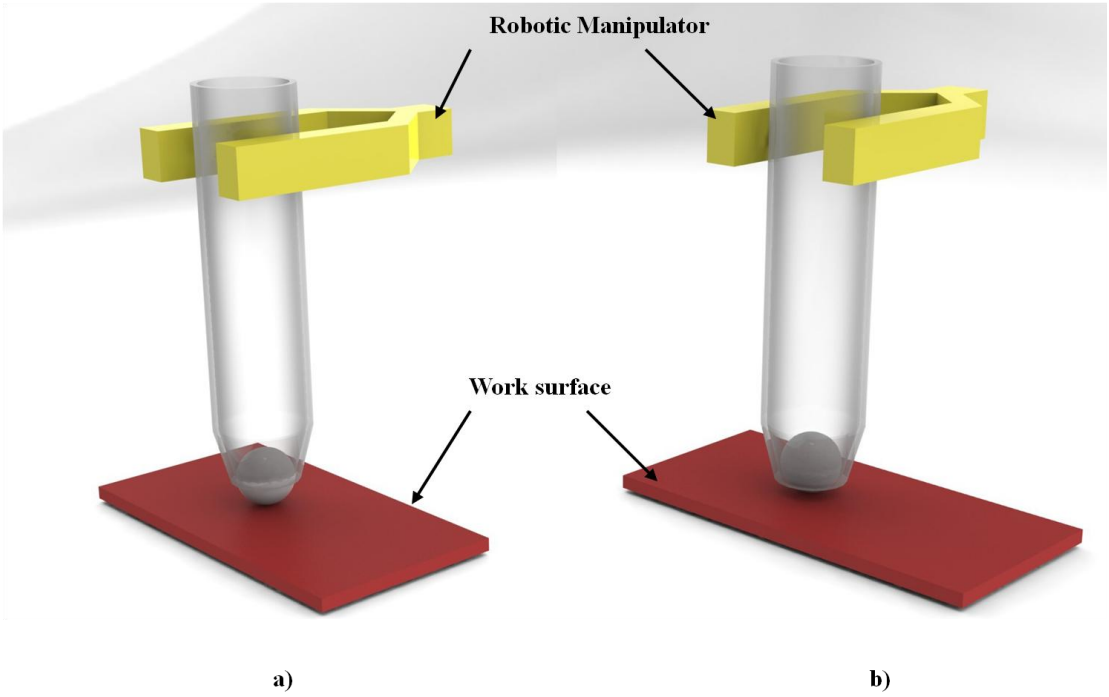

Figure 4.1: Sensor 3 is attached to the robotic manipulator. a) The spherical component is barely in contact with the work surface, b) the spherical component is fully displaced into the hollow cylindrical body.

4.3 Calibration of sensors

4.3.1 Calibration of the optical sensing scheme

In order to establish the operating range of the optical sensing scheme, the sensor was mounted to the Mitsubishi manipulator. The sensor was positioned in such a way that the spherical component of the sensor was scarcely in contact with the work surface as displayed in Figure 4.1a). The sensor was then lowered in its vertical direction by increments of 0.1 mm by using the robotic manipulator Mitsubishi RV-6SL which had a resolution of 0.02 mm. As a result of such movements, the spherical component was gradually displaced into the hollow cylindrical body of the sensor. This process

was stopped when the spherical component was entirely displaced into the hollow cylindrical body which was reached after 2.3 mm as seen in Figure 4.1b). The reverse process was then performed by moving the robotic manipulator in the opposite direction to gradually return the spherical component back to its original position.

The respective voltage reading of the photosensitive diode and the gradual displacement of the spherical component into and out of the hollow cylindrical body were then correlated for the loading and unloading process. The importance of ascertaining the behaviour of the sensor during the loading and unloading processes was to establish whether there was any significant hysteresis. The process of loading and unloading behaviour of the sensor is displayed in Figure 4.2. The level of hysteresis is minimal as seen from Figure 4.2. In Figure 4.3, the normalised behaviour of the sensor is shown, which can be approximated by the function

$$y = -0.1167x^3 + 0.6835x^2 - 1.4008x + 1.0207 \quad \textbf{(4-1)}$$

where,

y, is the normalised voltage output signal of the photosensitive diode

x, is the distance from the mirrored sphere.

The function used for this approximation has an $R^2 = 0.9993$. Thus the position of the spherical component can be determined using the output signal of the photosensitive diode by using the aforementioned function where the output signal and the distance from the mirrored sphere are y and x, respectively.

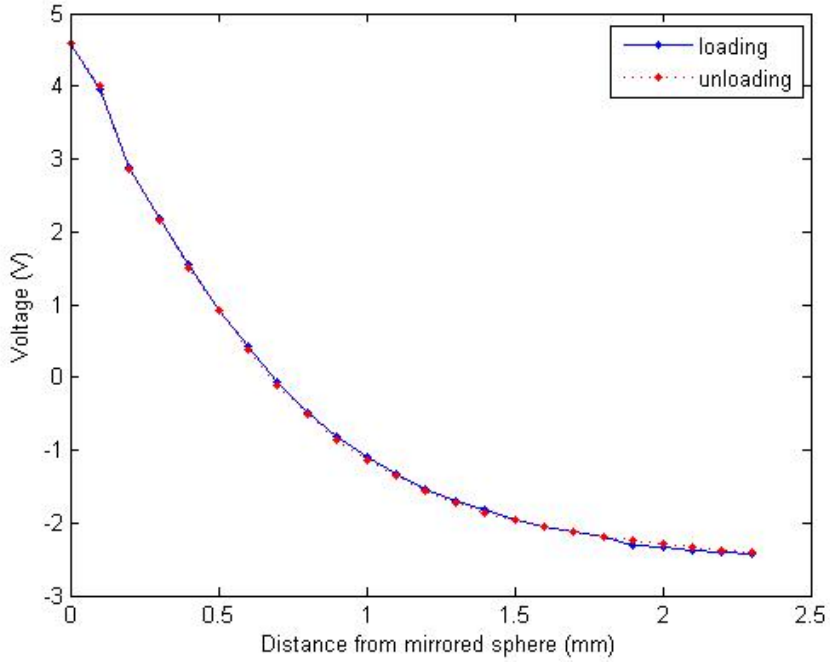

Figure 4.2: The behaviour of the sensor during the loading process is displayed in blue with a solid line and the unloading process is displayed in red with a dotted line

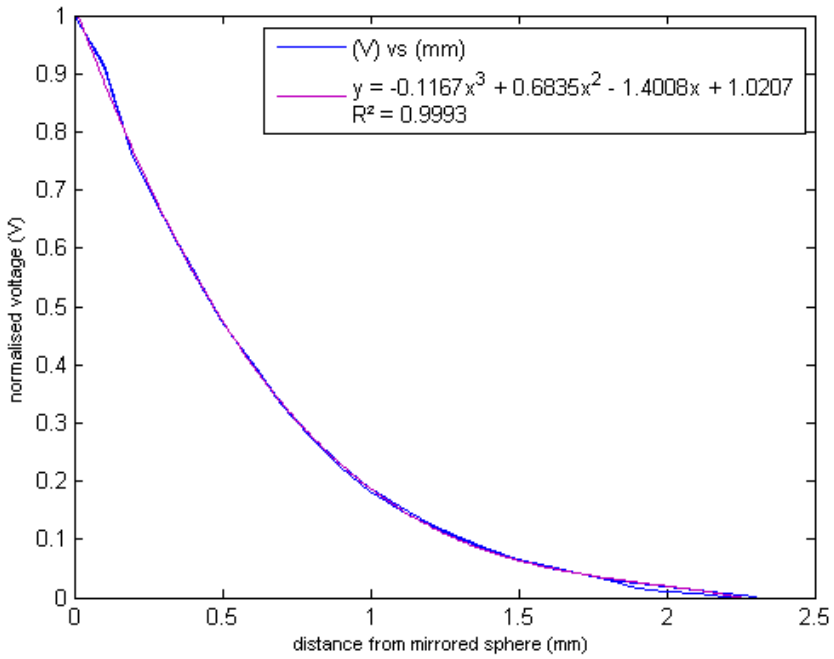

Figure 4.3: The normalised behaviour of the sensor can be approximated by the function $y = -0.1167x^3 + 0.6835x^2 - 1.4008x + 1.0207$ with an $R^2 = 0.9993$.

Number of cycles	20
Linear operating range	0.1-1.8 mm
Hysteresis from	0.0-0.1 and 1.8-2.3 mm distance from sphere
Resolution	0.1 mm
Function of normalised behaviour of the sensor	$y = -0.1167x^3 + 0.6835x^2 - 1.4008x + 1.0207$
R^2 of linear approximation	0.9993

Table 4.1: Summary of the experimental results of the calibration of the optical sensing scheme.

The experimental results of the calibration of the optical sensing scheme are summarised in Table 4.1.

4.3.2 Calibration of the pressure sensors

Sensor 3 was designed to operate with two pressure sensors; a pressure sensor that monitored the pressure fluctuation inside the hollow cylindrical body of the sensor was named P_{inside} and the pressure sensor which monitored the pressure variation at the outlet of the compressor was called P_{comp}. P_{inside} and P_{comp} were calibrated to establish the correlation between the output voltage signals and the pressure measurements.

For the calibration of the pressure sensors, an experimental setup was required that generated specific pressures. This was achieved by setting up the pressure sensor in a closed pressure system. A mechanically actuated syringe was used to increase and

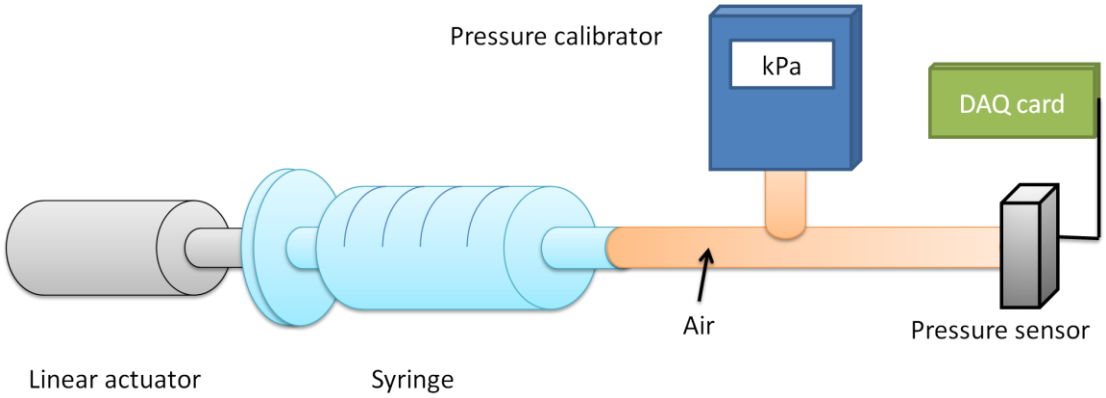

Figure 4.4: The experimental setup used to calibrate the pressure sensor is displayed.

decrease the pressure in the closed system. The closed system was composed of the actuated syringe, a pressure calibrator which was used to measure the pressure of the system and the pressure sensor that was being calibrated. Measurements were taken every time the pressure was increased by correlating the output signal voltage of the pressure sensor with the readings of the measurements of the pressure calibrator. This process was repeated every time the pressure of the system was decreased.

The layout of the experimental setup used to calibrate the pressure sensor is displayed in Figure 4.4. The identical process was used to calibrate both pressure sensors. The behaviour of P_{inside} and P_{comp} are shown in Figure 4.5a and Figure 4.5b, respectively. P_{inside} and P_{comp}, both follow a perfect linear behaviour with no hysteresis.

a)

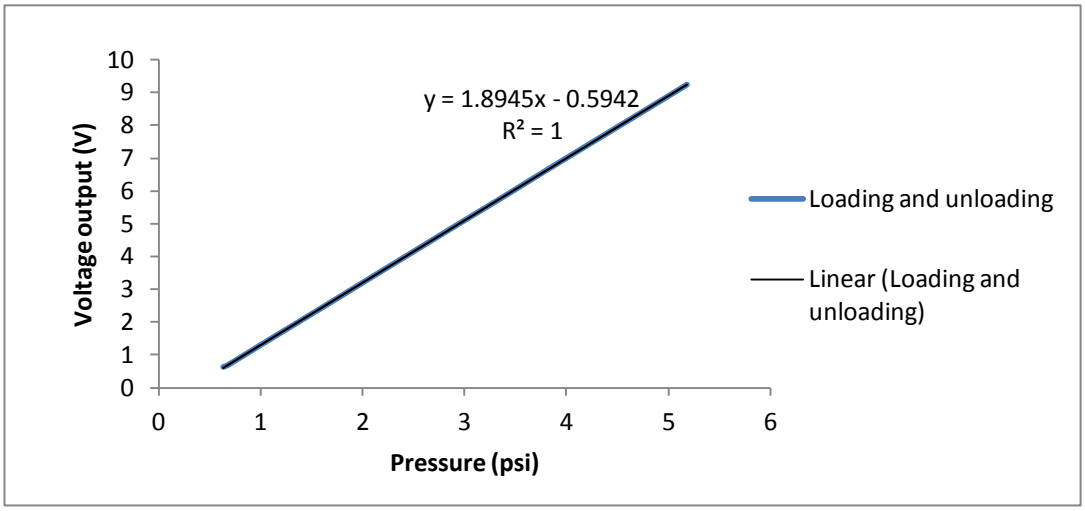

b)

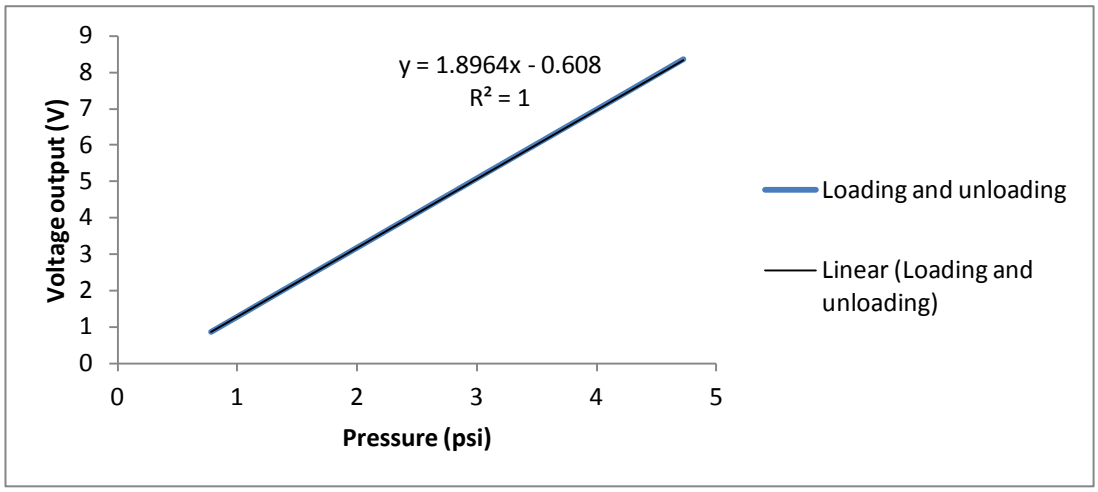

Figure 4.5: a) The behaviour of P_{inside} is entirely linear during loading and unloading and is given by the function y = 1.8945x - 0.5942 b) The behaviour P_{inside} is entirely linear during loading and unloading and is given by the function y = 1.8964x - 0.0608.

The linear relationship for P_{inside} between the variation of the output signal and the corresponding pressure is given by

$$V = 1.8945\, p - 0.5942 \qquad \textbf{(4-2)}$$

	P_{inside}	P_{comp}
Number of cycles	20	20
Linear operating range	0.633-5.186 psi	0.780-4.722 psi
Hysteresis from	n/a	n/a
Resolution	0.001 psi	0.001 psi
Function of behaviour of the sensor	$V = 1.8945\,p - 0.5942$	$V = 1.8964\,p - 0.6080$
R^2 of linear approximation	1	1

Table 4.2: Summary of the experimental results of the calibration of pressure sensors P_{inside} and P_{comp}.

where,

V is the voltage output,

P, is the pressure measurement.

This relationship is valid for pressure measurements that range from 0.633 psi to 5.186 psi.

The linear relationship for P_{comp} between the variation of the output signal and the corresponding pressure is given by

$$V = 1.8964\,p - 0.6080 \quad \textbf{(4-3)}$$

where,

V is the voltage output,

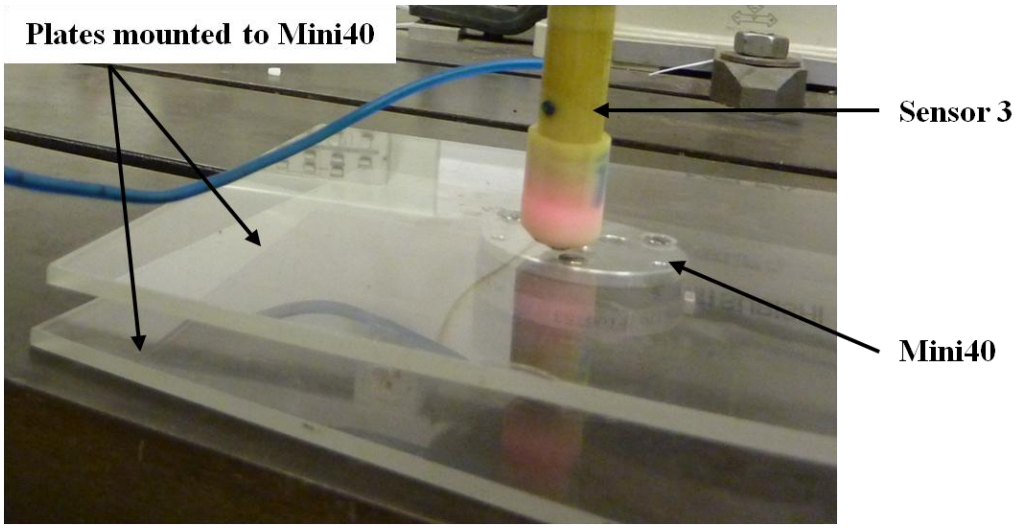

Figure 4.6: Sensor 3 is positioned just above the plates that are connected to the Mini40.

P, is the pressure measurement.

This relationship is valid for pressure measurements that range from 0.780 psi to 4.722 psi.

The experimental results of the calibration of the optical sensing scheme are summarised in Table 4.2.

4.4 Force estimation experiment

4.4.1 Experimental setup and procedure

In order to establish experimentally a correlation between the variations in pressures in the system which were measured by P_{inside} and P_{comp}, and the force exerted by the spherical component of Sensor 3 onto the surface under investigation, a force sensor had to be used.

The force/torque sensor used was the Mini40 (ATI). It was mounted onto two plates to increase its sensing area and stability and was placed onto the work surface.

The force torque sensor was connected to a DAQ card and the software used to interface it was provided by ATI.

Sensor 3 was mounted onto the distal tip of a Mitsubishi RV-6SL 6-DOF robotic manipulator. Sensor 3 was then positioned in such a way that the spherical component of the sensor was 1 mm above the sensing surface of the force/torque sensor as shown in Figure 4.6.

The sensor which was controlled by the robotic manipulator was then lowered in its vertical direction onto the sensing surface of the force/torque sensor until the spherical component was fully displaced into the hollow cylindrical body of the sensor, then at the same speed the sensor was returned to its starting position. The output signals of the photosensitive diode, the pressure sensors and the force sensor were collected during this process. This cycle was repeated ten times for a set pressure. This was then repeated for a range of pressures. The range of pressures used was based on the measurements of P_{comp}. These initial measurements were 0.86 psi, 1.01 psi, 1.22 psi, 1.44 psi, 1.60 psi, 1.66 psi, 1.68 psi, 1.73psi, 1.76 psi, 1.79 psi, 1.80 psi, 1.84psi and used for experiments 1 to 12, respectively. For each experiment, the most representative cycle was used to plot the output signals of the photosensitive diode, the pressure sensors and the force sensor against time. The force sensor measurements were plotted against the respective pressure measurements of each sensor and the force measurements were plotted against the displacement measurements.

4.5 Experimental results

The experimental results of Experiment 1 to Experiment 12 are presented in this section, For each experiment, the first Figure shows four plots. The graph in the top left corner is representative of the displacement of the mirrored spherical component versus time, the graph in the top right corner displays the pressure variation inside the hollow cylindrical body of Sensor 3 against time, the graph in bottom left corner illustrates the measurements recorded at the outlet of the compressor versus time, and the graph in the bottom right corner shows the variation in force measured by the force sensors versus time. The time period used was the same one for each plot. The second figure shows the plot of the force exerted against the corresponding pressure measurements from P_{inside}. The third figure shows the plot of the force exerted against the corresponding pressure measurements from P_{comp}. The fourth figure shows a graph of the force against the displacement. For the second, third and fourth figures of each experiment a corresponding best fit function is plotted (where appropriate) displaying the equation and the matching Norm of Residuals (NoR).

4.5.1 Experiment 1

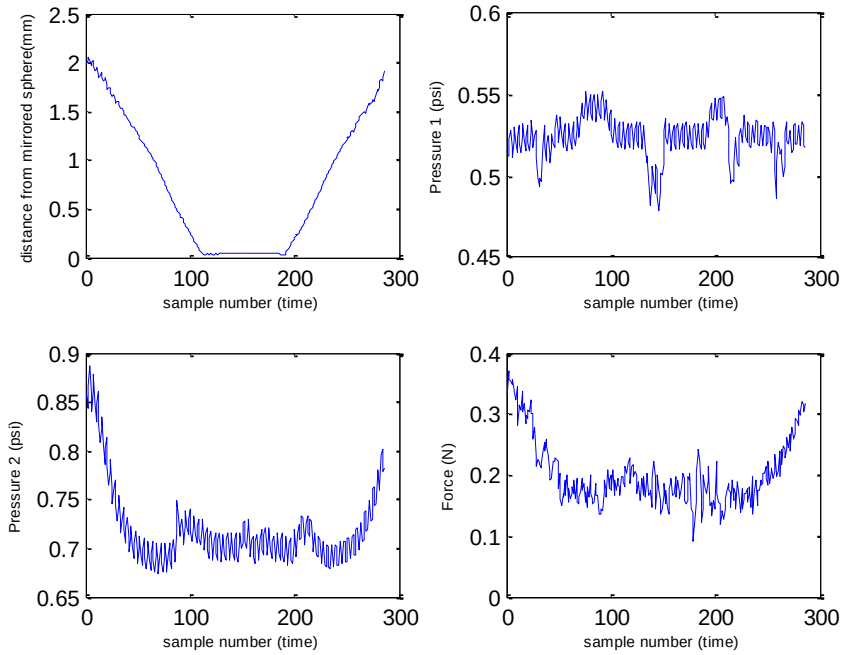

Figure 4.7: Experiment 1, the output signals of the photosensitive diode, P_{inside}, P_{comp} and the force sensor are individually plotted versus the same time period.

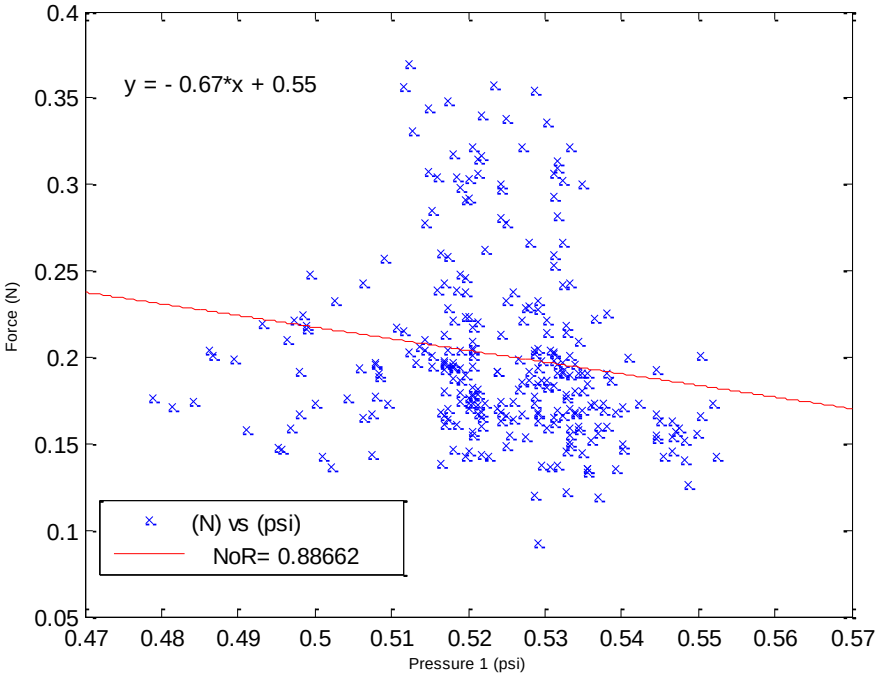

Figure 4.8: Experiment 1, force measurements versus P_{inside} measurements.

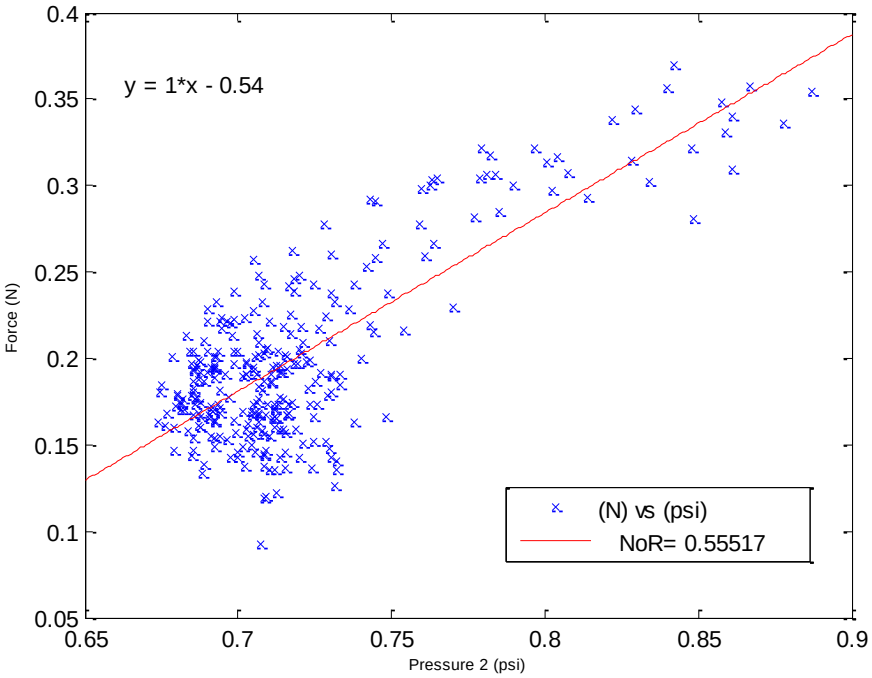

Figure 4.9: Experiment 1, force measurements versus P_{comp} measurements.

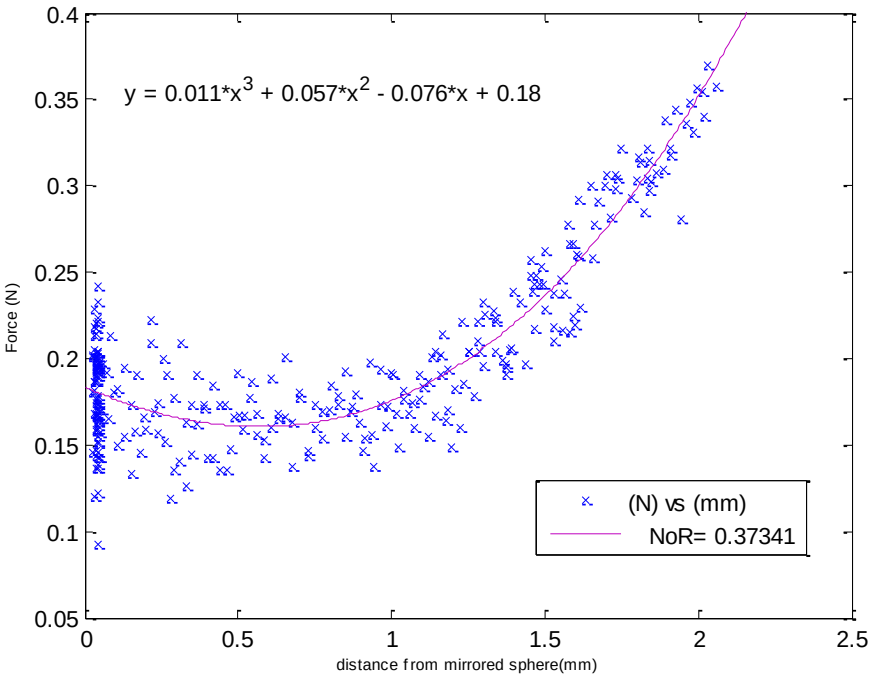

Figure 4.10: Experiment 1, force measurements versus distance from the sphere.

4.5.2 Experiment 2

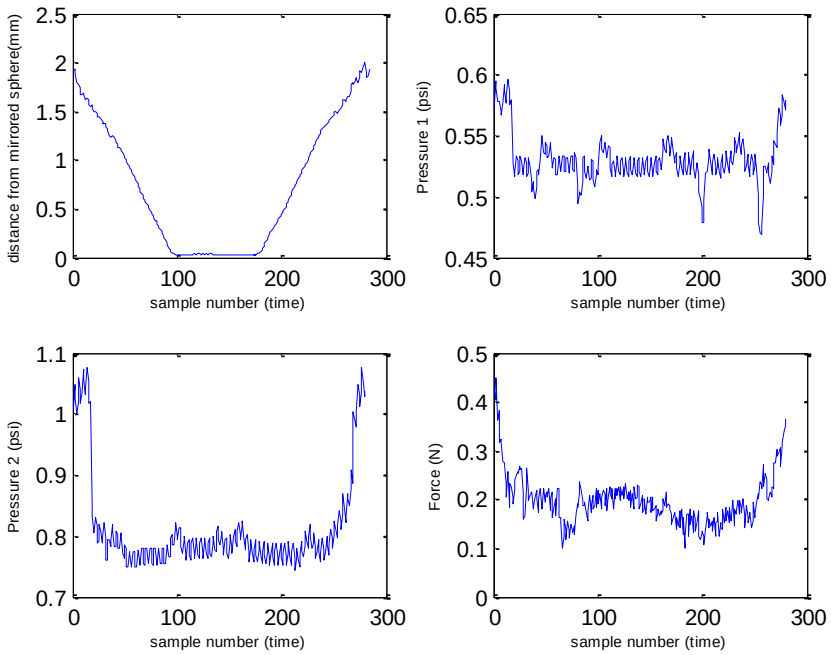

Figure 4.11: Experiment 2, the output signals of the photosensitive diode, P_{inside}, P_{comp} and the force sensor are individually plotted versus the same time period.

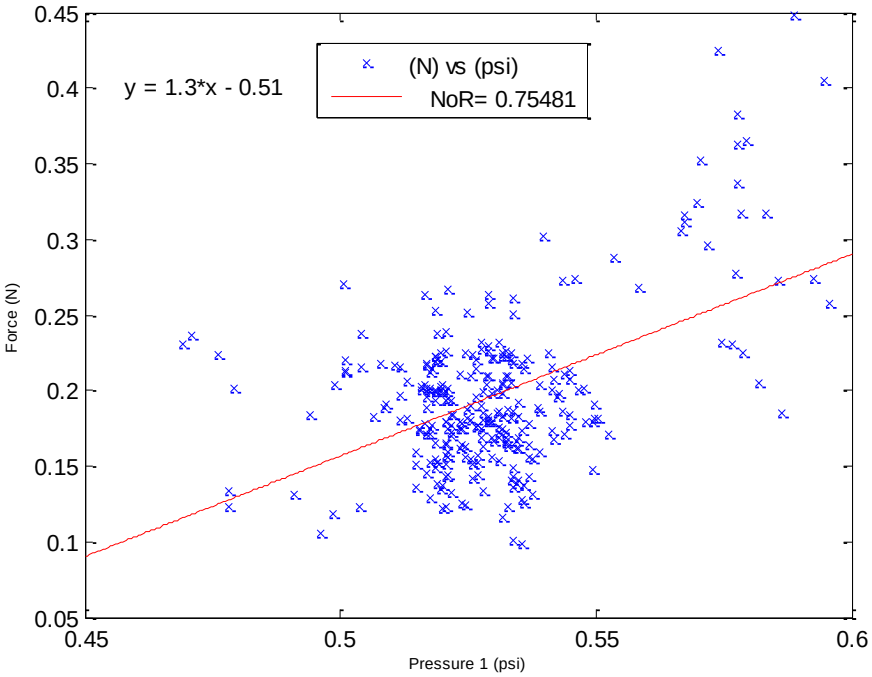

Figure 4.12: Experiment 2, force measurements versus P_{inside} measurements.

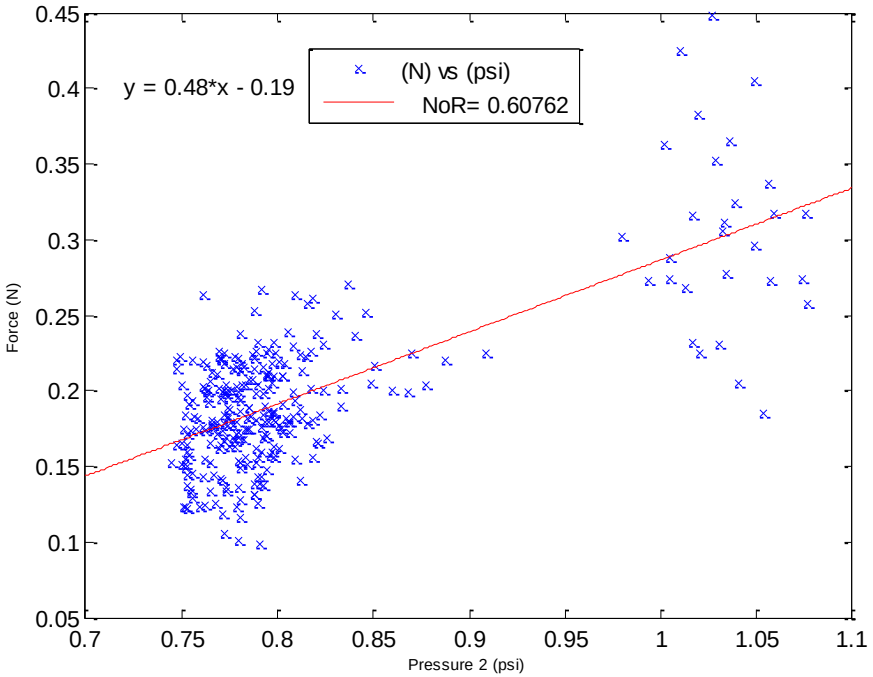

Figure 4.13: Experiment 2, force measurements versus P_{comp} measurements.

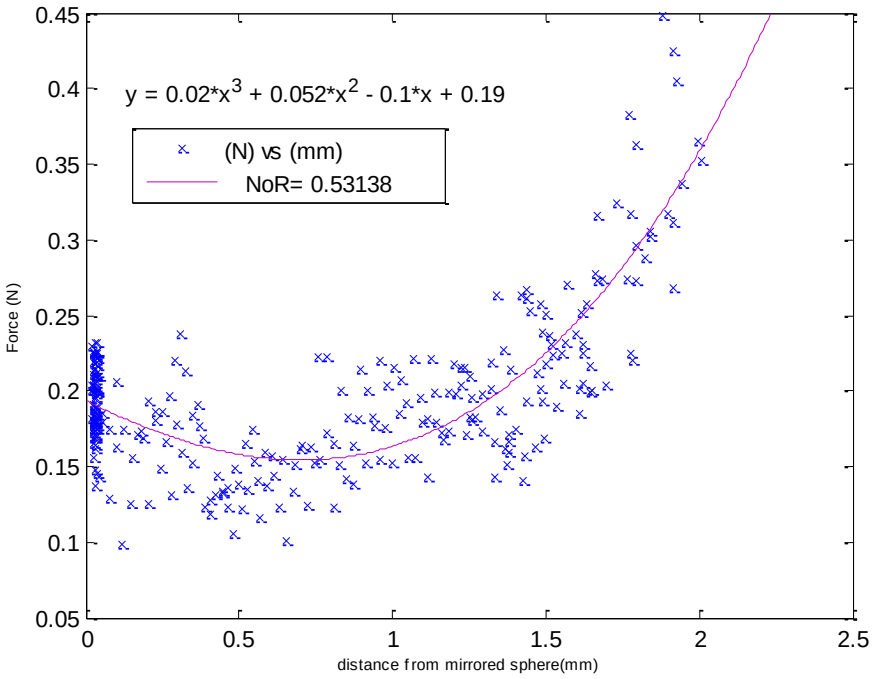

Figure 4.14: Experiment 2, force measurements versus distance from the sphere.

4.5.3 Experiment 3

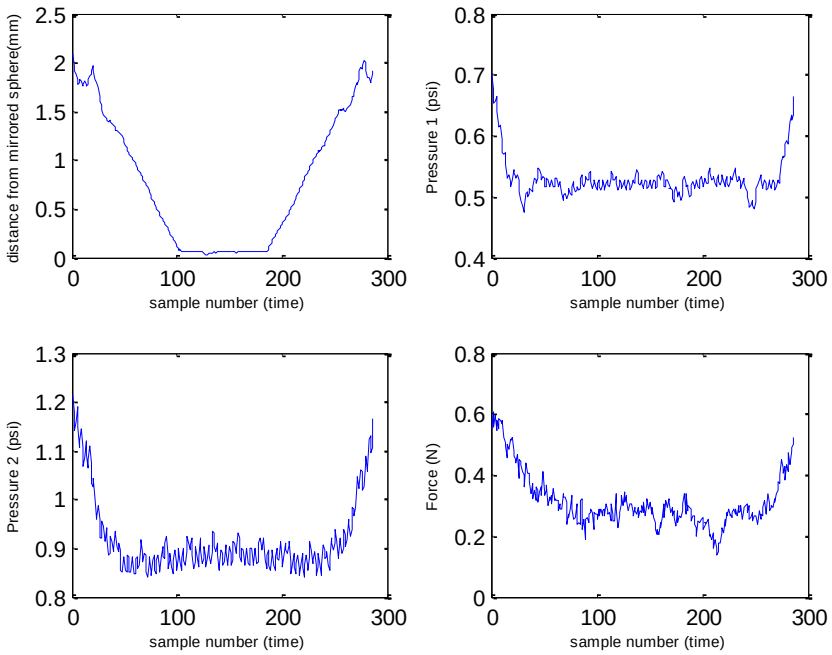

Figure 4.15: Experiment 3, the output signals of the photosensitive diode, P_{inside}, P_{comp} and the force sensor are individually plotted versus the same time period.

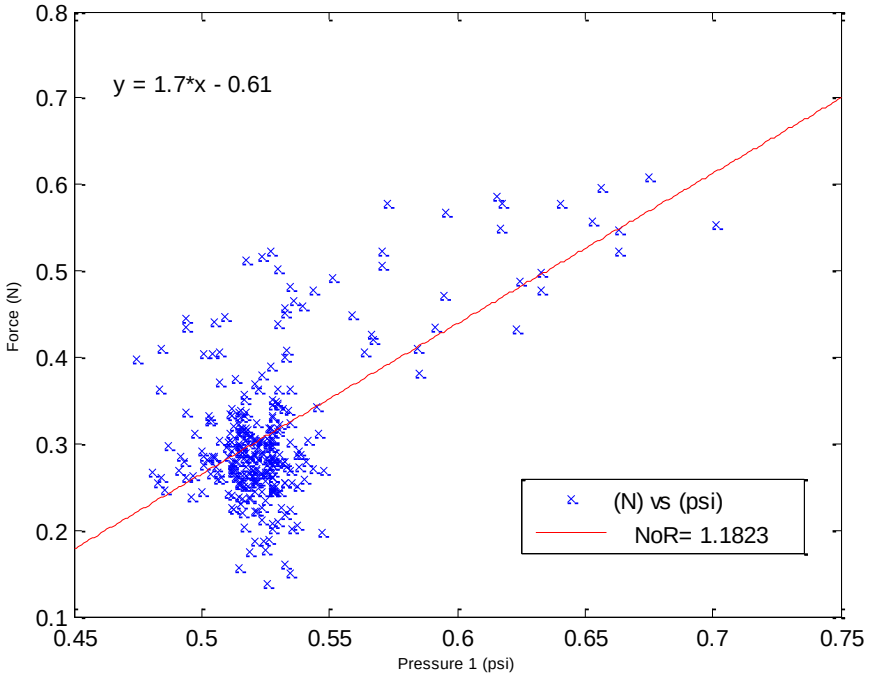

Figure 4.16: Experiment 3, force measurements versus P_{inside} measurements.

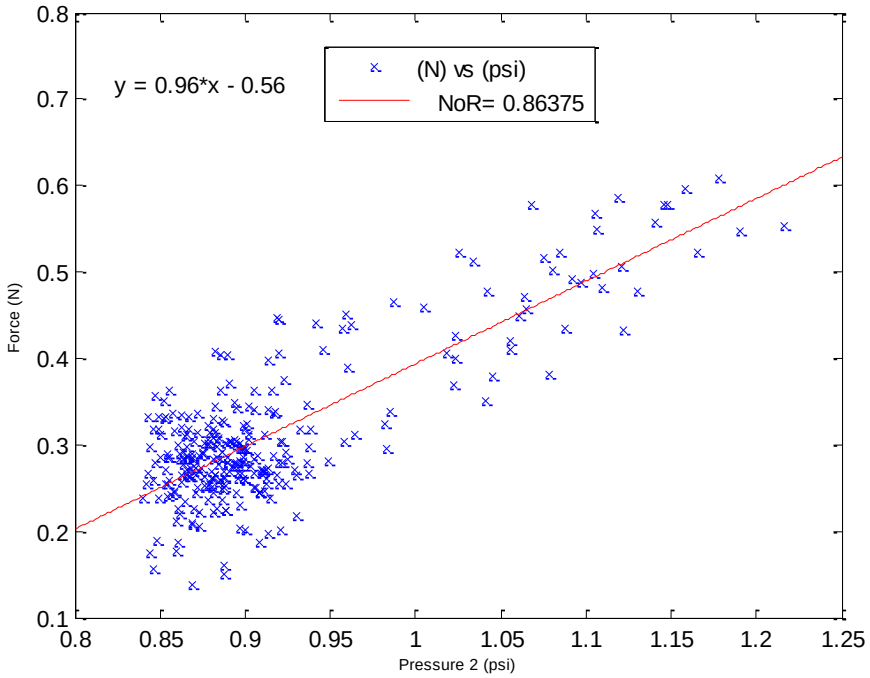

Figure 4.17: Experiment 3, force measurements versus P_{comp} measurements.

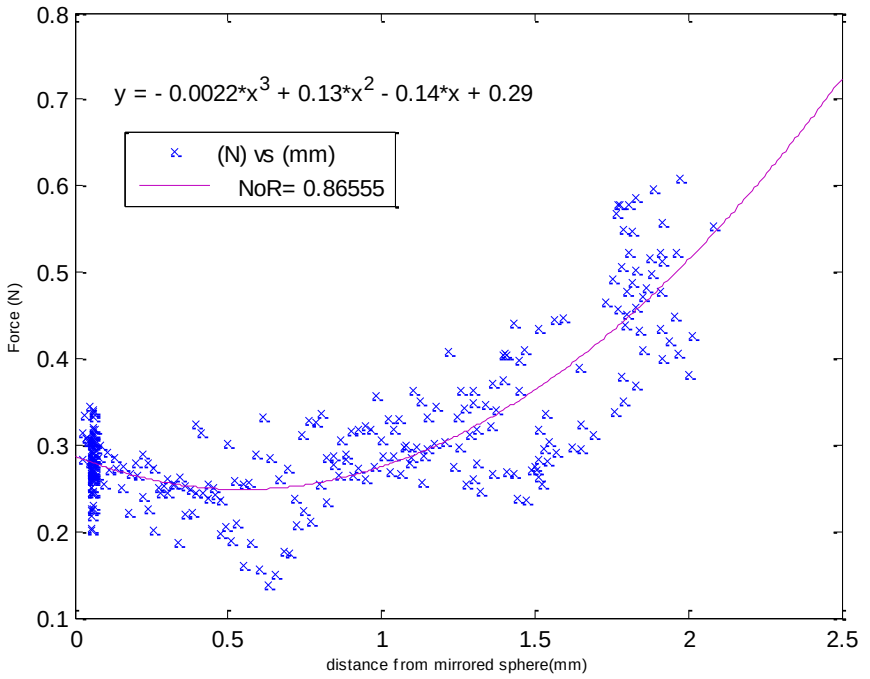

Figure 4.18: Experiment 3, force measurements versus distance from the sphere.

4.5.4 Experiment 4

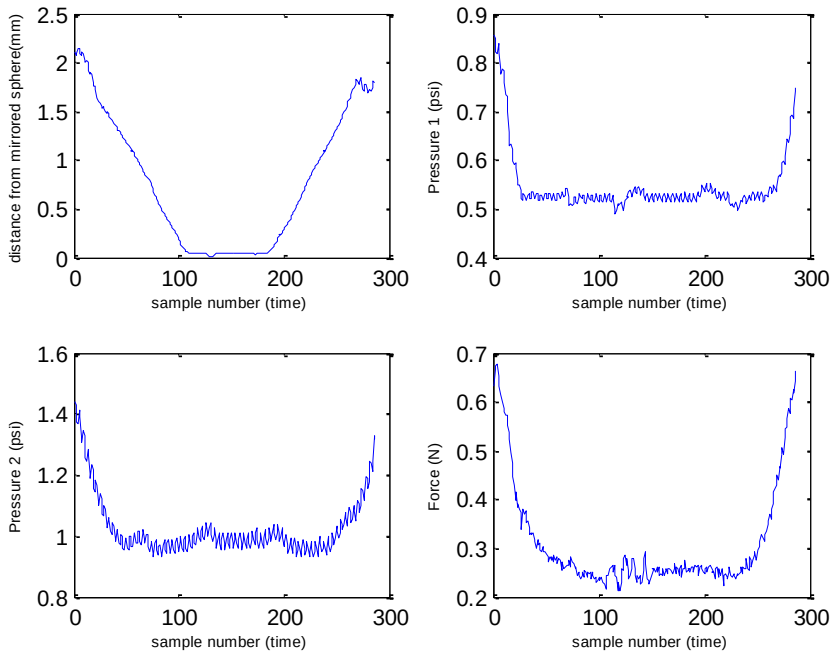

Figure 4.19: Experiment 4, the output signals of the photosensitive diode, P_{inside}, P_{comp} and the force sensor are individually plotted versus the same time period.

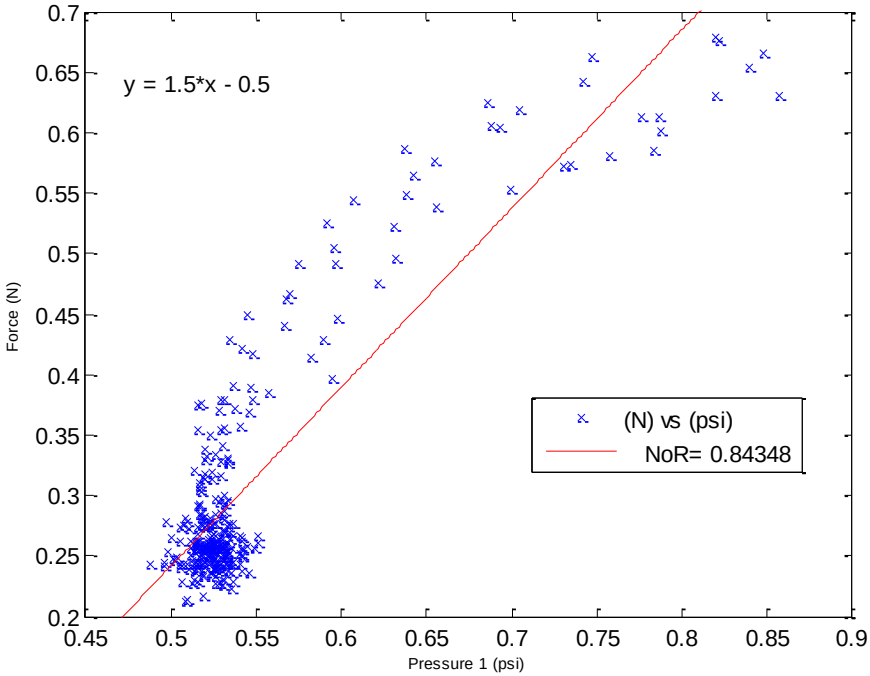

Figure 4.20: Experiment 4, force measurements versus P_{inside} measurements.

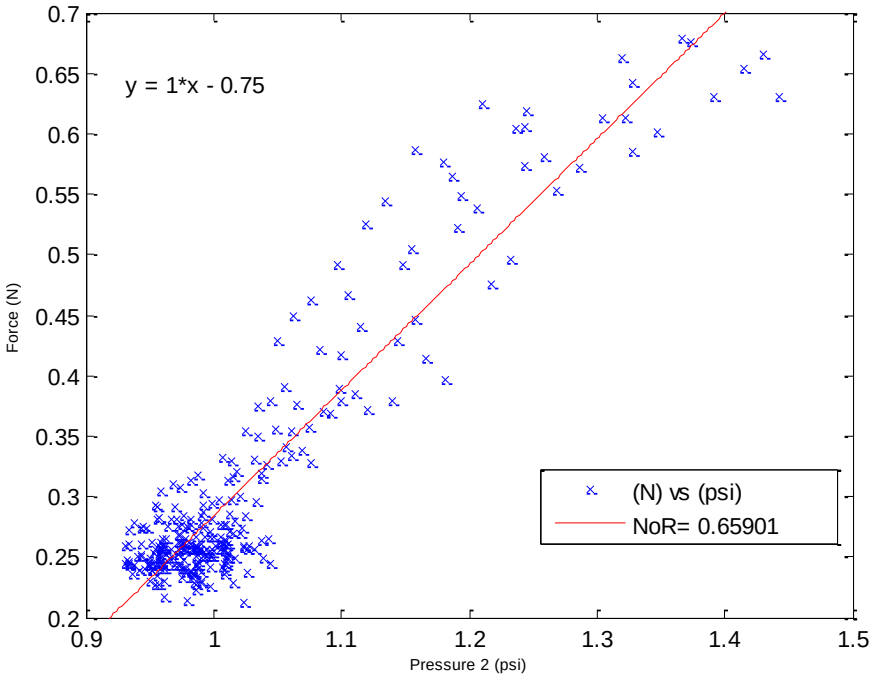

Figure 4.21: Experiment 4, force measurements versus P_{comp} measurements.

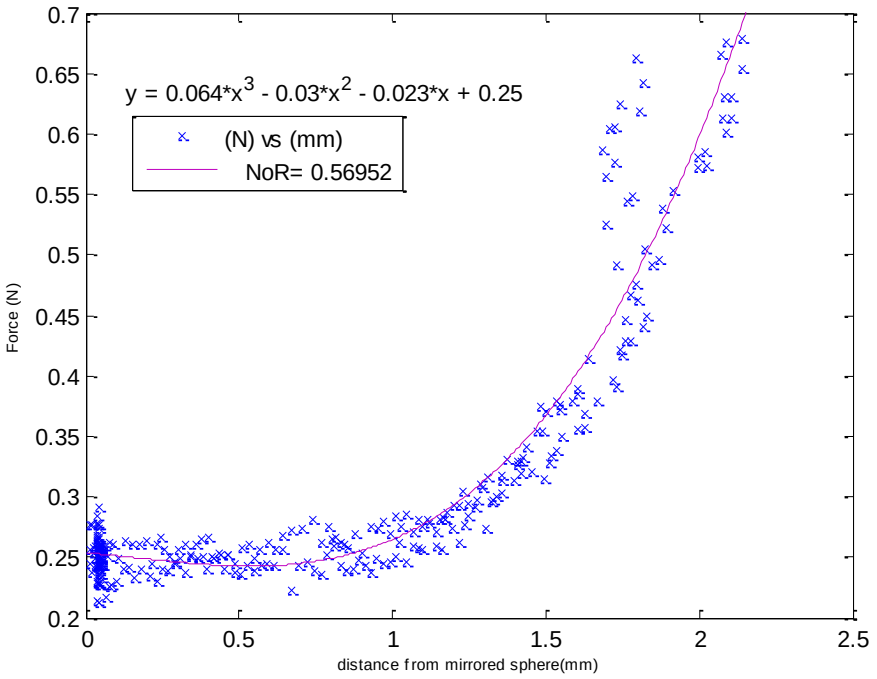

Figure 4.22: Experiment 4, force measurements versus distance from the sphere.

4.5.5 Experiment 5

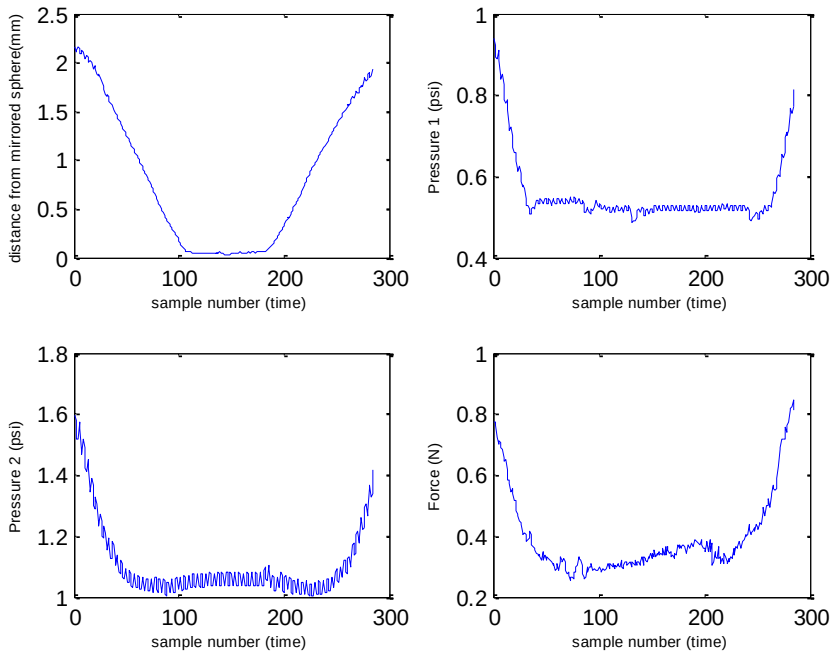

Figure 4.23: Experiment 5, the output signals of the photosensitive diode, P_{inside}, P_{comp} and the force sensor are individually plotted versus the same time period.

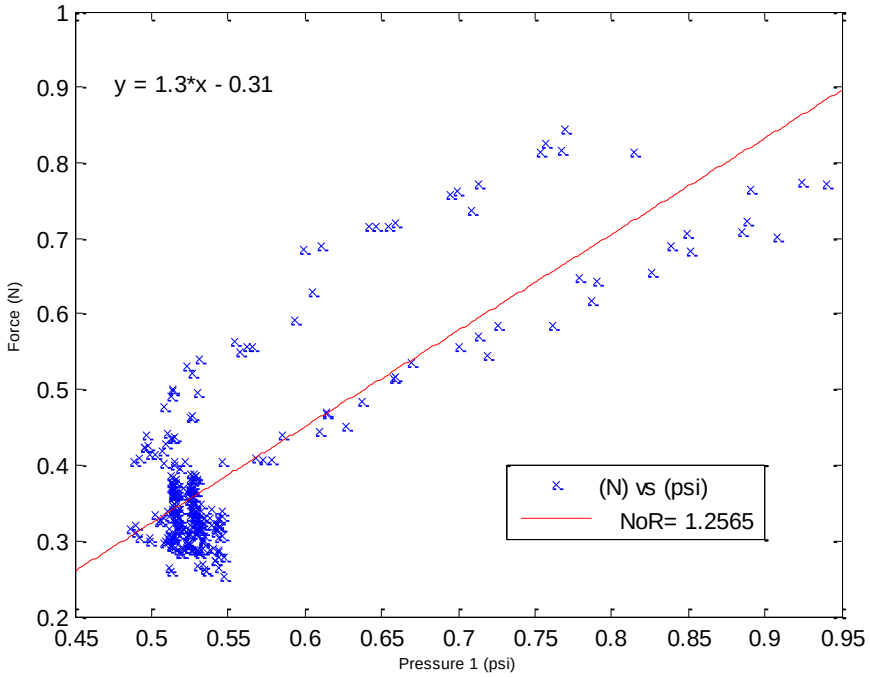

Figure 4.24: Experiment 5, force measurements versus P_{inside} measurements.

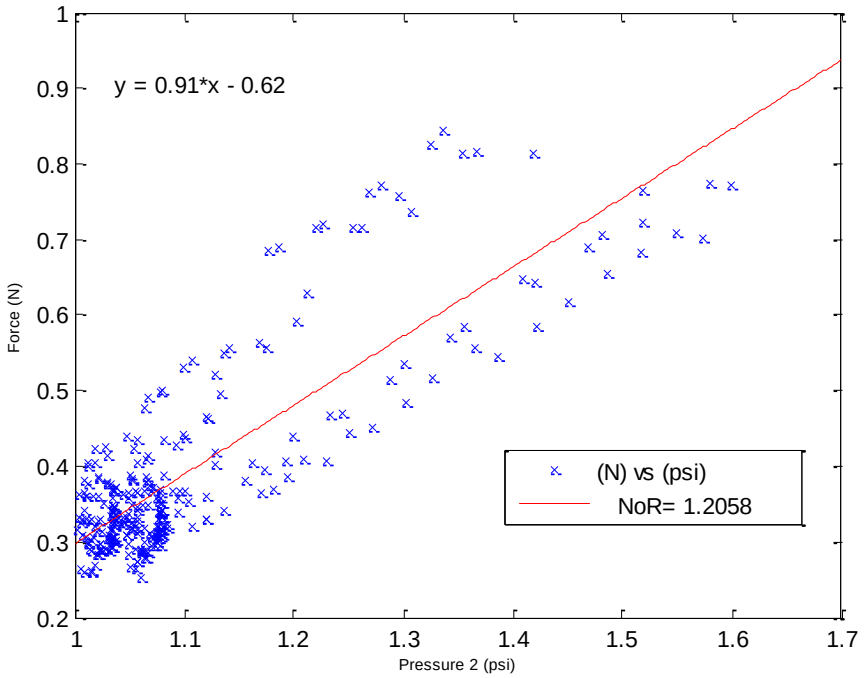

Figure 4.25: Experiment 5, force measurements versus P_{comp} measurements.

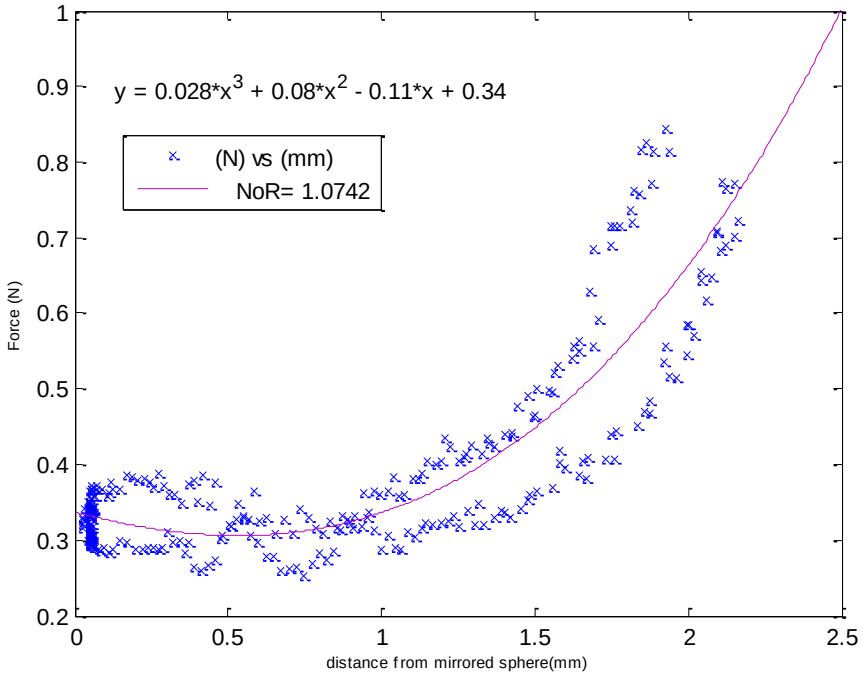

Figure 4.26: Experiment 5, force measurements versus distance from the sphere.

4.5.6 Experiment 6

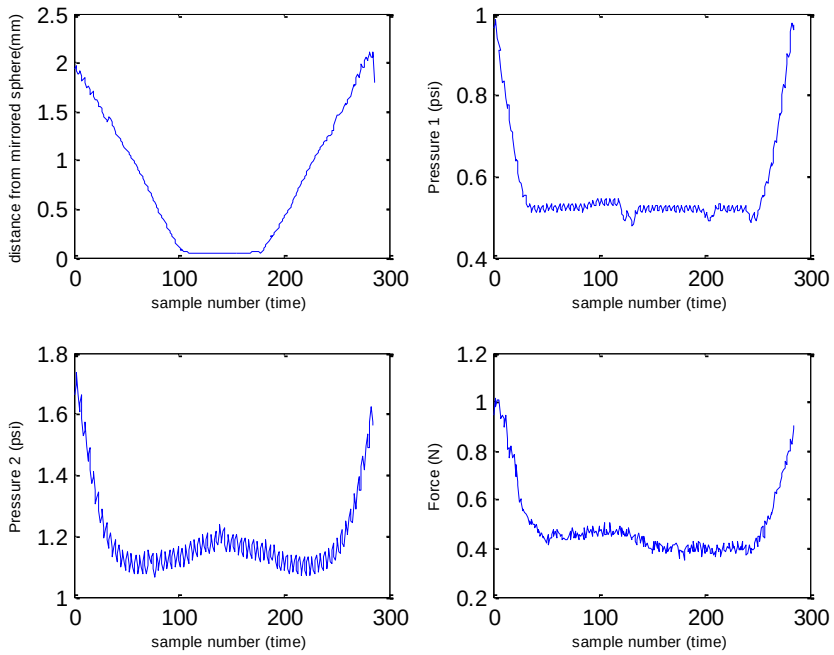

Figure 4.27: Experiment 6, the output signals of the photosensitive diode, P_{inside}, P_{comp} and the force sensor are individually plotted versus the same time period.

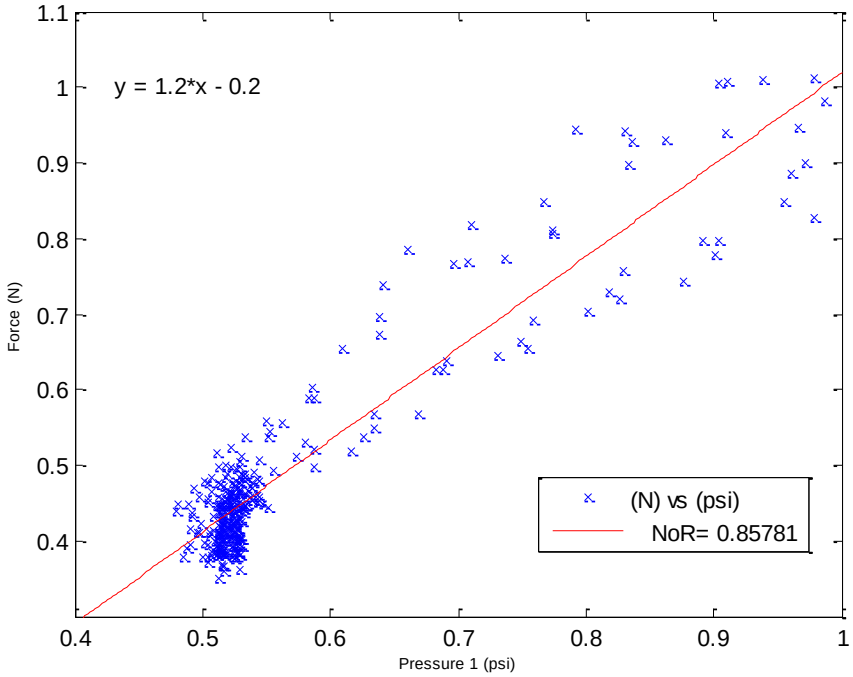

Figure 4.28: Experiment 6, force measurements versus P_{inside} measurements.

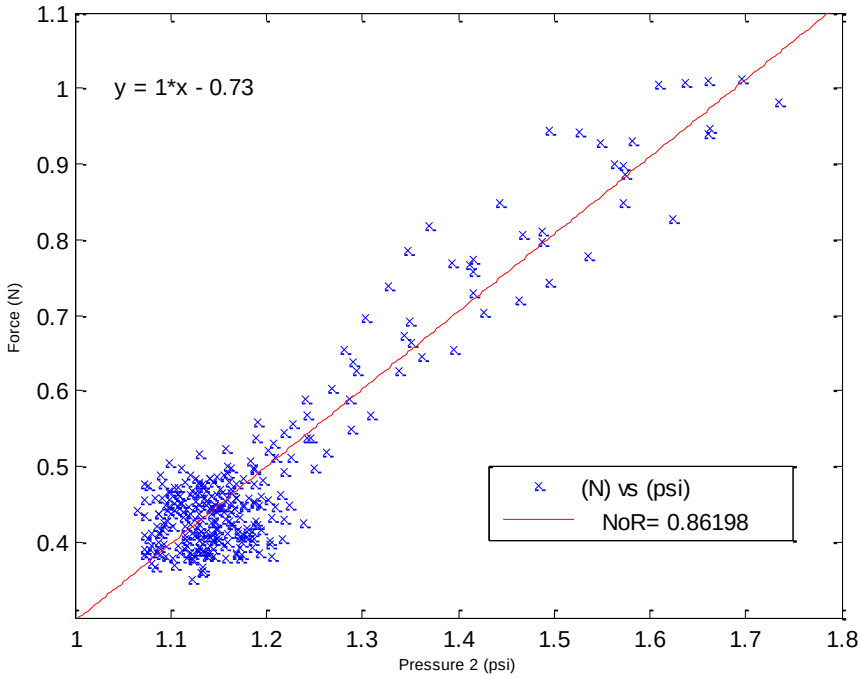

Figure 4.29: Experiment 6, force measurements versus P_{comp} measurements.

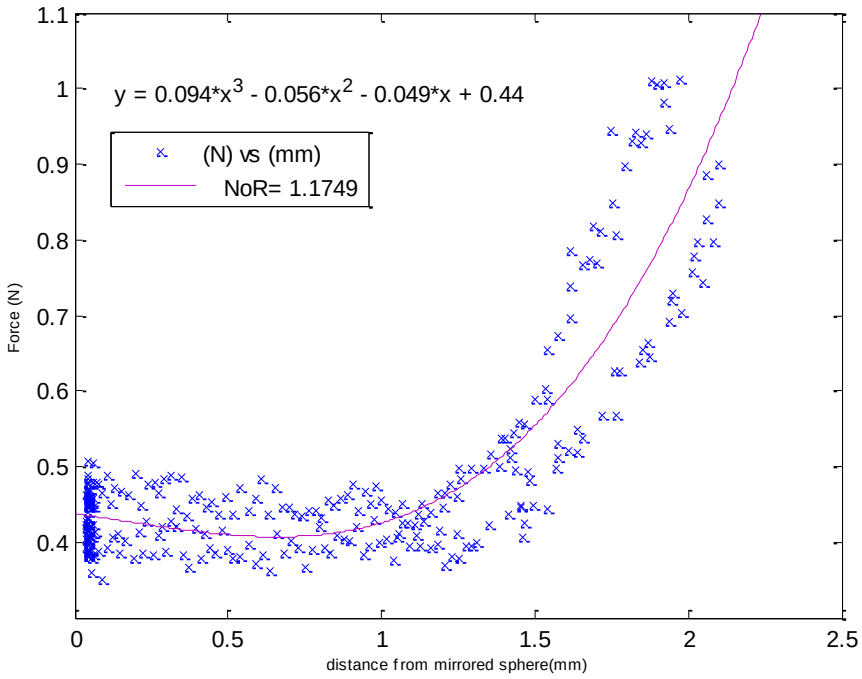

Figure 4.30: Experiment 6, force measurements versus distance from the sphere.

4.5.7 Experiment 7

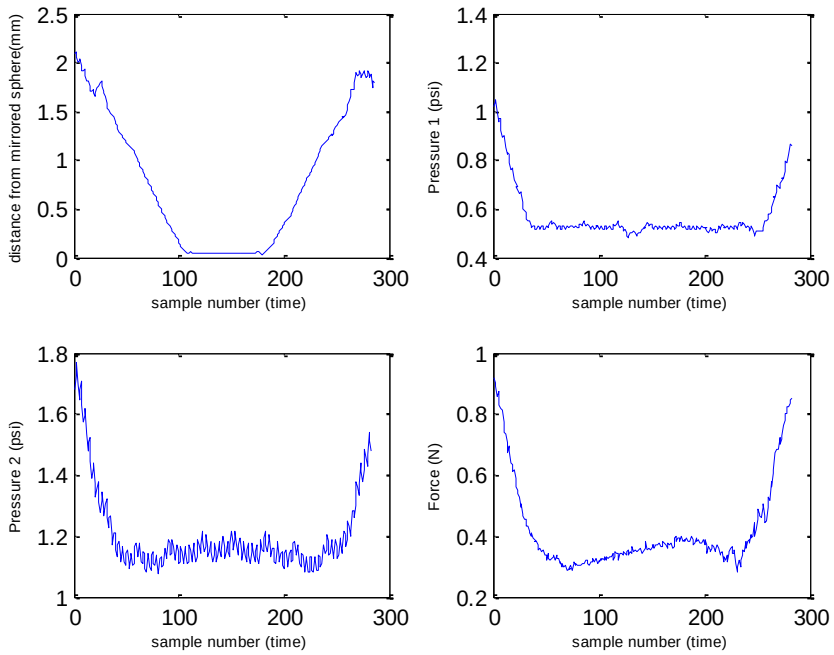

Figure 4.31: Experiment 7, the output signals of the photosensitive diode, P_{inside}, P_{comp} and the force sensor are individually plotted versus the same time period.

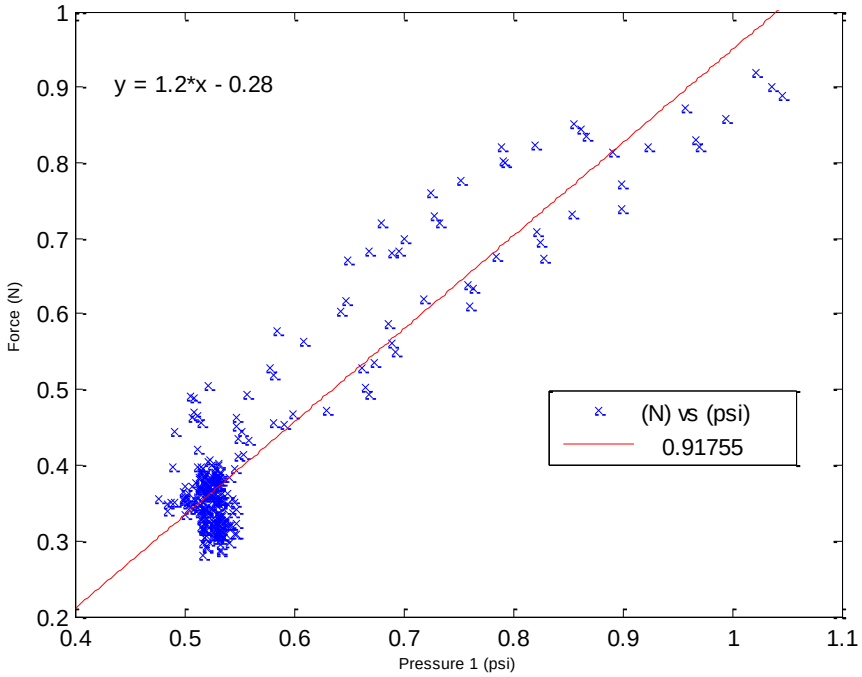

Figure 4.32: Experiment 7, force measurements versus P_{inside} measurements.

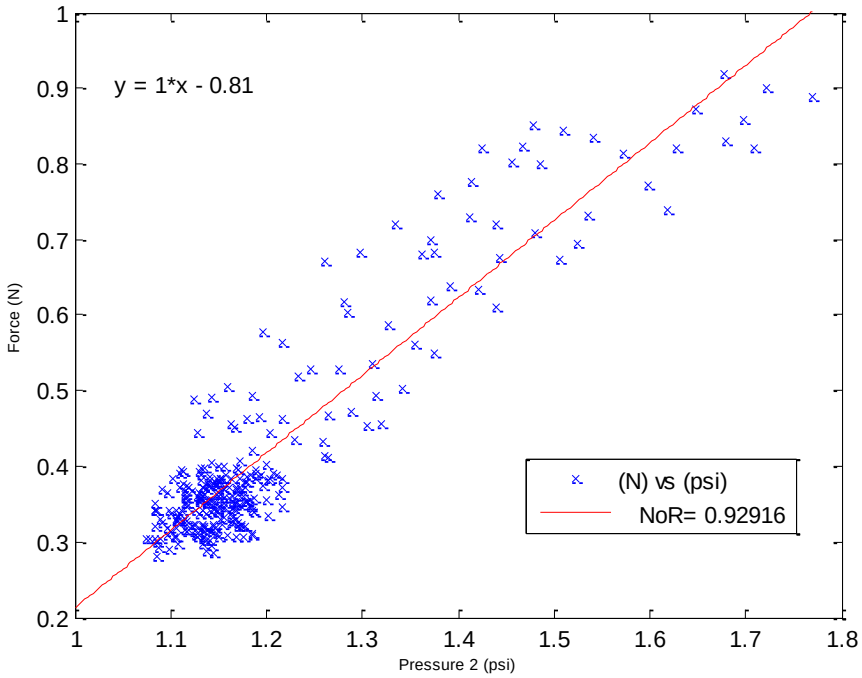

Figure 4.33: Experiment 7, force measurements versus P_{comp} measurements.

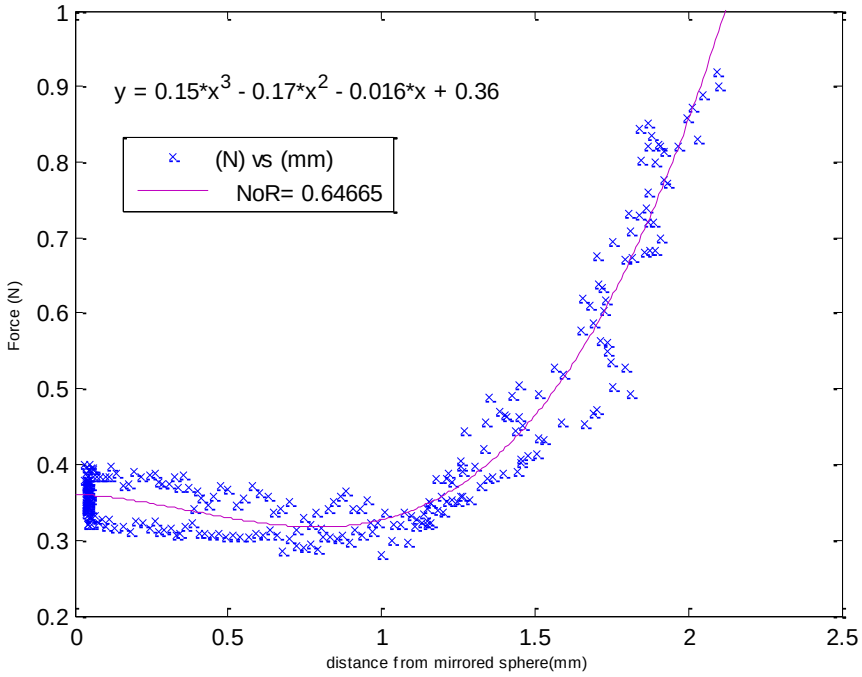

Figure 4.34: Experiment 7, force measurements versus distance from the sphere.

4.5.8 Experiment 8

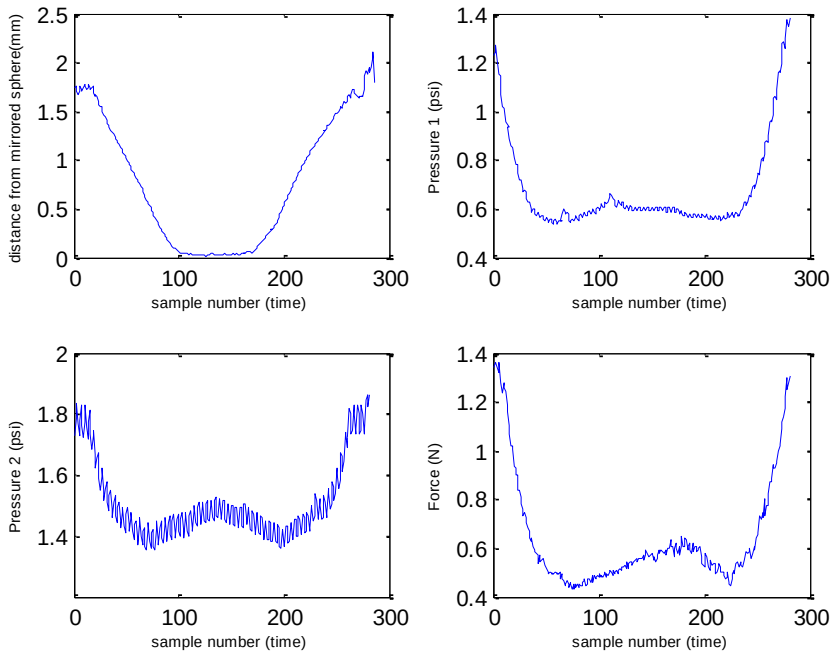

Figure 4.35: Experiment 8, the output signals of the photosensitive diode, P_{inside}, P_{comp} and the force sensor are individually plotted versus the same time period.

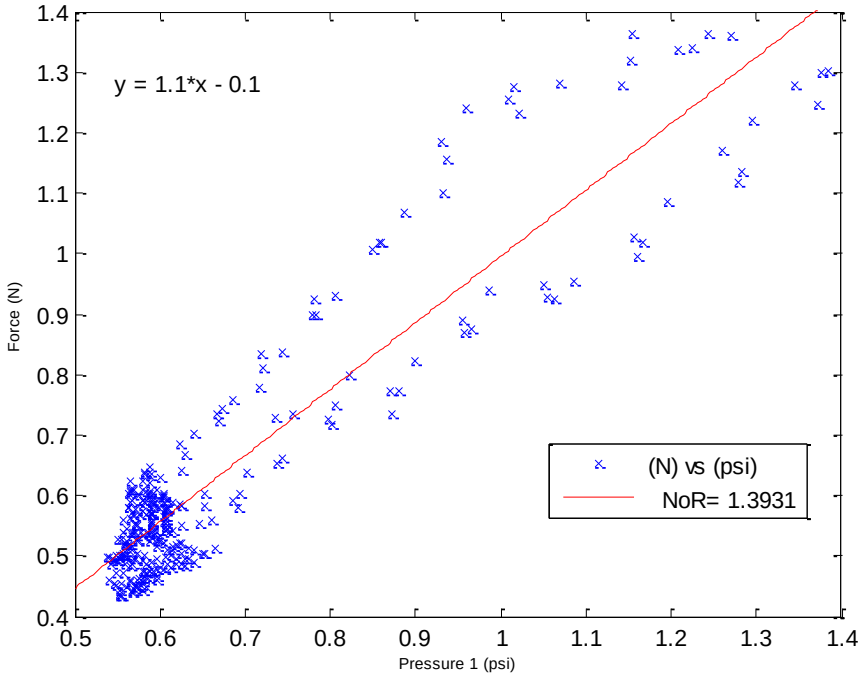

Figure 4.36: Experiment 8, force measurements versus P_{inside} measurements.

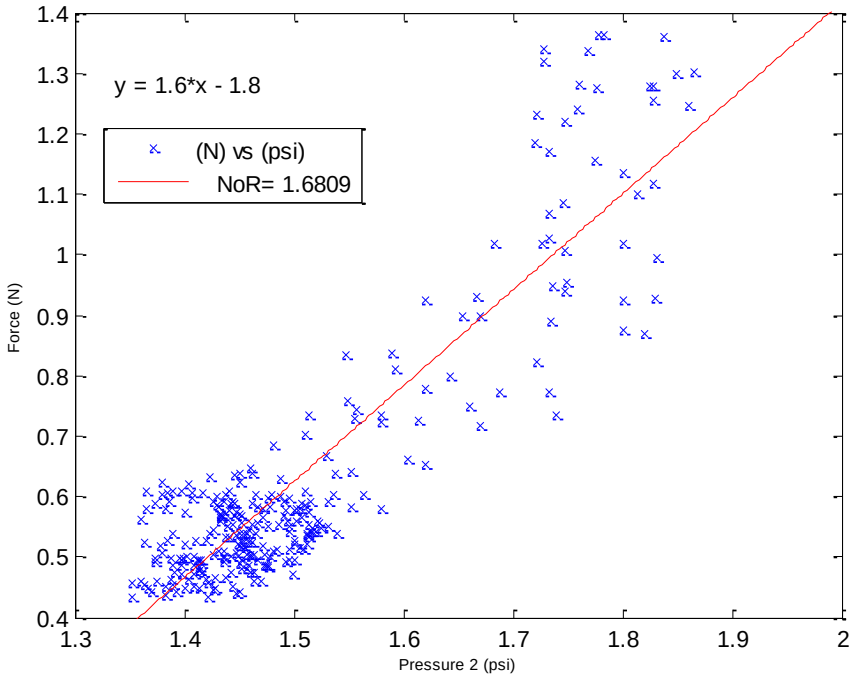

Figure 4.37: Experiment 8, force measurements versus P_{comp} measurements.

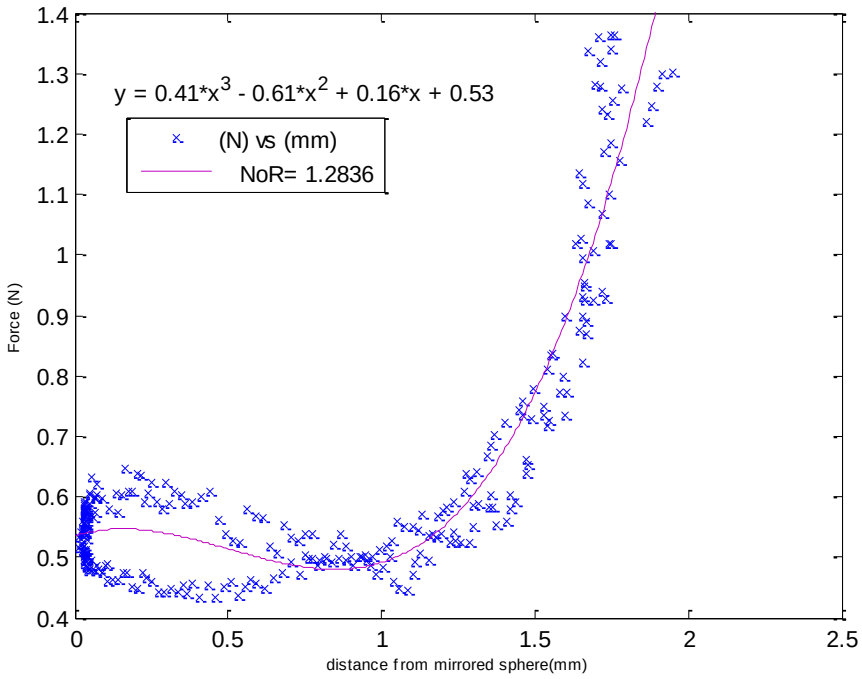

Figure 4.38: Experiment 8, force measurements versus distance from the sphere.

4.5.9 Experiment 9

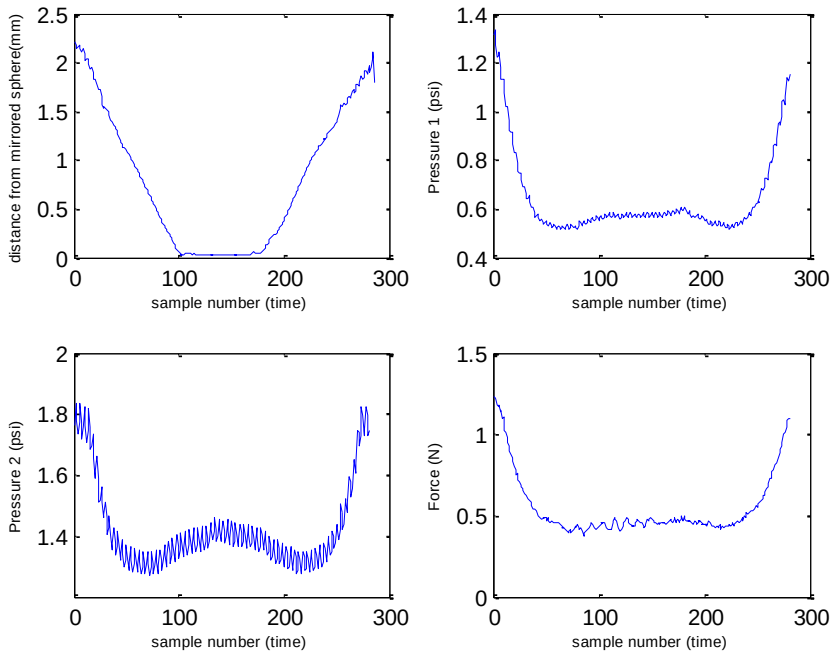

Figure 4.39: Experiment 9, the output signals of the photosensitive diode, P_{inside}, P_{comp} and the force sensor are individually plotted versus the same time period.

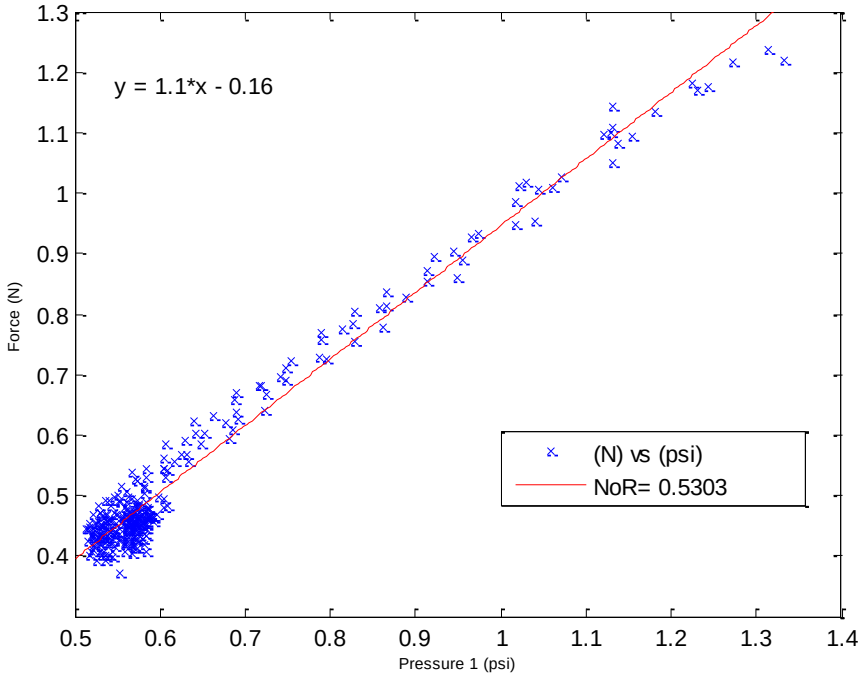

Figure 4.40: Experiment 9, force measurements versus P_{inside} measurements.

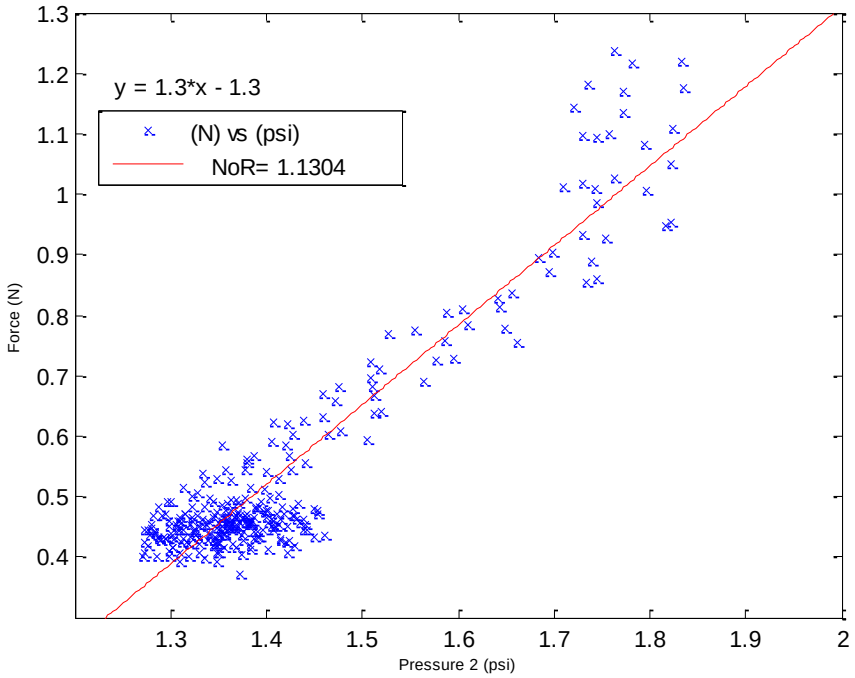

Figure 4.41: Experiment 9, force measurements versus P_{comp} measurements.

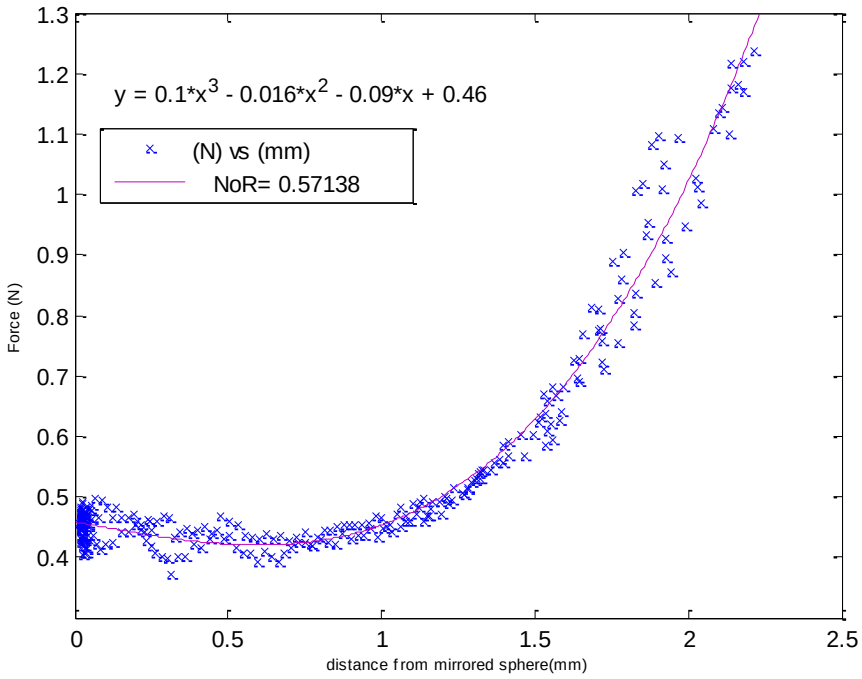

Figure 4.42: Experiment 9, force measurements versus distance from the sphere.

4.5.10 Experiment 10

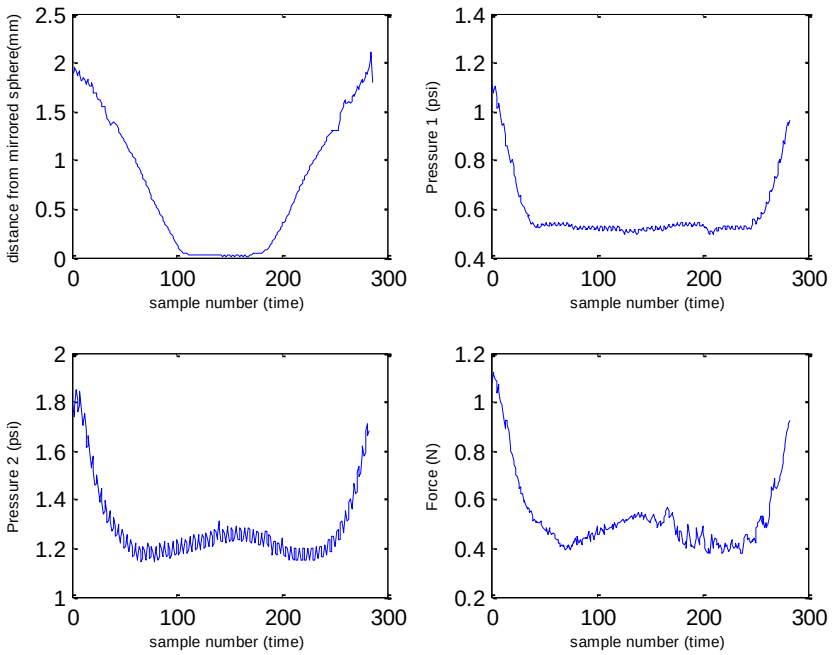

Figure 4.43: Experiment 10, the output signals of the photosensitive diode, P_{inside}, P_{comp} and the force sensor are individually plotted versus the same time period.

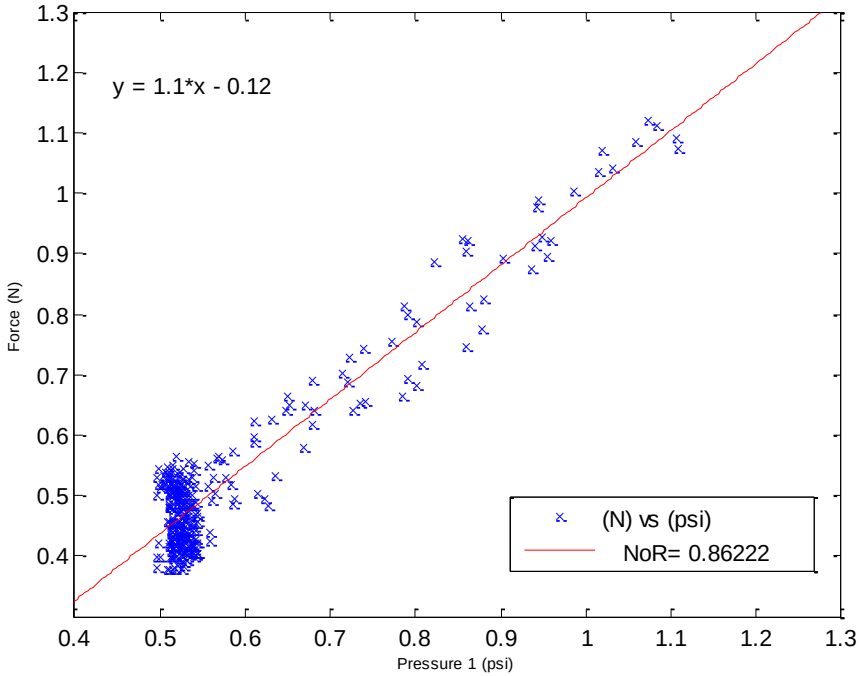

Figure 4.44: Experiment 10, force measurements versus P_{inside} measurements.

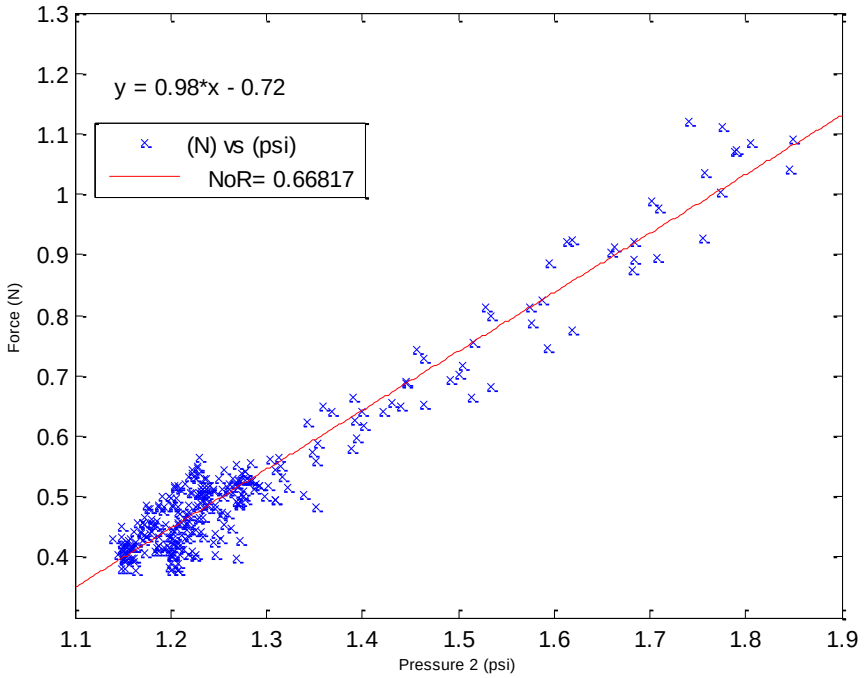

Figure 4.45: Experiment 10, force measurements versus P_{comp} measurements.

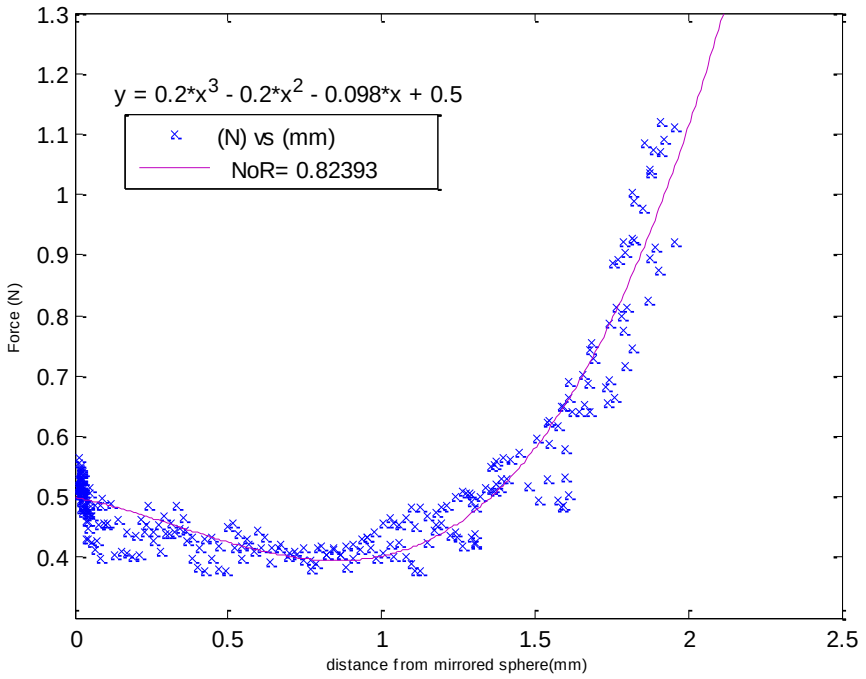

Figure 4.46: Experiment 10, force measurements versus distance from the sphere.

4.5.11 Experiment 11

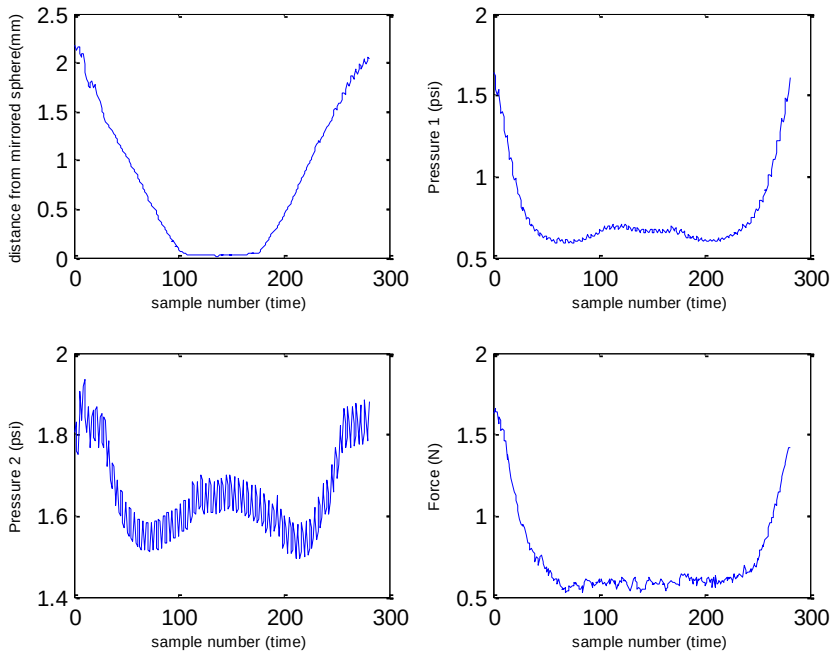

Figure 4.47: Experiment 11, the output signals of the photosensitive diode, P_{inside}, P_{comp} and the force sensor are individually plotted versus the same time period.

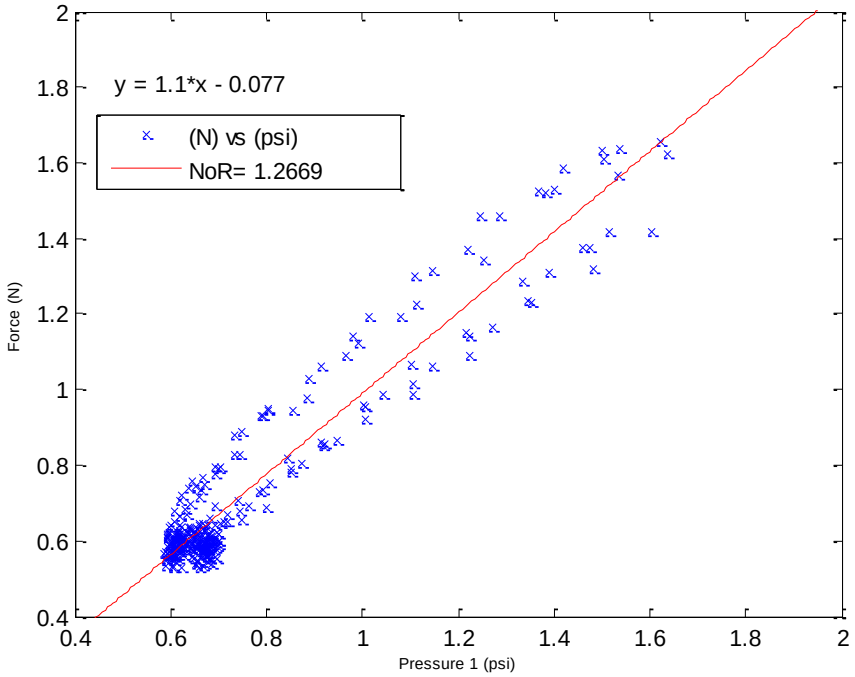

Figure 4.48: Experiment 11, force measurements versus P_{inside} measurements.

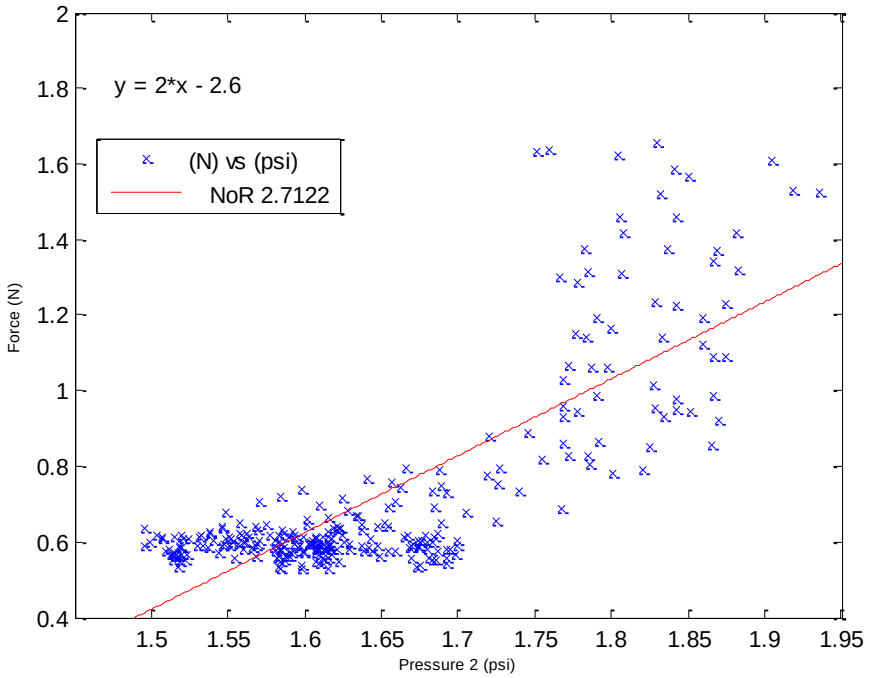

Figure 4.49: Experiment 11, force measurements versus P_{comp} measurements.

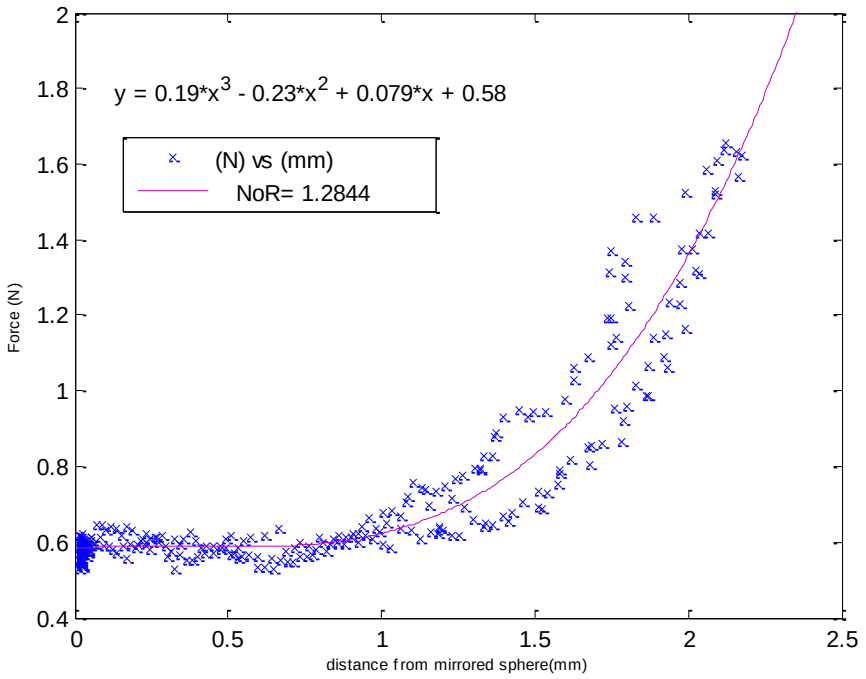

Figure 4.50: Experiment 11, force measurements versus distance from the sphere.

4.5.12 Experiment 12

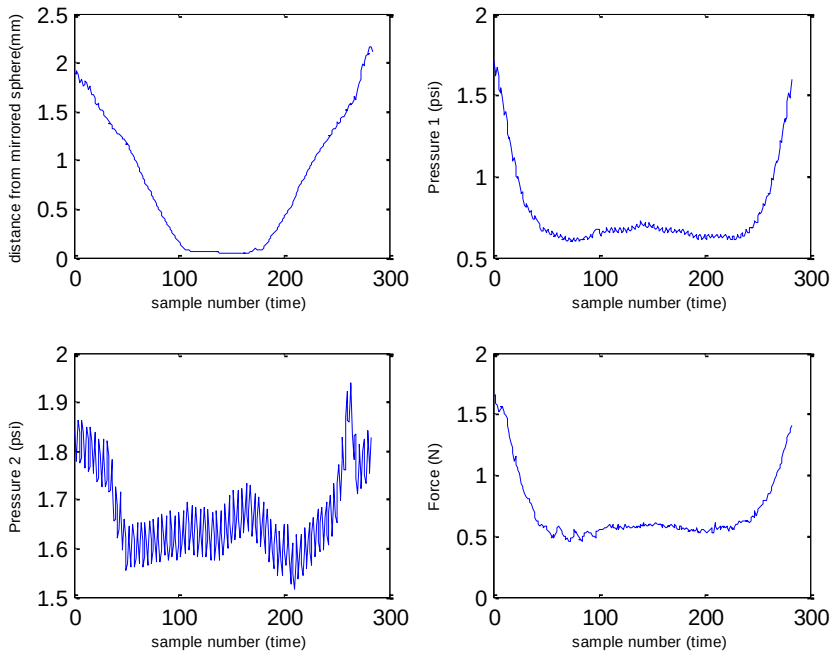

Figure 4.51: Experiment 12, the output signals of the photosensitive diode, P_{inside}, P_{comp} and the force sensor are individually plotted versus the same time period.

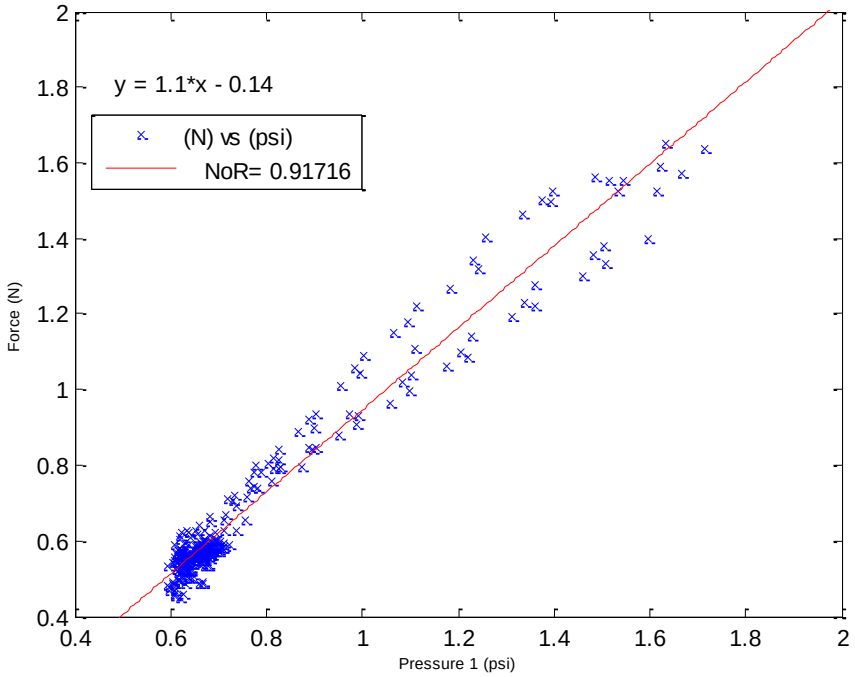

Figure 4.52: Experiment 12, force measurements versus P_{inside} measurements.

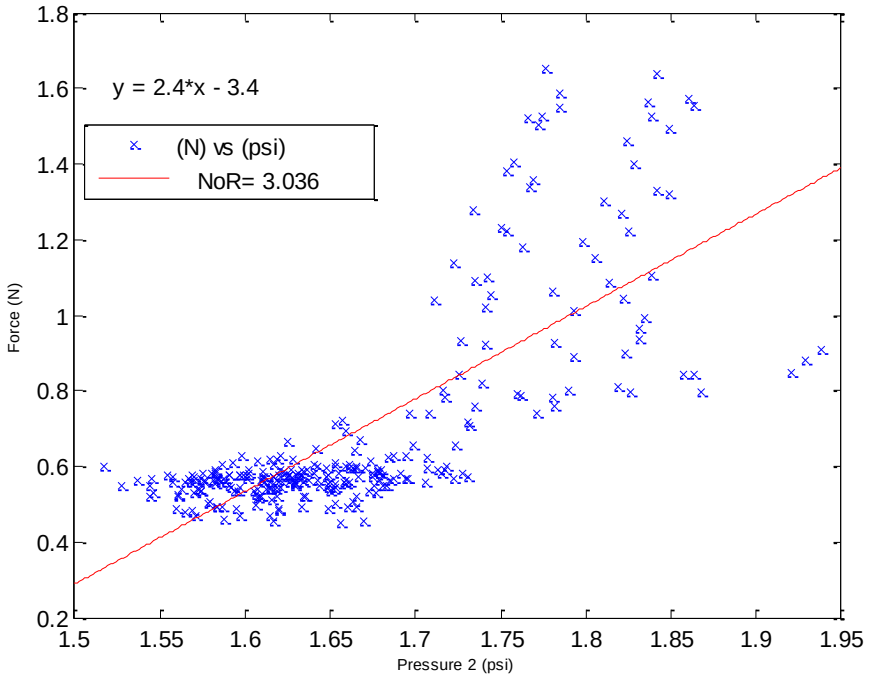

Figure 4.53: Experiment 12, force measurements versus P_{comp} measurements.

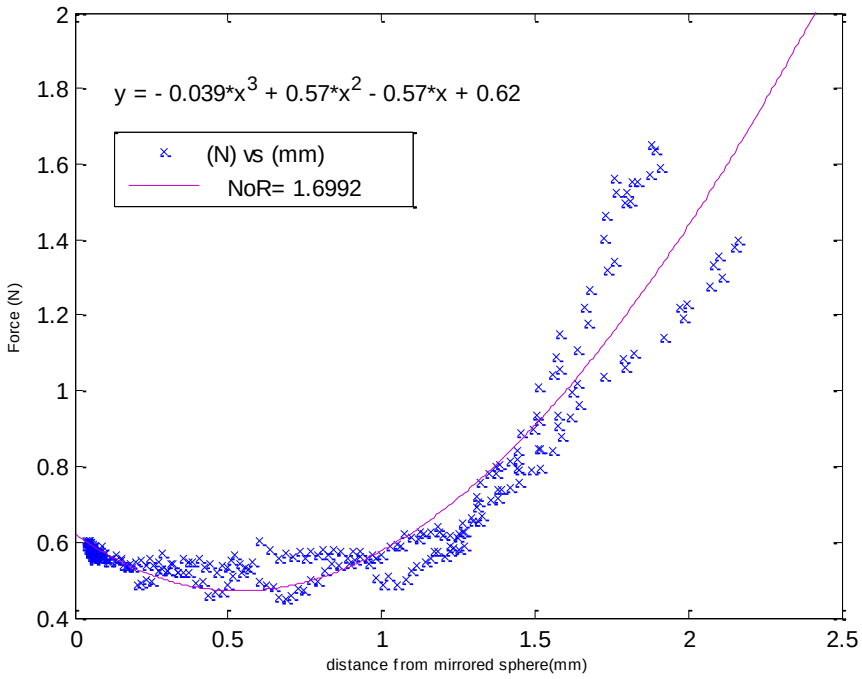

Figure 4.54: Experiment 12, force measurements versus distance from the sphere.

4.6 Discussion

The relationship between the force exerted by the spherical component and the pressure measurements of P_{comp} can be approximated by a linear function for initial pressure measurements of 1.22 psi, 1.44 psi, 1.6 psi, 1.66 psi, 1.68 psi, 1.73 psi, 1.76 psi, 1.79 psi as seen in experiments 3 to 10, respectively. The relationship between the force exerted by the spherical component and the pressure measurements of P_{inside} can be approximated by a linear function for initial pressure measurements (of P_{comp}) of 1.6 psi, 1.66 psi, 1.68 psi, 1.73 psi, 1.76 psi, 1.79, 1.80 psi, 1.84 psi as seen in experiments 5 to 12, respectively. The relationship between the force exerted by the spherical component and its displacement for set initial pressures is approximated by a cubic function for pressure measurements (based on P_{comp} measurements) of 0.86 psi, 1.01 psi, 1.22 psi, 1.44 psi, 1.6 psi, 1.66 psi, 1.68 psi, 1.73 psi, 1.76 psi, 1.79 psi, 1.80 psi, 1.84 psi as seen in experiments 1 to 12.

The functions that can be used for set pressures are summarised in the Table 4.3. It must be noted that these functions only give an approximate value for the force exerted by the spherical component.

Initial Pressure P2 (psi)	F(N) vs P1(psi)	F(N) vs P2 (psi)	F(N) vs distance (mm)
0.86			$y = 0.011x^3+0.057x^2 - 0.076x +0.18$
1.01			$y = 0.02x^3+0.052x^2 - 0.1x +0.19$
1.22		y = 0.96x - 0.56	$y = -0.0022x^3+0.13x^2 - 0.14x +0.29$
1.44		y = 1x - 0.75	$y = 0.064x^3-0.03x^2 - 0.023x +0.25$
1.6	y = 1.3x – 0.31	y = 0.91x – 0.62	$y = 0.028x^3+0.08x^2 - 0.11x +0.34$
1.66	y = 1.2x -0.2	y = 1x - 0.73	$y = 0.094x^3-0.056x^2 - 0.049x +0.44$
1.68	y = 1.2x -0.28	y = 1x - 0.81	$y = 0.15x^3-0.17x^2 - 0.016x +0.36$
1.73	y = 1.1x - 0.1	y = 1.6x - 1.2	$y = 0.41x^3-0.61x^2 + 0.16x +0.53$
1.76	y = 1.1x - 0.16	y = 1.3x – 1.3	$y = 0.1x^3-0.016x^2 - 0.09x +0.46$
1.79	y = 1.1x - 0.12	y = 0.98x - 0.72	$y = 0.2x^3-0.2x^2 - 0.098x +0.5$
1.80	y = 1.1x - 0.077		$y = 0.19x^3-0.23x^2 + 0.079x +0.58$
1.84	y = 1.1x - 0.14		$y = -0.039x^3+0.57x^2 - 0.57x +0.62$

Table 4.3: A summary is given of the functions that can be used to approximate the force exerted by the spherical component for a set initial pressure.

4.7 Conclusion

The design of Sensor 3 lends itself to a tactile and force sensor. The operating range of the optical sensing scheme has been determined and the corresponding force estimation relationships have been established of this sensor. The ability of this sensor to detect tissue abnormalities and provide force maps of the area under investigation is tested in Chapter 5.

Chapter 5 – Sensor applications

5.1 Introduction

In Chapter 3, the conceptual structure and principle of the proposed sensor was introduced with its three designs and their respective sensing principles. This chapter focuses on the experimental protocol which was employed to operate the sensors and their range of applications. The sensors are then used experimentally to establish their abilities as MIS sensors, with the results presented and discussed. Sensor 1 was tested in an non elastic environment. Sensor 1, Sensor 2 and Sensor 3 were tested on silicon phantoms with embedded nodules. Sensor 1 and Sensor 3 were also tested in an ex vivo setting on animal livers. The experimental results that are presented in experiments 1 to 4 have been published by the author in (Zbyszewski, Bhaumik, Althoefer, & Seneviratne, 2008), (Althoefer, et al., 2008), (Zbyszewski, Polygerinos, Seneviratne, & Althoefer, A Novel MRI Compatible Air-Cushion Tactile Sensor for Minimally Invasive Surgery, 2009), (Zbyszewski, Althoefer, Liu, Seneviratne, Challacombe, & Dasgupta, 2009).

5.2 Experimental procedures with Sensor 1

5.2.1 Experiment 1: Tactile sensing (feasibility study)

The first experiment that was carried out to assess the effectiveness and feasibility of Sensor 1 was to determine whether it could detect a subtle irregularity when rolled over a flat surface. The testing surface was made up of a 6 mm diameter paper clipping acquired from a paper hole puncher with a thickness of 103 μm and a number of A4 paper sheets with the same thickness each placed on top of the paper clipping. Experiments were conducted with different numbers of "covering" sheets varying from 1 to 7. The sensor was connected to the distal tip of the manipulator to achieve controlled movements of the sensor in the plane of the paper sheets. The z-axis was normal to the paper sheets (all the sheets of paper used for this experiment were A4,

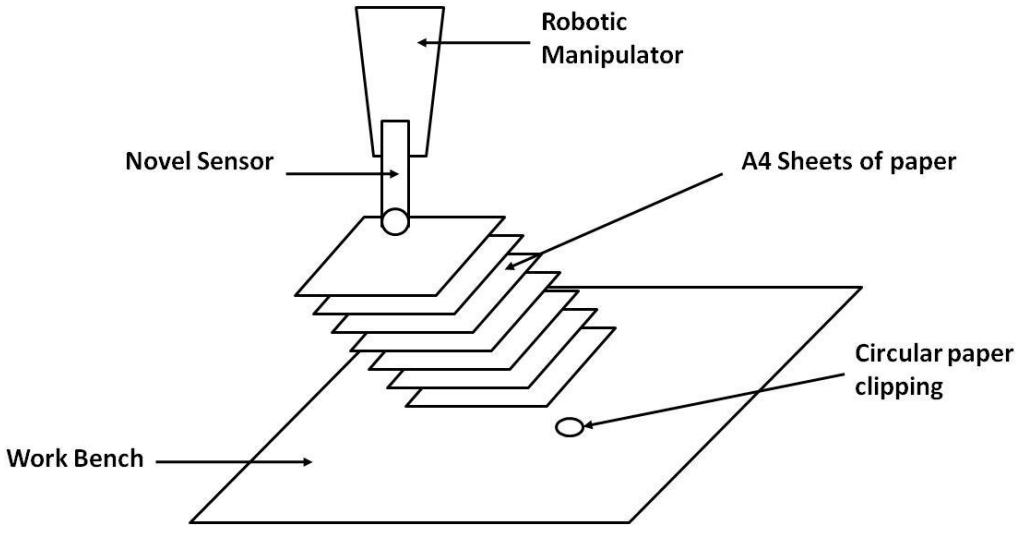

Figure 5.1: A schematic of the experimental setup illustrating the circular paper clippings and the range of A4 paper sheets that are used to cover it. The novel sensor is attached to the robotic manipulator and is normal to the surface under inspection.

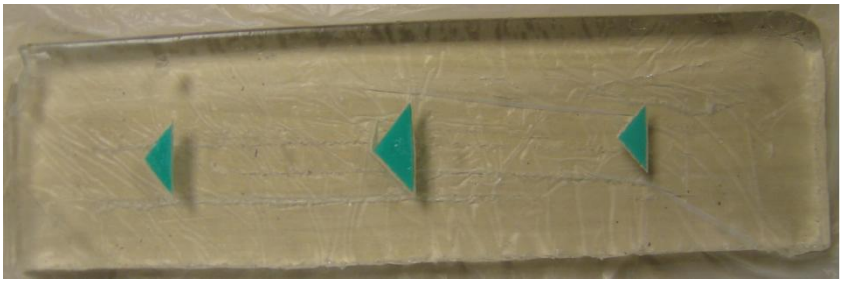

Figure 5.2: A picture of the silicone phantom used with all three embedded nodules.

80 g/m^2). A schematic of the experimental setup is illustrated in Figure 5.1.

The robotic manipulator was then instructed to roll the sensor over the paper at a constant height and at a constant speed of 4 cm/s to evaluate whether the novel sensor would detect the "buried" disc of paper. The experiment was repeated by adding an additional sheet of paper on top of the disc until it was covered by 7 layers of paper.

5.2.2 Experiment 2: Silicone Phantom

Following the sensor's performance in the previous experiment in a non elastic environment, there was a need to establish its ability on an elastic-tissue like surface. In this experimental study, the silicone phantom with the embedded nodules was used to approximate the behaviour of the sensor when rolled over areas of tissue with abnormalities.

The silicone rectangloid that was used had a length of 184 mm, a width of 60 mm, and a height of 17 mm, it is illustrated in Figure 5.2. In Figure 5.2, the triangle on the far left was triangle 1, the centre one was triangle 2 and the one on the far right was triangle 3. The dimensions of the three nodules are clearly illustrated in Figure 5.3.

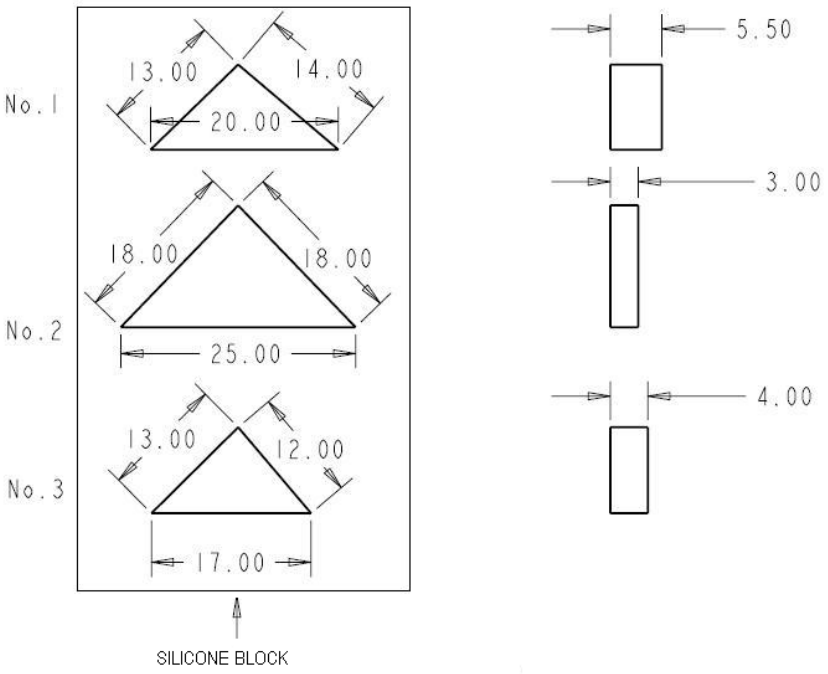

Figure 5.3: The dimensions of all triangular nodules are in milimeters.

The three nodules of varying dimensions were lodged in the silicone phantom. The nodules were aligned along the central strip of the silicone block with 60 mm separating one another.

At the start of the experiment, the compressor was set to generate an air pressure of 14kPa. The sensor which was normal to the silicone phantom was positioned in such a way that its spherical component was in the top right hand corner of the silicone phantom and was rolled at a constant speed of 4 cm/s to the bottom right hand corner of the phantom while the signal outputs of the photosensitive diode were recorded for that roll. The sensor was then placed back to the top of the phantom but shifted to the left by 3 mm from its original position. Another set of data was collected for that second roll. This process was repeated 13 times so that the sensor would have rolled over the entire phantom in 13 strips. The distance between the sensor and the silicone

phantom was kept constant at all times. The speed at which the rolls were carried out was also kept constant.

5.2.3 Experiment 3: Excise porcine liver

An experimental procedure using animal tissue was carried out to establish the capabilities of Sensor 1. The chosen surface under inspection was an excised sample of porcine liver. The liver sample was approximately 50x55x20 mm. The liver sample was placed onto a polystyrene board accompanied by 5mm diameter pin heads that acted as abnormalities within the porcine liver. These were placed in the board and under the liver. The first, second, and third pin heads were located beneath liver thicknesses of 21, 19, and 17 mm, respectively. During this trial the compressor generated a pressure of 14 kPa while connected to Sensor 1. The sensor was rolled over the porcine liver at a constant speed of 4 cm/s in 10 parallel and adjacent paths of length 50 mm. The constant parameters for this experiment were the vertical position of the sensor and the speed of rolling. The output signals acquired from the photosensitive diode were recorded.

5.3 Experimental results with Sensor 1

5.3.1 Experiment 1: Tactile sensing (feasibility study)

The sensor successfully detected the circular clipping of paper placed under the various layers of papers. The readings given by the sensor when it was rolled over flat, undisturbed sections of the sheet was 10V. The photosensitive diode was calibrated at a reading of 10V for this vertical position, so that any vertical displacement of the sphere would be detected. The voltage reading when the sensor

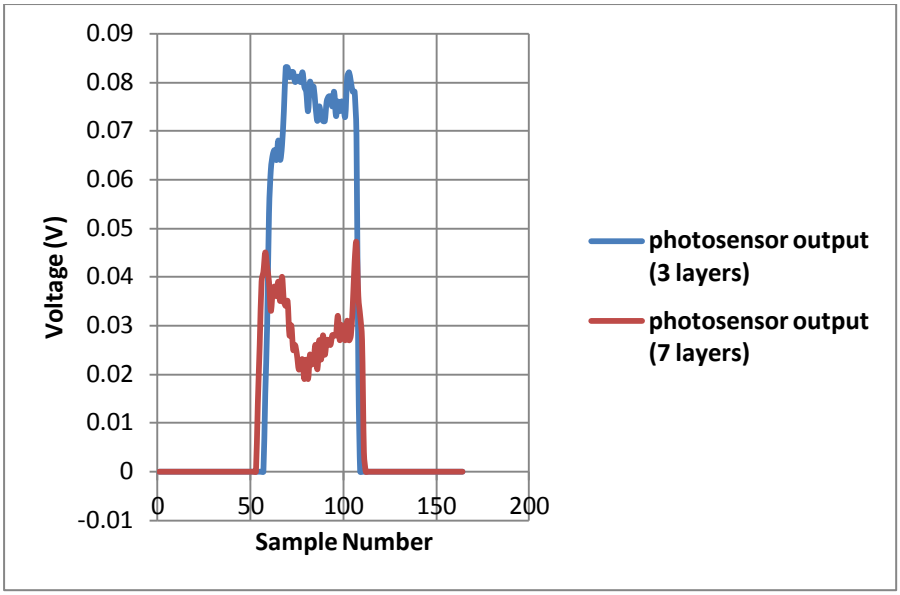

Figure 5.4: The voltage outputs of the sensor when it is rolled over the circular paper clipping that is hidden under 3 layers of paper (in blue) and under 7 layers of paper in (in red).

was rolled over the circular paper clipping that was covered by 3 layers of paper was 9.917V and was 9.953V when the number of layers was increased to 7. In order to facilitate the interpretation and plotting of the data, the readings were inverted generating peak values of 0.083 V and 0.047V for the output voltages of the photosensitive diode for 3 and 7 layers respectively. The output voltages are plotted in Figure 5.4.

In Figure 5.4Figure 5.4, the red graph shows the trace of the disk clipping that under 7 layers of paper and the blue graph illustrates the trace under 3 layers of paper. The dip in voltage between both peaks for both graphs is a reflection of the outer ridges of the circular paper clipping obtained through the use of a paper hole puncher. The difference in voltage between the two peaks is 0.036V. The thickness of one layer of A4 (80 g/m^2) paper is estimated at 0.103 mm. This difference in layers is four layers of A4 paper which generate a thickness of 0.412 mm and a sensitivity of 0.036V. The

outcome is a displacement of 0.1 mm leading to a change in voltage of 0.087V. These results are only indicative as the sensor was tested on a non-elastic surface and do not predict the behaviour of the sensor on a soft tissue surface. Independent tests conducted manually where the researchers probed the test environment with their fingers showed that the clipping was virtually undetectable under 7 layers of paper.

5.3.2 Experiment 2: Silicone Phantom

Following the experiment, the data for each of the 13 parallel and adjacent rolls over the silicone block which was generated by the photosensitive diode was processed. Each roll was plotted to observe whether the nodules were detected by the sensor. Once again, in order to facilitate the interpretation and plotting of the data, the readings were inverted. The plots of the 6th, 7th and 8th roll are illustrated in Figure 5.5, Figure 5.6 and Figure 5.7 respectively.

In Figure 5.5, Figure 5.6 and Figure 5.7, the plots visibly illustrate the presence of the 3 embedded nodules detected during each roll. As the plots clearly illustrate the accuracy and ability of the sensor at detecting the three embedded nodules, a three dimensional map of the silicone phantom can be generated, as shown in.

The three dimensional representation of the silicone block and the position of its three nodules within the block are clearly portrayed in Figure 5.8.

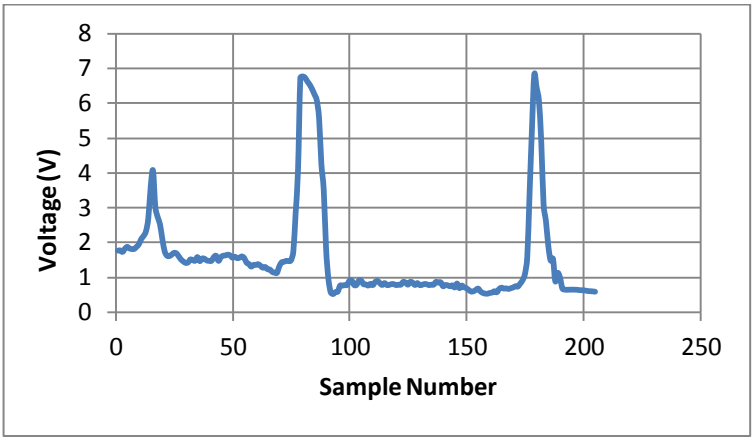

Figure 5.5: The graph of the 6th roll showing the three peaks representing the three embedded nodules.

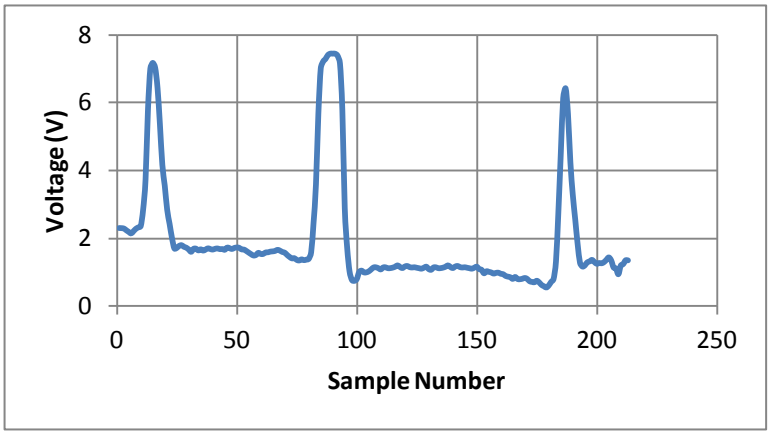

Figure 5.6: The graph of the 7th roll showing the three peaks representing the three embedded nodules.

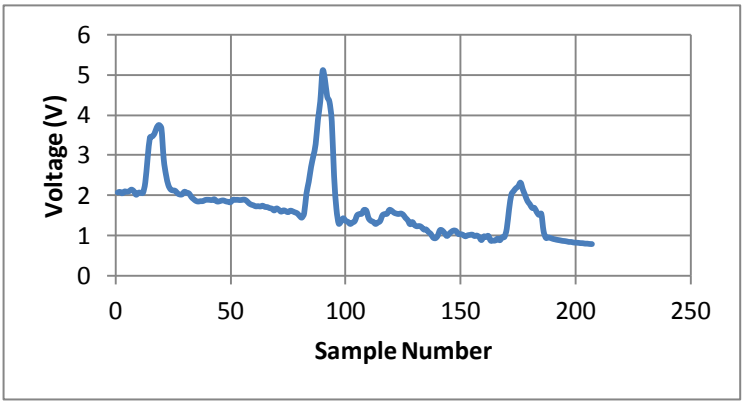

Figure 5.7: The graph of the 8th roll showing the three peaks representing the three embedded nodules.

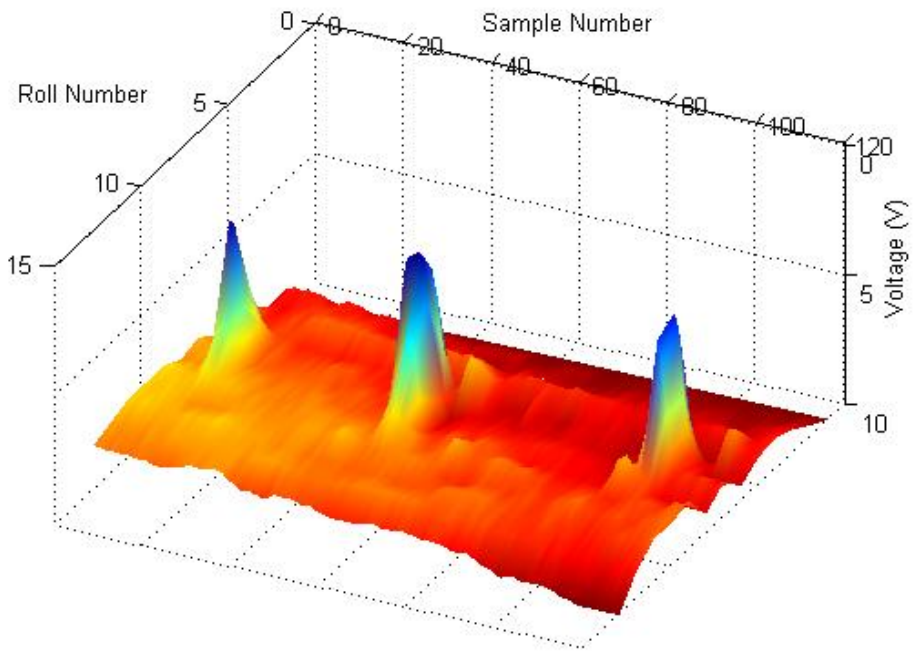

Figure 5.8: A rolling map of the silicone phantom with the location of the three embedded nodules.

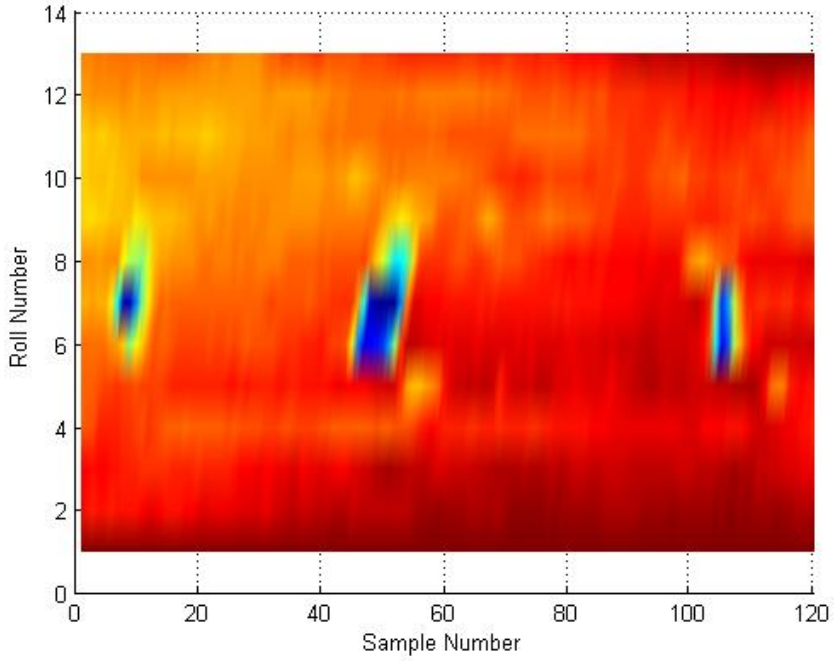

Figure 5.9: The top view of the silicone phantom rollover map map clearly illustrating in blue the location of the three embeddded nodules.

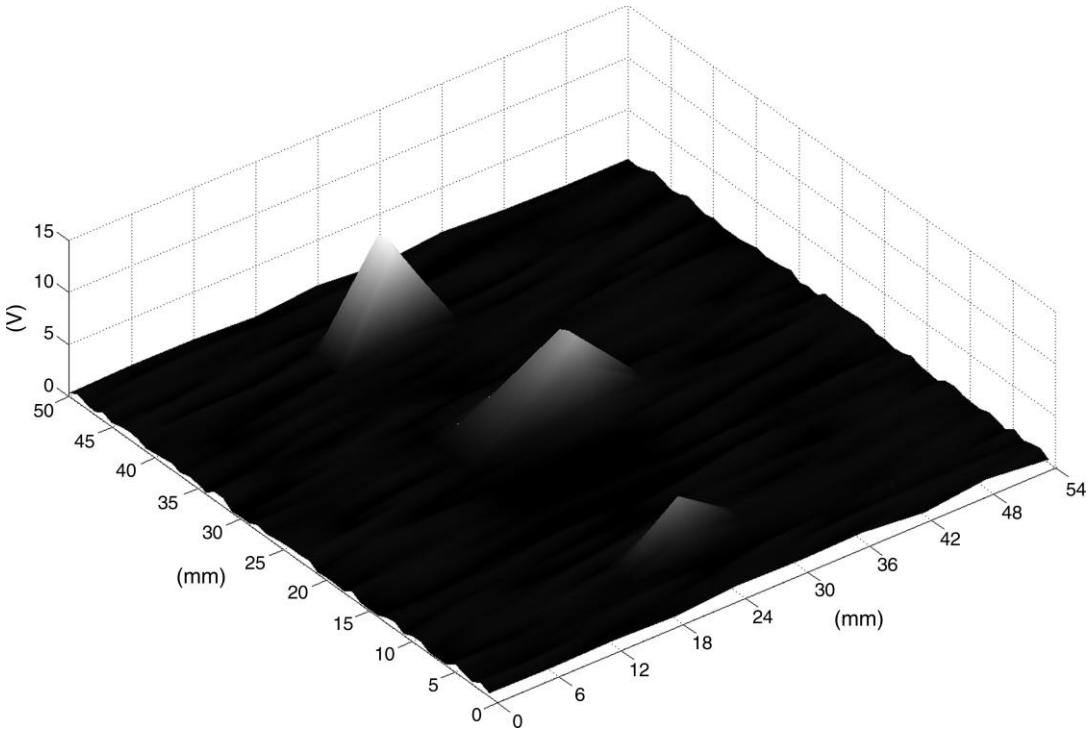

Figure 5.10: Rolling map of the excised porcine liver and the location of the three embedded pins.

The areas of blue coloration in Figure 5.8 and Figure 5.9 indicate an area of greater stiffness which represents the locations of the embedded nodules in the silicone phantom. The dimensions of the peaks and their width are also proportional to the size of the nodules

The conducted experimental study showed the potential of this sensing concept in locating and mapping different levels of tissue stiffness. The next step to validate this sensor was to perform an experimental study on an organ with embedded abnormalities. Due to the ethical and clinical restrictions in the United Kingdom of using human organs for experimental studies; this had to be performed on either an excised porcine liver or an excised porcine kidney as they are some of the organs that resemble the closest in shape and size their human equivalent organs.

Figure 5.11: Rolling map of the excised porcine liver and the location of the three embedded pins.

5.3.3 Experiment 3: Excised porcine liver

A stiffness map of the liver surface under investigation is shown in Figure 5.10. The areas of lighter colouring represent areas of increased stiffness. It can be observed three such areas are clearly visible on the map. The areas of increased stiffness are an accurate representation of the location of the pinheads that where placed under the excised liver. The sensor accurately detected the position of the pin heads under the varying thicknesses of porcine liver.

5.4 Experimental procedures with Sensor 2

5.4.1 Experiment 4: Silicone phantom rollover – Comparative study

This experiment was carried out to establish the feasibility of Sensor 2 as a tactile sensor for MIS and to compare its ability to the wheeled probe sensor described in

(Liu H. , Noonan, Althoefer, & Seneviratne, 2008). The wheel probe sensor used an expensive high resolution industrial force/torque sensor whereas Sensor 2 was a low cost sensor. The comparison study was performed to establish whether despite these differences, Sensor 2 was fit for purpose. The wheel force sensor was made of an aluminium wheel which had a diameter of 8 mm and a width of 8 mm which was used as the end-effector. The wheel was grooved with 12 teeth along its circumference to avoid slip during rolling; this is illustrated in Figure 5.11. A Force/Torque sensor (ATI Nano 17) was paired with a DAQ card (NI PCI 6034E 16-bit resolution DAQ) and was mounted between the cylindrical wheel and the distal tip of the robotic manipulator.

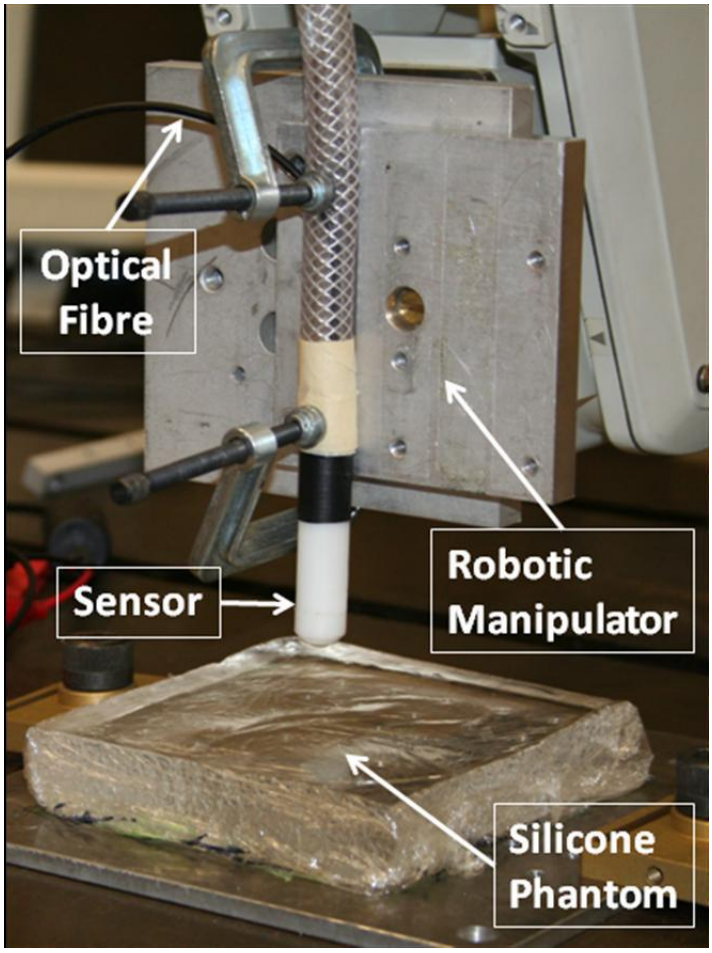

Figure 5.12: The experimental set-up of the silicone rollover experiment displaying the silicone phantom, the sensor attached to the robotic manipulator and the optical fibre that is hermetically inserted into the sensor through the tube that is connected to the compressor.

The sensor were used to investigative a silicone phantom. The phantom had dimensions of 100 mm x 100 mm and thickness 20 mm. The experimental set up is illustrated in Figure 5.12. Two soft silicone nodules were placed under the silicone phantom to approximate the behaviour of the sensor when rolled over areas of tissue with abnormalities. The use of soft nodules made the task of finding areas of increased stiffness more difficult due to their elasticity. These conditions approached more closely an in vivo environment where tissue abnormalities such as tumour have a certain degree of elasticity. The two nodules were name Nodule A an Nodule B.

They were of cylindrical shape with a diameter of 5 mm and with heights of 6 mm and 2 mm for Nodule A and Nodule B, respectively. The nodules are illustrated in Figure 5.14 next to a one Pound Sterling coin. The nodules were positioned vertically under the silicone phantom just as they are displayed in Figure 5.13and Figure 5.14.

At the start of the experiment the compressor was set to generate a pressure of 6.9kPa, creating a constant air flow. Sensor 2 was rolled over the silicone phantom at a constant speed of 4 cm/s in 8 parallel and adjacent rolls to cover the area under which the nodules were buried. For each roll the signal output of the photosensitive diode was collected.

The force torque sensor was also rolled over the silicone phantom in 8 parallel and adjacent paths to detect the silicone nodules. The force measurements of the force/torque sensor were recorded during this process.

The speed at which the rolls were carried out was kept constant for both sensors. The indentation depth of the sensors onto the silicone phantom was set to 1.5 mm.

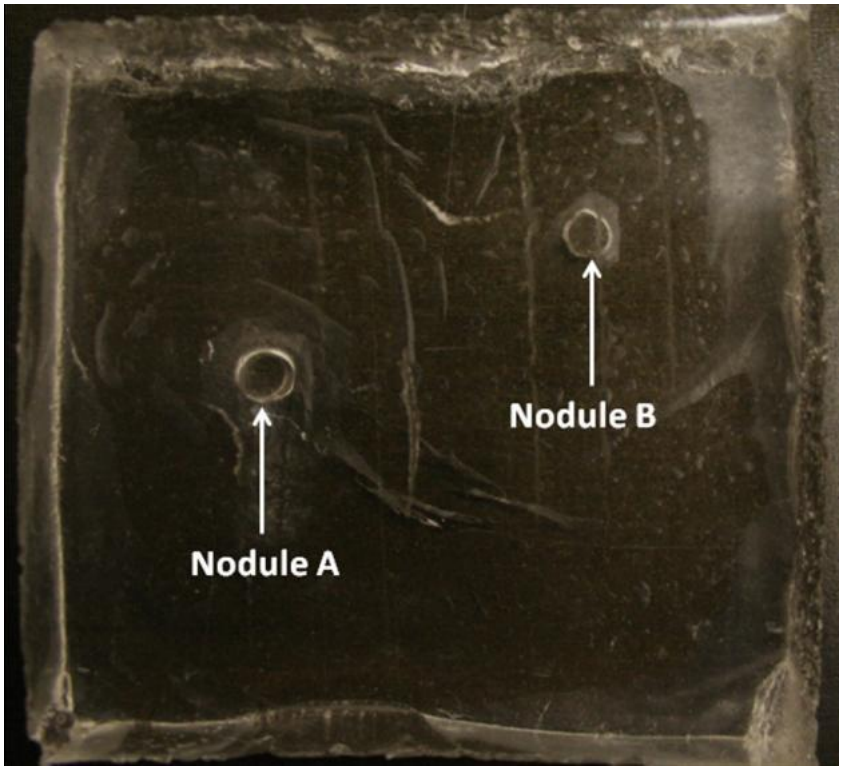

Figure 5.13: Nodule A and nodule B covered with the silicone phantom to generate "abnormalities".

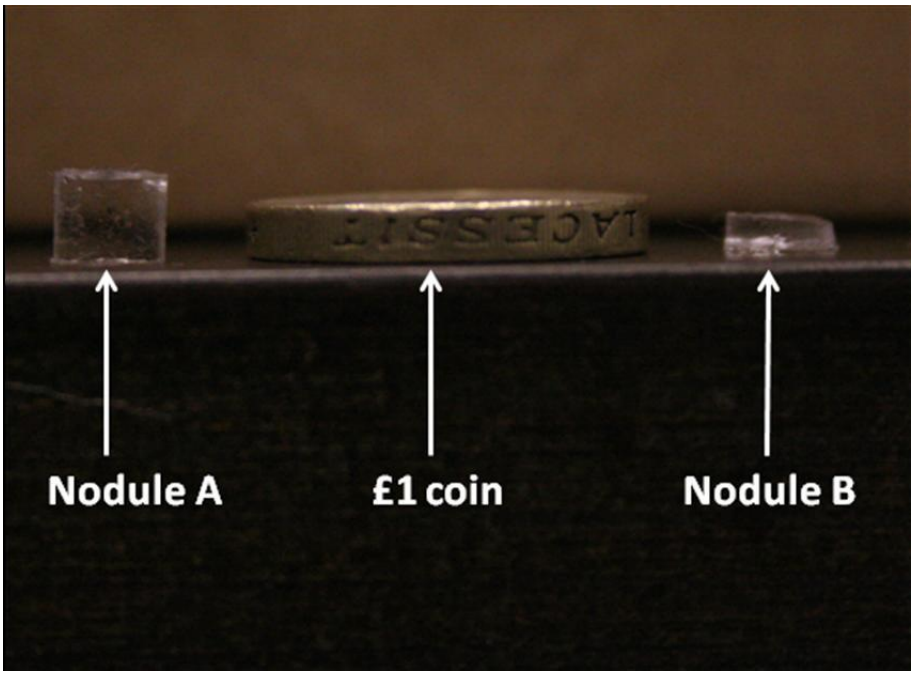

Figure 5.14: Nodule A and Nodule B next to a Pound Sterling coin

5.5 Experimental Results with Sensor 2

5.5.1 Experiment 4: Silicone Phantom Rollover – Comparative study

The signal outputs recorded by the photosensitive diode for Sensor 2 and the ones recorded by the force/torque sensor for the wheeled probe sensor during the process of rolling indentation were used to generate stiffness maps of the area under investigation.

The map generated by using the signal outputs of the photosensitive diode for Sensor 2 is shown in Figure 5.15. The red colour indicates the highest stiffness area where as the yellow area indicates an area of lesser stiffness and with the blue colour indicating an area of low stiffness Nodule A can clearly be identified where as nodule B is less prominent. The reason for which Nodule A is surrounded by a vast yellow area is that its height of 6 mm raises the surrounding area of the top of the nodules consequently raising the silicone phantom from underneath. The same phenomenon happens with Nodule B but this is less visible as it has a height of 2 mm.

The map generated by using the output signals of the force/torque sensor for the wheeled probed is illustrated in Figure 5.16. The same colouring scheme is used as in Figure 5.15 to identify areas of greater stiffness. The locations of Nodule A and Nodule B were successfully detected by the wheel probe sensor was it can be seen on the stiffness map.

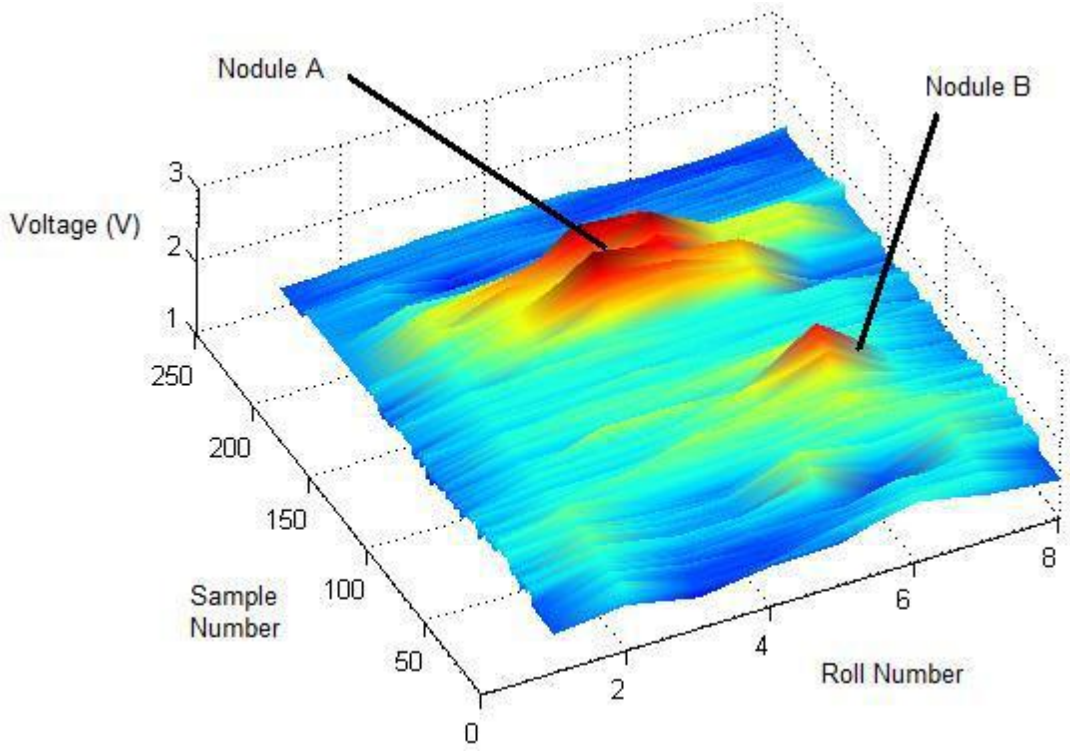

Figure 5.15: A three dimensional plot of the silicone block illustrating the positions of nodule A and nodule B.

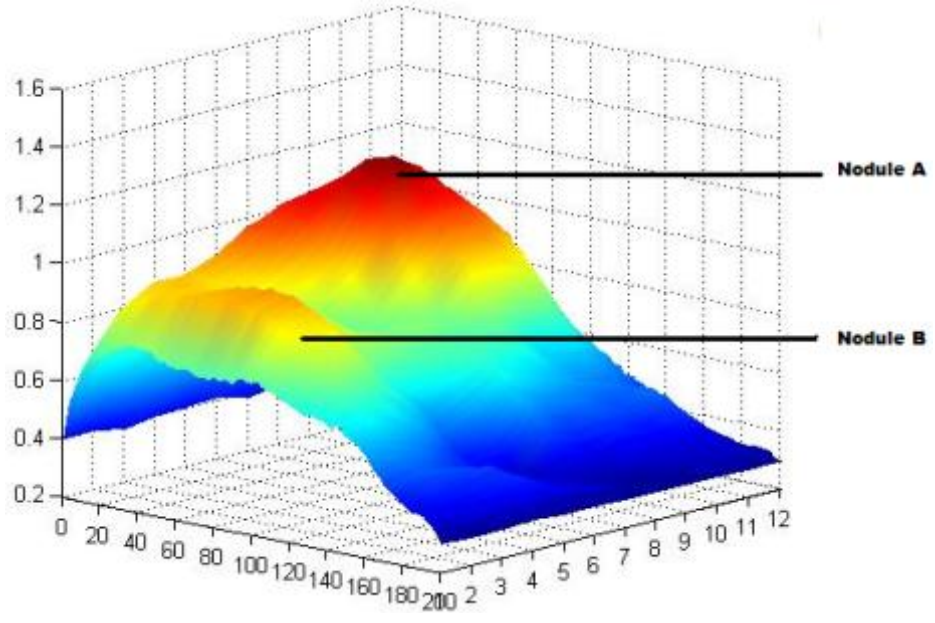

Figure 5.16: A stiffness map of the silicone phantom illustrating the location of Nodule A and Nodule B.

5.6 Experimental Procedures with Sensor 3

5.6.1 Experiment 5: Silicone Phantom

In this experiment, Sensor 3 was used to attempt to detect embedded nodules in a silicone phantom. The silicone phantom used had a surface of dimensions 100 mm by 100 mm and a thickness of 20 mm. There were 9 embedded nodules positioned in a three row by three column grid. Each row was composed of three spherical nodules of different sizes. The first, second and third nodules, were named Nodule 1, Nodule 2 and Nodules 3 and had a diameters of 9 mm, 6 mm and 5 mm, respectively. The nodules in the first row were embedded 1 mm below the surface of the silicone phantom. The second row of nodules were embedded in middle of the thickness of the phantom so that Nodule 1,Nodule 2 and Nodule were 6 mm, 7 mm and 8 mm, respectively, below the surface of the silicone phantom. The third row of nodules were located below the surface of the phantom at depth of 11 mm, 14 mm and 15 mm for Nodule A, Nodule B and Nodule C, respectively. A picture of the silicone phantom with the location of its nine nodules set up in three rows is illustrated in Figure 5.17.

Sensor 3 was rolled over each row individually in 3 parallel and adjacent paths at a constant speed of 4 cm/s. This process was repeated for a range of pressures and indentation depth until the nodules was detected. The signal output of the photosensitive diode was used to plot the corresponding stiffness map. Force maps were plotted using the force estimation relationship established between the distance of the spherical component and the force exerted given for a set pressure.

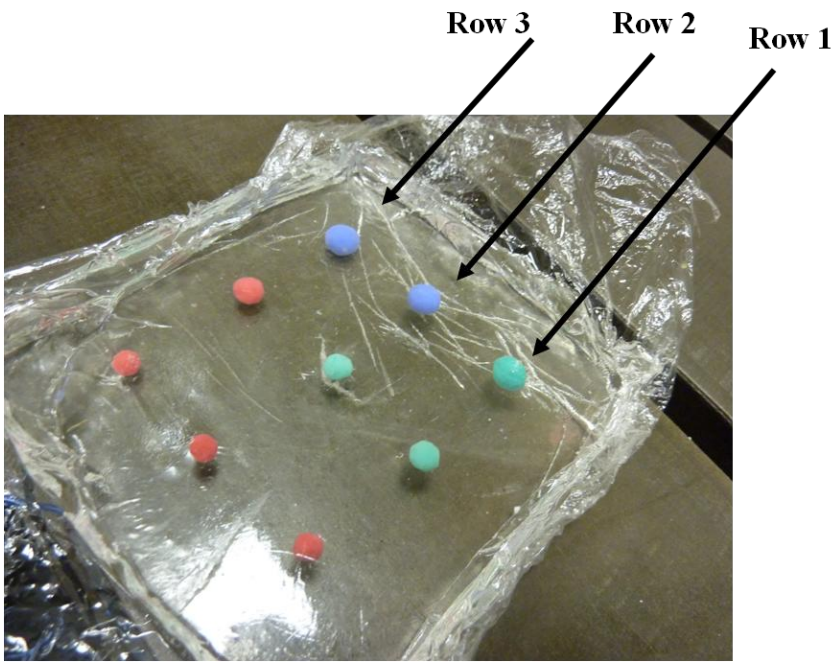

Figure 5.17: The silicone phantom with its 9 nodules in 3 rows.

5.6.2 Experiment 6: Excised porcine liver

This experiment was carried out to establish Sensor 3's ability at detecting soft and hard nodules in an animal organ. An excised porcine liver was used as it is an organ that resembles the closest in shape and size its human equivalent. The area of the liver used had dimensions of 800 mm by 560 mm. Its thickness ranged from 12 mm to 26 mm .The liver was embedded two soft nodules and two hard nodules. The two soft nodules were spherical in shape and had diameters of 5.3 mm. The two hard nodules were also spherical and had a diameter of 4.5 mm. A soft and a hard nodule were placed inside the liver through lateral incisions at a depth of 15 mm in a smooth area of the liver. In a rugged area of the liver that had a embedded connecting tissues, one soft and one hard nodules were placed through lateral incisions at a depth of 23 mm from the surface of the liver.

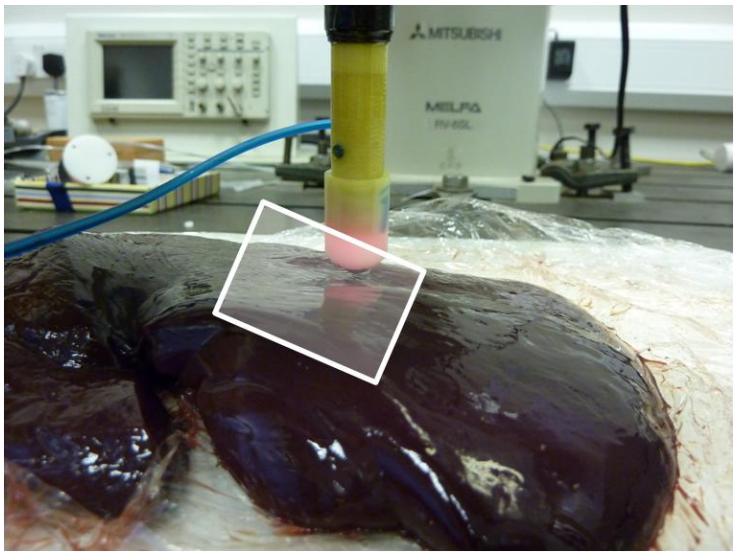

Figure 5.18: The excised porcine liver with the area under inspection highlighted.

The excised liver was placed on a polystyrene board and the sensor was rolled at a constant speed of 4 cm/s over it for a range of pressures. The area of the liver that was inspected is illustrated in Figure 5.18.

The resulting signal output of the photosensitive diode was used to plot the corresponding stiffness maps. Force maps were plotted using the force estimation relationship established between the photosensitive output signal and the force exerted given for a set pressure.

5.7 Experimental results with Sensor 3

5.7.1 Experiment 5: Silicone Phantom

The first row of the silicone was inspected with an indentation depth of 3 mm and with a pressure of 1.22 psi. The stiffness and force plots are shown in Figure 5.19 and Figure 5.20.

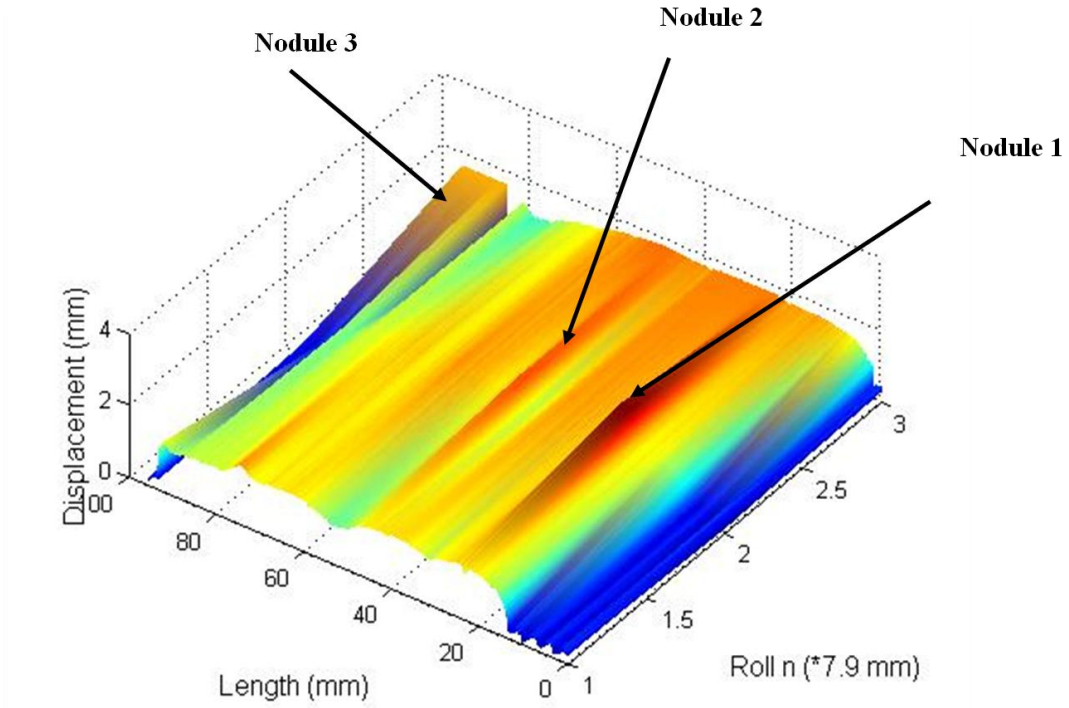

Figure 5.19: Stiffness map of row 1 illustrating the position of the nodules.

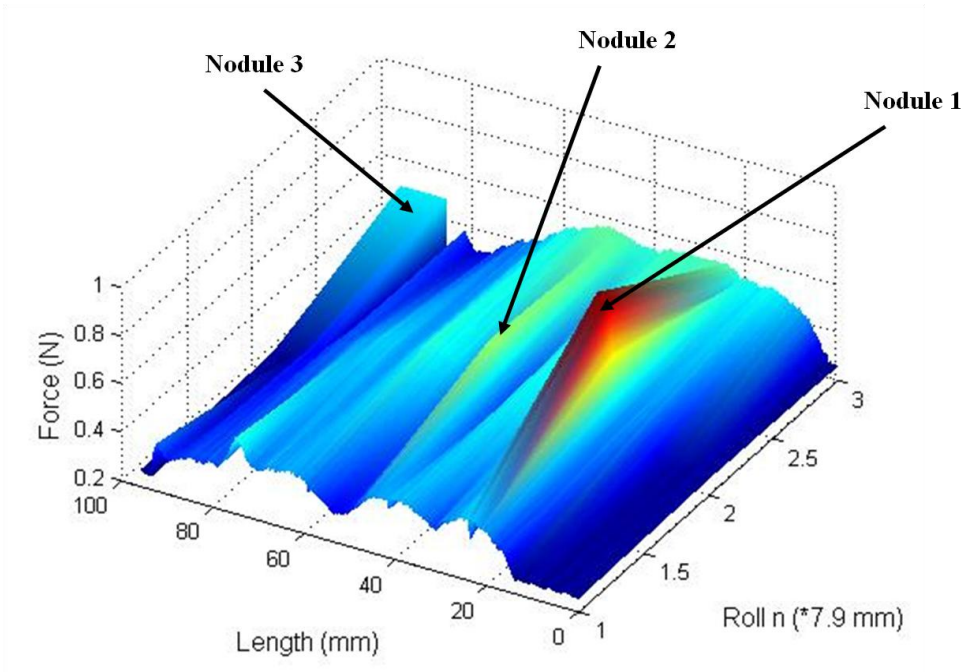

Figure 5.20: Force map of row 1 showing the force exerted by the nodules.

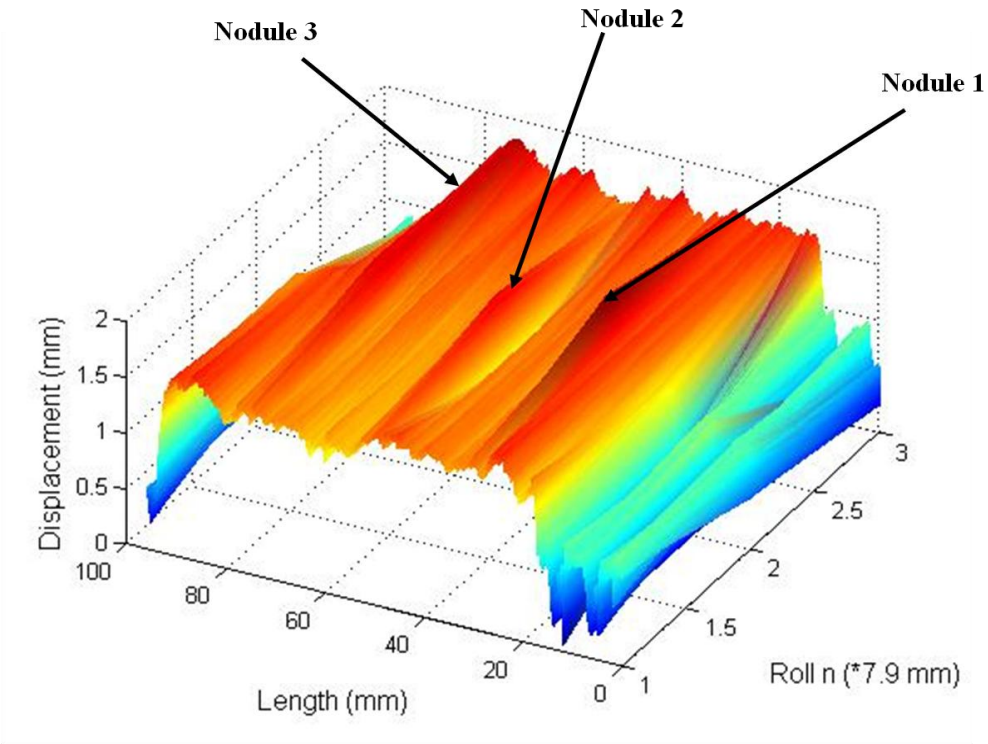

Figure 5.21: Stiffness map of row 2 illustrating the position of the nodules.

The second row of nodules was inspected at an indentation depth of 8 mm with a pressure of 1.76 psi. The stiffness map and force map are shown in Figure 5.21 and Figure 5.23.

The third row of the silicone phantom was inspected with a rolling indentation depth of up to 9 mm but Sensor 3 was unable to detect any of the three nodules. A stiffness map and a corresponding force map were generated for the inspection at 9 mm indentation depth and pressure of 1.73 psi as measured by P_{comp}. The stiffness map is displayed in Figure 5.23 and the force map in Figure 5.24.

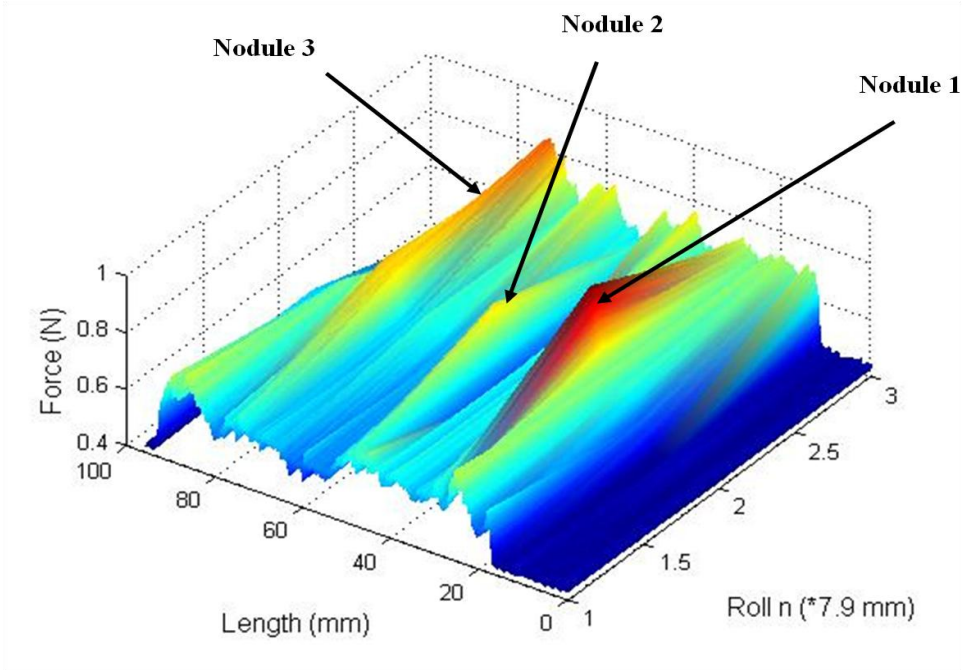

Figure 5.22: Force map of row 2 showing the force exerted by the nodules.

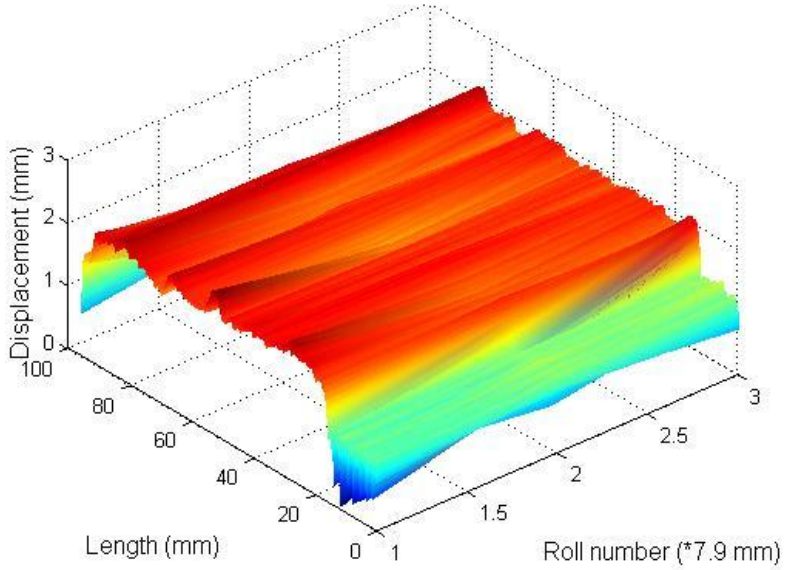

Figure 5.23: Stiffness map of the third row showing no nodules.

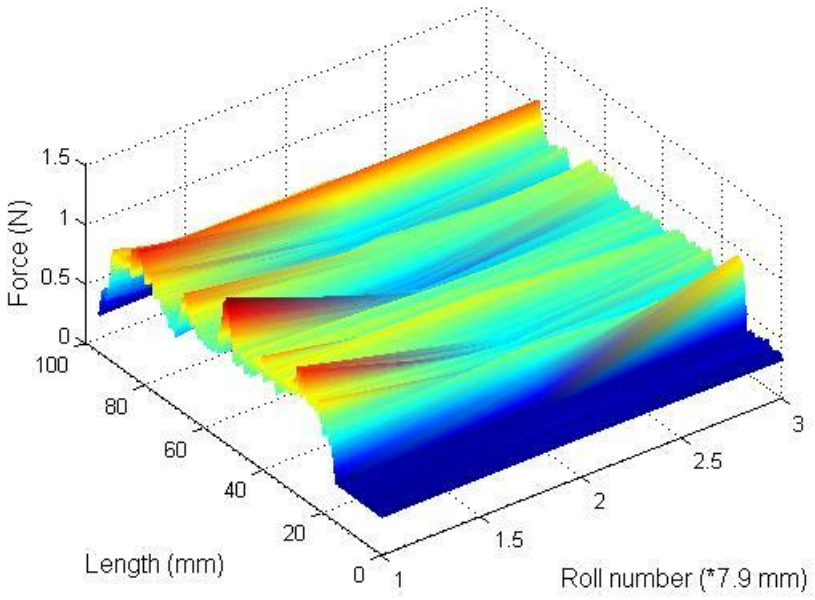

Figure 5.24: The force map of the third row showing no detected nodules.

5.7.2 Experiment 6: Excised Porcine Liver

Sensor 3 was rolled over the excised liver in 7 parallel and adjacent rolls. The indentation depth used was 5 mm. The liver was investigated at four different pressures. These were 0.86 psi, 1.22 psi, 1.44 psi, 1.80 psi. At a pressure of 0.86 psi, the soft and hard nodules that were embedded at 15 mm below the surface were detected with an area of high stiffness in red as seen in Figure 5.25. The red area is representative of rugged area of the liver that had a embedded connecting tissues. The other two nodules that were embedded at a depth of 23 mm are detected on the force map in Figure 5.26. At a pressure of 1.22 psi, the stiffness map and the force map in Figure 5.27and Figure 5.28, respectively, show the location of the two hard nodules and of one soft nodule. At a pressure of 1.44 psi, the soft nodule embedded at 15 mm is no longer detected but its counterpart that is embedded at 23 mm is observed and so are the other two hard nodules as seen in the stiffness map in Figure 5.29. The force map of the liver at that pressure in Figure 5.30, only illustrates the presence of the two

hard nodules. For a pressure of 1.44 psi the only nodule that is detected is the hard nodule that was embedded at 15 mm below the surface. This is reflected in the stiffness and force maps in Figure 5.31 and Figure 5.32, respectively. The increased area of stiffness illustrated in of all the above stiffness and force maps at the start of every roll was due to the slopping nature of the liver and to the starting position of the sensor.

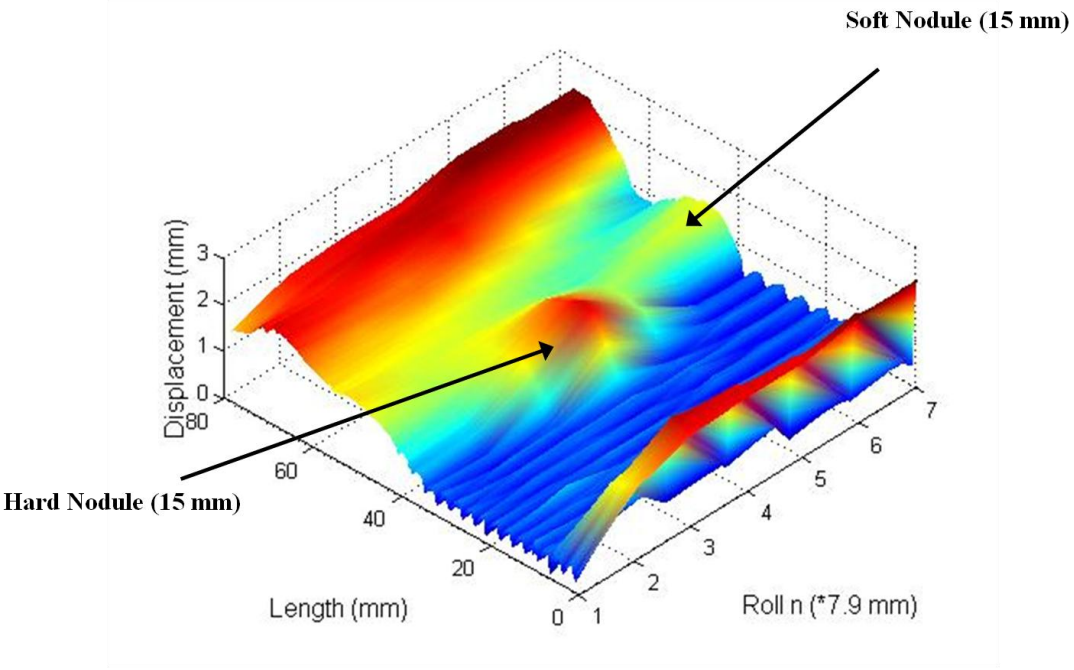

Figure 5.25: A stiffness map of the liver for a pressure of 0.86 psi with two nodules visible.

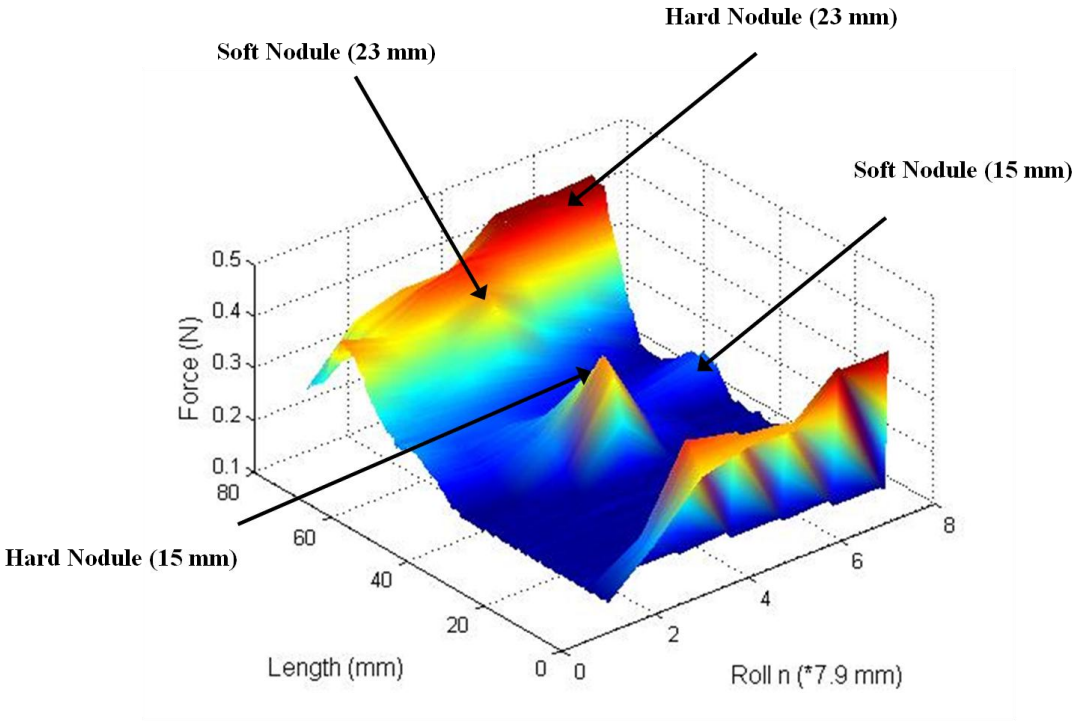

Figure 5.26: A force map of the liver for a pressure of 0.86 psi showing the location of all 4 embedded nodules.

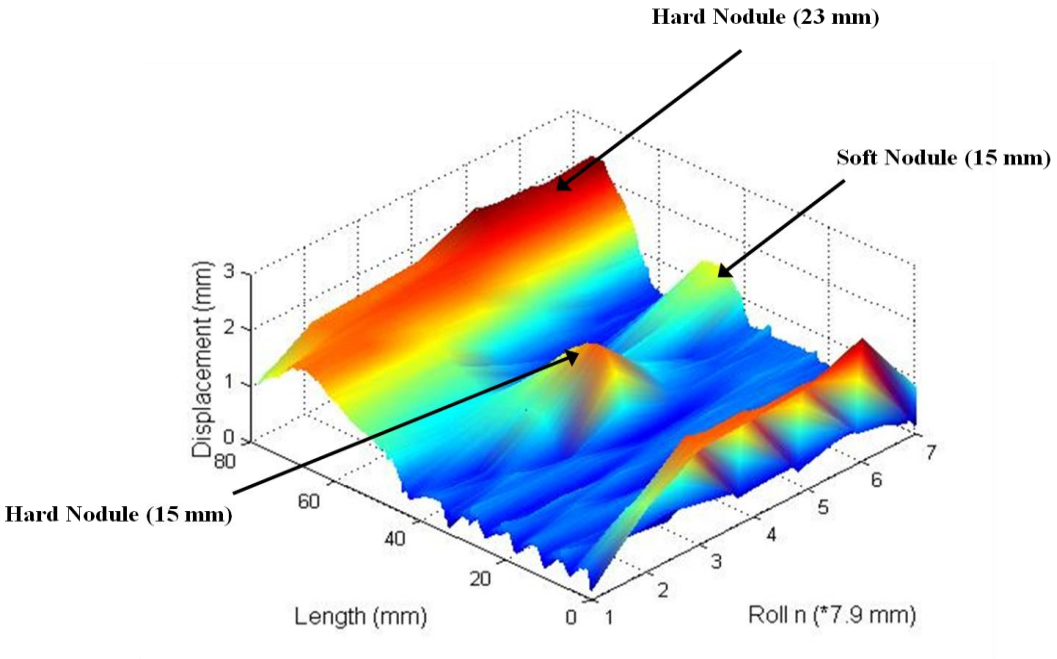

Figure 5.27: A stiffness map of the liver for a pressure of 1.22 psi showing the location of 3 nodules.

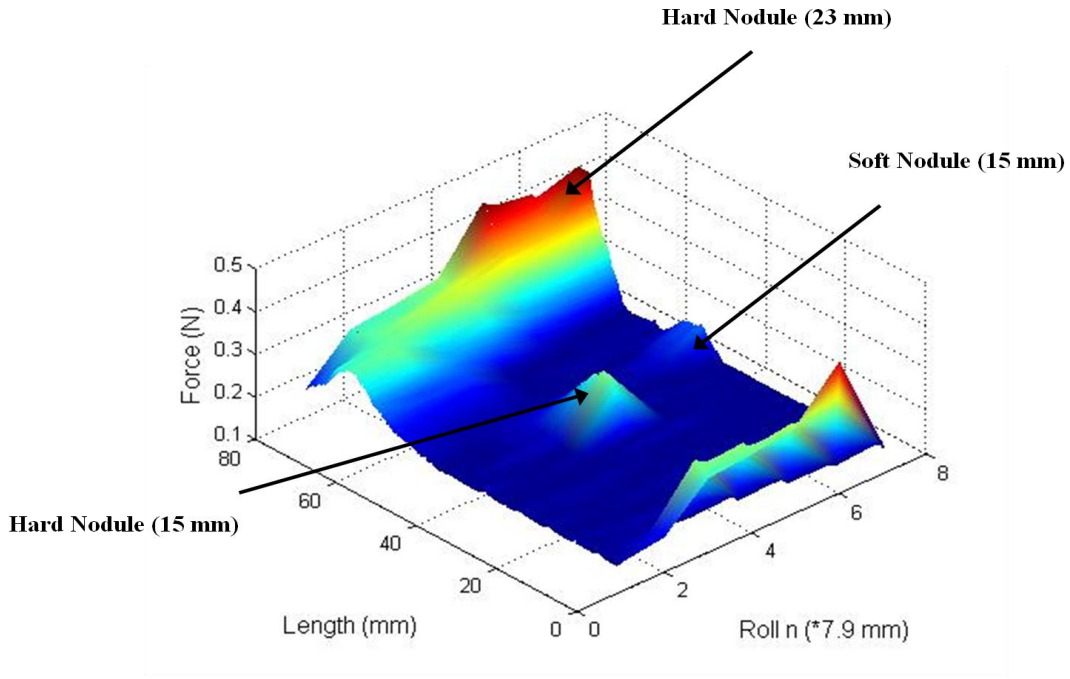

Figure 5.28: A force map of the liver at a pressure of 1.22 psi illustrating the location of the nodules and their force distribution.

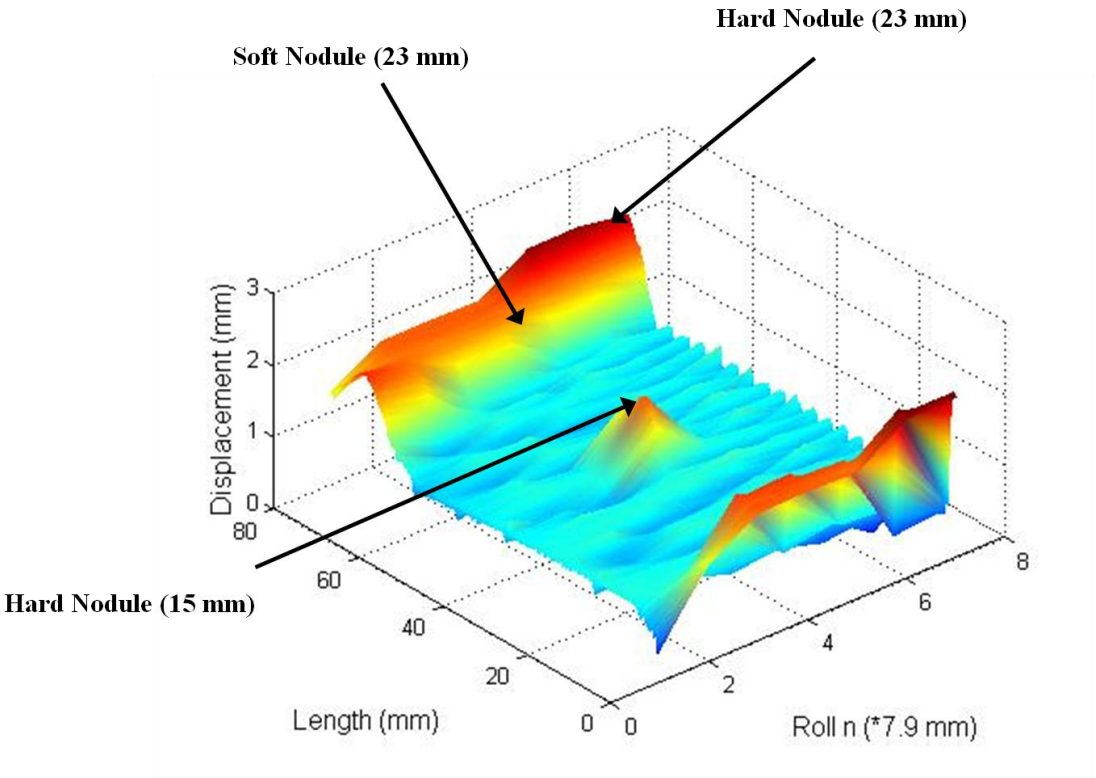

Figure 5.29: A stiffness map of the liver for a pressure of 1.44 psi illustrating the location of the two hard nodules.

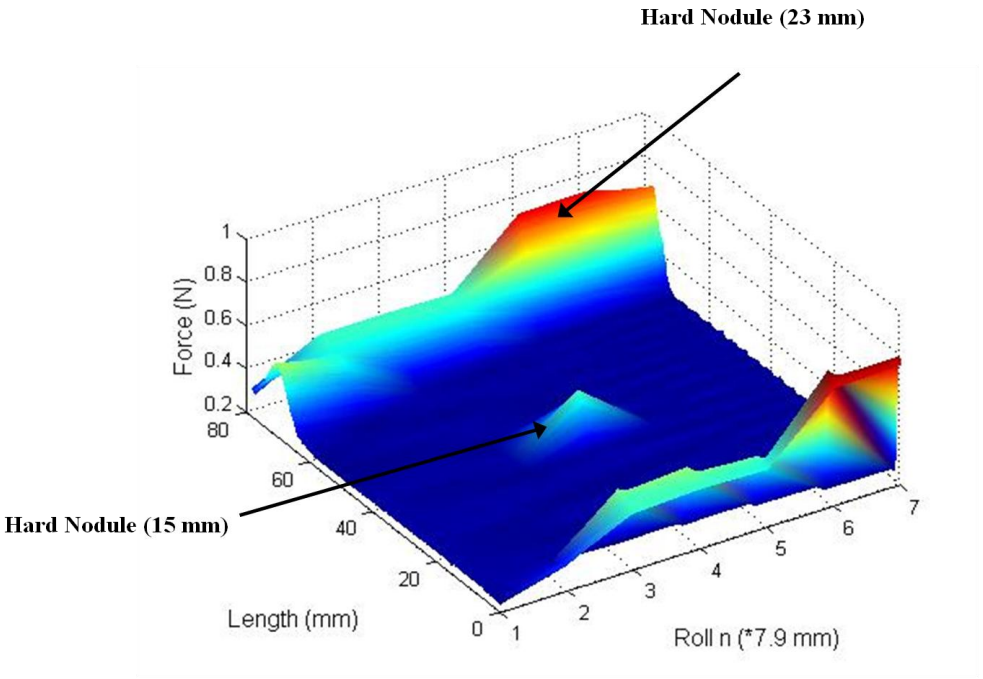

Figure 5.30: For a pressure of 1.44 psi, the force map illustrates the reaction forces of the liver and the location of the two hard nodules.

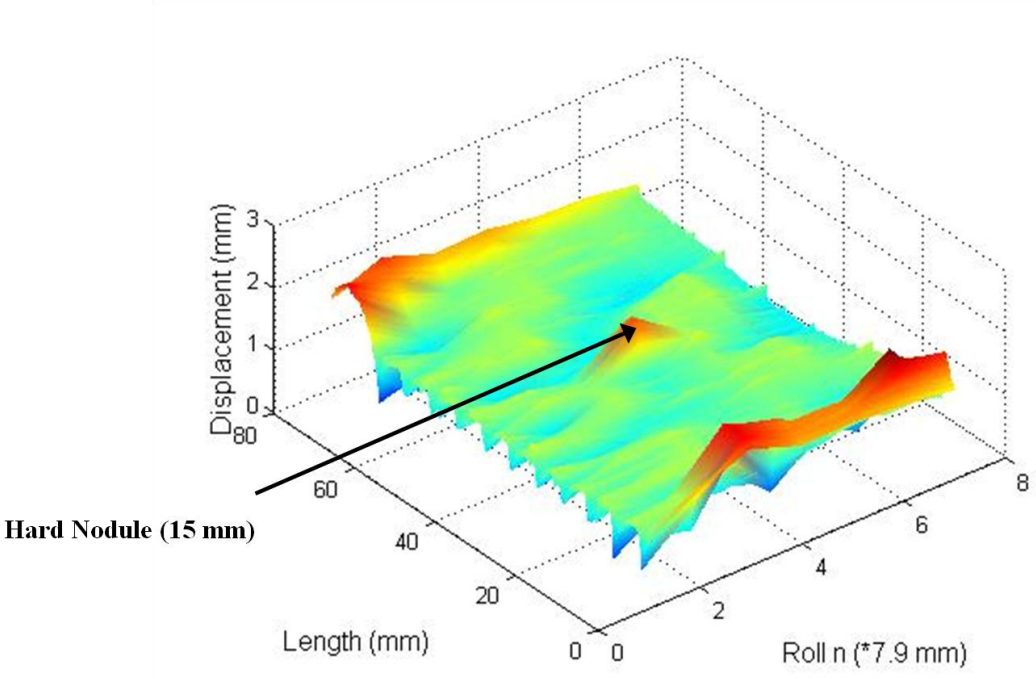

Figure 5.31: A stiffness map of the liver displaying only one nodule for a pressure of 1.44psi.

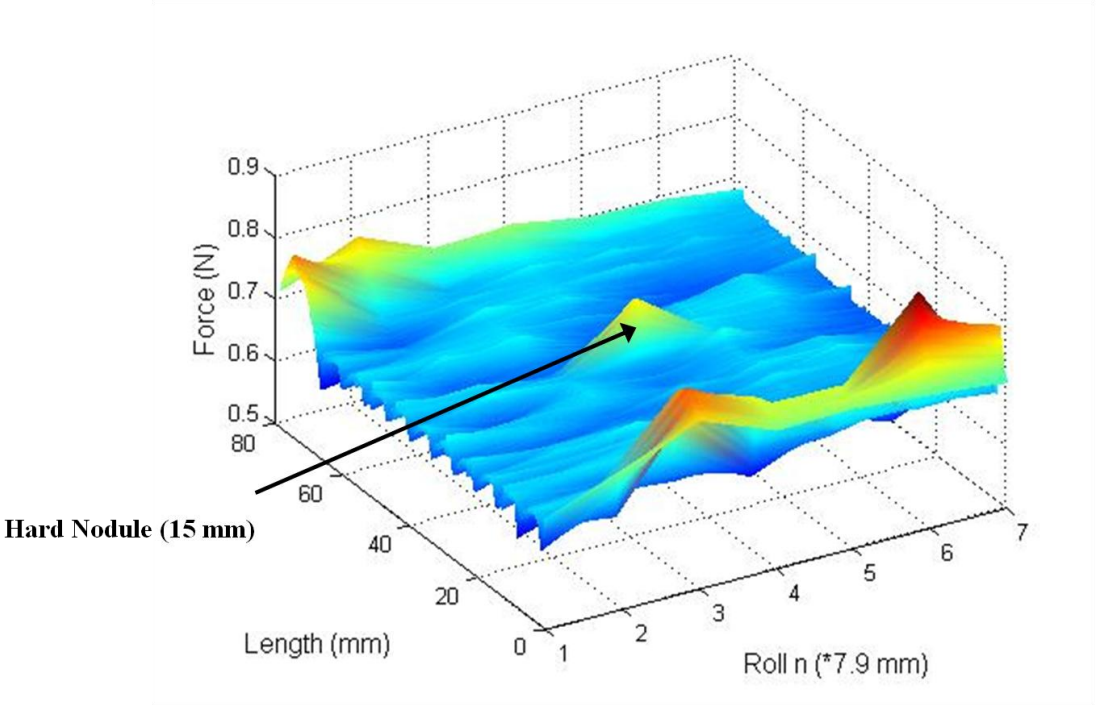

Figure 5.32: A force map of the deliver for a pressure of 1.44 psi, illustrating the reaction force distribution of the tissue and showing the presence of one hard nodule.

5.8 Discussion

Throughout Experiments 1 to 6, the ability of Sensor 1, Sensor 2 and Sensor 3 were tested. The results of experiments 1 to 3 demonstrated the sensor's ability as a tactile sensor by successfully detecting the paper thin nodules in a non elastic environment and by locating embedded nodules at various depths in a silicone phantom and an excised porcine liver. The ability of Sensor 2 was compared to the wheel probe sensor in Experiment 4 that required both sensors to locate the position of two soft nodules in a silicone phantom. The two sensors successfully detected the nodules, showing that Sensor 2 was a competent tactile sensor despite its low manufacturing cost. Experiments 5 and 6 were designed to assess Sensor 3's ability as a tactile and force sensor for MIS. In Experiment 5, the sensor showed its ability at detecting 6 out of the 9 embedded nodules. The difficulty in detecting the nodules in row 3 was due to

their embedded depth and to the high reaction forces of the silicone phantom. In row 1 and row 2, Nodule three is not aligned with Nodule 1 one and Nodule 2 as seen in Figure 5.19, Figure 5.20, Figure 5.21, and Figure 5.22. This is a true reflection of the location of Nodules 3 in the silicone phantom. Experiment 6, was a test that attempted to assess the ability of Sensor 3 in an environment that was approached MIS conditions by using an excised porcine liver with two soft and two hard embedded nodules. The force maps of the experiment demonstrated that by using too high pressures certain nodules may not be detected and reversely by using too low pressures it can be difficult to distinguish the location of the nodules.

5.9 Conclusion

The ability of Sensor 1, Sensor 2 and Sensor 3 were tested to establish their potential as MIS sensors. The results that were presented were promising as the sensors were capable of detecting tissue “abnormalities” on different surfaces. The tactile and force maps generated by the sensors do however sometimes require prior knowledge of the nature of tissue. As organs may have areas of increase stiffness that naturally occur in them without the presence of tissue abnormalities. It must be noted that during surgery, surgeons do not always rely solely on the haptic examination of an organ to determine whether any tissue abnormalities are present but also use pre-operative scans achieved by using ultrasounds, CT and MRI scans. Therefore the surgeons do have a prior knowledge of whether tissue abnormalities exist and of their location. Thus Sensor 1, Sensor 2 and Sensor 3 could be used for medical applications based on their ability at detecting tissue abnormalities.

Chapter 6 – Conclusion

6.1 Introduction

The general absence of tactile and force feedback has been an ongoing concern in the field of Minimally Invasive Surgery. A number of sensors have been developed in an attempt to overcome this lack of haptic feedback.

The sensors proposed in this PhD employed a novel design to address the problem. The concept of an air-cushion sensor for MIS was presented. The concept employed a spherical component that was surrounded by a cushion of air to be rolled over the surface under investigation in a near frictionless manner. Any movement of the spherical component along the longitudinal axis of the sensor was monitored using an optical scheme. Any abnormalities in the tissue under investigation displaced the spherical component during the rolling process.

Three sensor designs that embraced this novel concept were presented and built. The sensors were named Sensor 1, Sensor 2 and Sensor 3. Sensor 1 was designed with an inbuilt optical sensing scheme that employed an LED and a photosensitive diode to

monitor the displacement of the spherical component. Sensor 2 was an MIS tactile sensor that was fully MRI compatible as it was built entirely of ABS plastic. The sensing scheme employed a single optical fibre to monitor the displacement of the sphere. Sensor 3 was an MIS tactile sensor with force estimation capabilities that was designed and built to address certain limitations of Sensor 2.

The behaviour of Sensor 3 as a force sensor was experimentally studied and a model was found that estimated the force exerted by the spherical component as a function of its displacement and the pressure of the air employed.

All three sensors were experimentally tested and their ability at detecting tissue abnormalities was assessed. Sensor 3 was also used to generate force estimation maps of the surface under investigation.

6.2 Achievement of aims and objectives

The following aims and objectives set out at the start of this PhD are listed and how they were attained is explained.

- *The sensing component of the sensing device should be located in close proximity of the area under inspection so that any tissue interaction can be effectively detected and not be affected by any surrounding forces*. - This was achieved as the spherical component of Sensor 1, Sensor 2 and Sensor 3 are directly in contact with the tissue under investigation. The spherical component of the sensors enables them to be rolled in any direction over the tissue under investigation.
- *The sensing component and the sensing device must not exceed an outer diameter of 12 mm so that they can be inserted through a standard size of*

trocar port. – This was attained for Sensor 2 and Sensor 3 as their outer diameter is 12 mm.

- *The sensing device must provide the surgeon with tactile information of the tissue under inspection through visual, auditory or haptic display.* – All three sensors provide the surgeon with tactile feedback in the form of a tactile map that illustrates the areas of increased stiffness.
- *The sensing components of the sensing device should be sterilisable.*- The designs and components of Sensor 2 and Sensor 3 lend themselves to sterilisation due to their plastic structure. The optical fibre used is not however compatible with the autoclave process and therefore would need to be replaced with a more robust silica optical fibre.
- *The sensor should also be of an overall low manufacturing cost.* – The use of an optical fibre as a sensing element and the plastic structure of Sensor 2 and Sensor 3 make them of a low manufacturing cost and could be used as disposable sensors.
- *It would be advantageous if the sensing components were Magnetic Resonance Imaging (MRI) compatible in order to be available for the upcoming tendency of performing Minimally Invasive Robotic Surgery (MIRS) under an MRI scanner.* – Sensor 2 is entirely MRI compatible as the optical sensing fibre is not affected by electromagnetic fields and the plastic structure of the sensor is safe to be used in an MR environment.
- *The sensing device should have the ability to generate the fast creation of mechanical images of the surface under investigation illustrating the stiffness and/or force distribution over that area.* – All three sensors generated

stiffness maps of the surfaces under investigation. Sensor 3 also generated an estimate of the force distribution of that area.

- *The sensing device should have the capability to acquire data of a large area with relative ease and at a reasonable speed.* – The spherical component of all three sensors enabled them to be rolled in any direction over the tissue under investigation with ease.
- *The sensor should maintain its condition during its application* – Due to the design of the sensors, the condition of the sensor is maintained as the pressurised fluid ensures that the spherical component is free of any transfer materials and fluids on its reflective portion.
- *To maintain a low manufacturing cost so that it can be used in a disposable manner and thus maintain its sterility.* – This was achieved by using an ABS structure which is of low cost and sterilisable.
- *To lead to a wide range of applications based on its purpose.* – The sensors applications have proved themselves in an elastic and non elastic environment. Which enables them to be used in a wide range of applications including non medical environments.
- *To evaluate and validate the sensing device for its intended use in MIS.* – Sensor 3 was tested under ex vivo conditions and successfully generated stiffness maps of the organ with the force distribution over the area.

6.3 Summary of Contributions

In order to assist surgeons with the well documented problem of reduced or lack of haptic feedback during MIS, a system was created in an attempt to overcome it. The design that was proposed in the form of Sensor 1, Sensor 2 and Sensor 3 addressed

this limiting factor. The major contributions and achievements of this PhD are summarised below:

- Three air cushion tactile sensor designs were proposed for tissue investigation.
- The proposed sensors are of low manufacturing cost and can be used to determine the variation in stiffness on the surface of soft materials as well as at levels at depth below the surface of the soft material.
- Sensor 3 is a tactile and force sensor as it can estimate the force distribution exerted during the process of rolling indentation.
- The application of these sensors is vast. They could be used on human or animal tissue to investigate internal organs such as liver and kidneys or blood vessels. The applications of these sensors are not limited to the internal organs; as they could be used on the outer body, such as on the skin, for example to aid in breast cancer diagnosis.
- The concept of the air cushion tactile sensors, their ability at detecting tissue abnormalities and their future applications have been widely praised and embraced by the medical community with which and for which they were designed, developed and built. This has resulted in the sensors collecting four international of awards.
- The design of Sensor 2 is a tactile air cushion sensor that could be used within an MR environment. This feature permits the sensor to be used as a tactile sensor during MRI-guided interventions which is considered an important step in the field of MRI guided surgery.
- An international patent was successfully granted for the designs and applications of the air cushion tactile sensors. The patent further reinforces the individuality of theses sensors.

6.4 Future Work

The air-cushion tactile sensors that were created as part of this research have demonstrated a good ability as tactile sensors with force estimation capabilities. Despite their good performance, the work on these sensors can be further improved in the following areas:

- **Clinical trials.** The ability of the sensors on human tissue has yet to be tested. In the United Kingdom such trial requires ethical approval which can be a long process.
- **Force modelling.** Despite having an experimental model to estimate the force exerted by the spherical component of the sensor, a Computational Fluids Dynamics (CFD) analysis would be preferred to accurately predict the flow of air in the system and the forces exerted by the sphere.
- **MRI environnent.** Sensor 2 was designed to be MR compatible; it should therefore be tested under MRI conditions to establish whether it is entirely MR-safe and MR-compatible.
- **Size.** Despite the size of Sensor 2 and Sensor 3 being within MIS dimensions, the sensor could be miniaturised further to be used on much smaller areas of the body. Although it must be noted that the sensing displacement range of this design is limited to less than the radius of the spherical component used.

This air-cushion sensor was designed to be used for MIS applications. It has yet to be tested in a clinical environment. The sensor's performance and design should be closely discussed with the surgeons evaluating it so as to improve it and gain an operational status. If the clinical tests are successful, this sensing design could pave the way for the use of low cost disposable sensors for MIS applications.

Bibliography

Alarcon, A., & Berguer, R. (1996). A comparison of operating room crowding between open and laparoscopic operations. *Surg Endosc 1996 , 10*, 916–919.

Albani, J. M. (2007). The role of robotics in surgery: a review. *Mo Med , 104* (2), 166–172.

Althoefer, K., Zbyszewski, D., Liu, H., Puangmali, P., Seneviratne, L., Challacombe, B., et al. (2008). Air-Cushion Force Sensitive Probe for Soft Tissue Investigation during Minimally Invasive Surgery. *7th IEEE Conference on Sensors,*, (pp. 827 – 830). Lecce, Italy.

Babb, J., & Bradley, C. (1995). Endoscope decontamination: where do we go from here? *Journal of Hospital Infection , 30*, 543-551.

Bargar, W. L., Bauer, A., & Börner, M. M. (1998). Primary and Revision Total Hip Replacement Using the Robodoc® System. *Clin Orthop Relat Res , 354*, 82-91.

Baumann, I., Plinkert, P., Kunert, W., & Buess, G. (2001). Vibrotactile characteristics of different tissues in endoscopic otolaryngologic surgery - in vivo and ex vivo measurements. *Min Invas Ther & Allied Technol , 10* (6), 323–327.

Bebek, O., & Cavusoglu, M. (2007). Whisker Sensor Design for Three Dimensional Position Measurement in Robotic Assisted Beating Heart Surgery. *IEEE International Conference on Robotics and Automation (ICRA)*, (pp. 225 - 231). Rome, Italy.

Berci, G., & Forde, K. A. (2000). History of Endoscopy: what Lessons Have we Learned from the Past? *Surg Endosc , 14* (1), 1-15.

Berguer, R., Forkey, D., & Smith, W. (1999). Ergonomic problems associated with laparoscopic surgery. *Surg Endosc , 13,* 466–468.

Bholat, O., Haluck, R., Murray, W., Gorman, P., & Krummel, T. (1999). Tactile feedback is present during minimally invasive surgery. *J Am Coll Surg , 189,* 349-255.

Bicchi, A., Canepa, G., De Rossi, D., Iacconi, P., & Scilingo, E. P. (1996). A sensorized minimally invasive surgery tool for detecting tissutal elastic properties. *Proc. IEEE Int. Conf. Robot. Autom.* (pp. 884-888). Minneapolis, MN: IEEE.

Bitterman, N. (2006). Technologies and solutions for data display in the operating room. *J Clin Monit Comput , 20*, 165-173.

Breedveld, P., Stassen, H., Meijer, D., & Jakimowicz, J. (2000). Observation in laparoscopic surgery: overview of impeding effects and supporting aids. *J Laparoendosc Adv Surg Tech A , 10*, 231–241.

Brouwer, I., Ustin, J., Bentley, L., Sherman, A., Dhruv, N., & Tendick, F. (2001). Measuring in vivo animal soft tissue properties for haptic modeling in surgical simulation. *Stud Health Technol Inform , 81*, 69-74.

Buchade, P. B., & Shaligram, A. (2006). Simulation and experimental studies of inclined two fiber displacement sensor. *Sensor Actuat. A-Phys. , 128* (2), 312–316.

Bucher, P., Pugin, F., Buchs, N., Ostermann, S., Charara, F., & Morel, P. (2009). Single Port Access Laparoscopic Cholecystectomy (with video). *World J Surg , 33*, 1015-1019.

Camarillo, D. B., Krummel, T. M., & Salisbury Jr., J. K. (2004). Robotic technology in surgery: past, present and future. *Am J Surg. , 18* (4A), 2S-15S.

Challacombe, B., Althoefer, K., & Stoianovici, D. (2010). Emerging Robotics. In P. Dasgupta, J. Fitzpatrick, R. Kirby, & I. Gill (Eds.), *New Technologies in Urology, New Techniques in Surgery Series* (Vol. 7, pp. 49-56). Springer.

Chaudharia, A. L., & Shaligram, A. D. (2002). Multi-wavelength optical fiber liquid refractometry based on intensity modulation. *Sensor Actuat. A-Phys , 100* (2-3), 160–164.

Chinzei, K., Kikinis, R., & Jolesz, F. (1999). MR compatibility of mechatronic devices: Design criteria. *Medical Image Computing and Computer-Assisted Intervention*, (pp. 1020-1031). Cambridge, UK.

Cleary, K., & Nguyen, C. (2001). State of the art in surgical robotics: Clinical applications and technology challenges. *Comput. Aided Surg , 6*, 312-328.

Craig, J. (2003). *Introduction to robotics: Mechanics and Control.* Englewood Cliffs, N.J: Prentice-Hall.

Cuschieri, A. (1995). Whither Minimal Access Surgery: TRibulations and Expectations. *The American journal of surgery , 169*, 9-19.

Dargahi, Najarian, S., & Ramezanifard, R. (2007). Graphical display of tactile sensing data with application in minimally invasive surgery. *Can. J. Elect. Comput. Eng. , 32* (3), 151-155.

Dargahi, J., & Najarian, S. (2003). An endoscopic force-position sensor grasper with minimum sensors. *Can. J. Elect. Comput. Eng. , 28*, 155-161.

Davies, B. (2000). A review of robotics in surgery. *Proc Inst Mech Eng , 214*, 129-140.

Elhawary, H., Tse, Z., Hamed, A., Rea, M., Davies, B., & Lamperth, M. (2008). The case for MR-compatible robotics: a review of the state of the art. *Int J Med Robot , 4* (2), 105-113.

Eltaib, M. E., & Hewit, J. R. (2003). Tactile sensing technology for minimal access surgery - a review. *Mechatronics , 13*, 1163-1177.

Encyclopædia Britannica, Science & Technology: Virtual Reality. (n.d.). Retrieved June 22, 2010, from Encyclopædia Britannica: http://www.britannica.com/EBchecked/topic/630181/virtual-reality

Francis, P. (2006). Home Study Program: Evolution of robotics in surgery and implementing a perioperative robotics nurse specialist role. *AORN J , 83* (3), 629-650.

Franklin, M. E., Rosenthal, D., Abrego-Medina, D., Dorman, J. P., Glass, J. L., Norem, R., et al. (1996). Prospective comparison of open vs laparoscopic colon surgery for carcinoma: five-year results. *Meeting of the American-Society-of-Colon-and-Rectal-Surgeons, 39(10)*, pp. S35-S46.

Fuchs, K. H. (2002). Minimally Invasive Surgery. *Endoscopy , 34*, 154-159.

Gallagher, A. G., McClure, N., McGuigan, J., Ritchie, K., & Shechy, N. P. (1998). An ergonomic analysis of the ‘fulcrum effect’ in endoscopic skill acquisition. *Endoscopy , 30*, 617–620.

Gangopadhyay, T. (2004). Prospects for Fibre Bragg Gratings and Fabry-Perot Interferometers in fibre-optic vibration sensing. *Sens. Actuators A-Phys. , 13* (1), 20-38.

Gill, I. S., Matin, S. F., Desai, M. M., Kaouk, J. H., Steinberg, A., Mascha, E., et al. (2003). Comparative Analysis of laparoscopic versus open partial nephrectomy for renal tumpurs in 200 patients. *J Urol. , 170* (1), 64-68.

Gloge, D. (1971). Weakly Guiding Fibers. *Applied Optics , 10* (10), 2252-2258.

Grattan, K., & Sun, T. (1999). Fiber optic sensor technology: an overview. *Sensors and actuators , 82* (1-3), 40-61.

Gross, S., & Kollenbrandt, M. (2009). Technical Evolution of Medical Endoscopy. *Acta Polytechnica Journal of Advanced Engineering , 49* (2), 15-19.

Guthart, ,. G., & Salisbury Jr., J. K. (2000). The intuitive telesurgery system: Overview and application. *IEEE Int. Conf. Robotics and Automation*, (pp. 618-621). San Francisco, CA.

Harris, S., Mei, Q., Hibberd, R., & Davies, B. (1997). Experiences using a special purpose robot for prostate resection. *International Conference on Advanced Robotics*, (pp. 161-166). Monterey,CA.

Hatzinger, M., Badawi, K., Langbein, S., & Hacker, A. (2005). The seminal contribution of Georpg Kelling to laparoscopy. *J. Endourol , 19* (10), 1154-1156.

Hecht, J. (1999). City of Light: The Story of Fiber Optics. Oxford University Press.

Hedrick, A., Hisada, M., & Mulloney, B. (2007). Tama-kugel: hardware and software for measuring direction, distance, and velocity of locomotion by insects. *J Neurosci Methods , 164* (1), 86-92.

Intuitive Surgical Product Images. (2005). Retrieved July 8, 2010, from Intuitive Surgical: http://www.intuitivesurgical.com/corporate/newsroom/mediakit/davinci_surgical_system.jpg

Jackson, D. (1985). Monomode optical fibre interferometers for precision measurement. *J. Phps. E: Sci. Instrum. , Vol. 18,* 981-1001.

Jacobaeus, H. C. (1910). Ueber die moeglichkeit die zystoskopie bei untersuchung seroeser. *Munich Med Wochenschr , 57,* 2090-2092.

Jacobsen, G., Berger, R., & Horgan, S. (2003). The role of robotic surgery in morbid obesity. *J Laparoendosc Adv Surg Tech A , 13* (4), 279-283.

JHM. (2009, February 2). *Hopkins transplant surgeons remove healthy kidney through donor's vagina.* Retrieved June 17, 2010, from Johns Hopkins Medicine: http://www.hopkinsmedicine.org/Press_releases/2009/02_02_09.html

Jones, D. B., Wu, J. S., & Sopper, N. J. (2004). *Laparoscopic Suregry: Principles and procedures* (2nd rev. ed. ed.). New York, NY: Marcel Dekker.

Kaczmarek, K., Webster, J., Bach-y-Rita, P., & Tompkins, W. (1991). Electrotactile and Vibrotactile display for sensory substitution systems. *IEEE transaction on biomedical engineering , 38* (1), 1-16.

Kim, V. B., Chapman, W. H., Albrecht, R. J., Bailey, M. B., Young, J. A., Nifong, W. L., et al. (2001). Early experience with telemanipulative robot-assisted laparoscopic cholecystectomy using da Vinci. *Surg Laparosc Endosc Percutan Tech. , 12* (1), 33-40.

Kitagawa, ,., Dokko, D., Okamura, A., & Yuh, D. (2005). Effect of sensory substitution on suture-manipulation forces for robotic surgical systems. *J Thorac Cardiovasc Surg , 129* (1), 151-158.

Klafter, R., Chmielewski, T., & Negin, M. (1989). *Robotic Engineering: An Integrated Approach.* Englewood Cliffs, N.J.: Prentice Hall.

Kobiela, J., Stefaniak, T., Mackowiak, M., Lachinski, A. J., & Sledzinski, Z. (2008). NOTES - thirdgeneration surgery. Vain hope or the reality of tomorrow? *Langenbecks Arch Surg. , 393* (3), 405-411.

Kulkarni, V. K., Lalasangi, A. S., Pattanashetti, I. I., & Raikar, U. S. (2006). Fiber optic micro-displacement sensor using coupler. *J. Optoelectron. Adv. M* , 1610 - 1612.

Kuo, C.-H., & Dai, J. (2009). Robotics for Minimally Invasive Surgery:A Historical Review from the Perspective of Kinematics. *International Symposium on History of Machines and Mechanisms*, (pp. 337-354).

Kwoh, Y. S., Hou, J., Jockheere, E. A., & Hayati, S. (1988). A robot with improved absolute positioning accuracy for CT guided stereotactic brain surgery. *IEEE Trans Biomed Eng , 35* (2), 153-160.

Lanfranco, A. R., Castellanos, A. E., & Desai, J. P. (2004). Robotic surgery: A current perspective. *Ann Surg , 239* (1), 14-21.

Lawall, J., & Kessler, E. (2000). Michelson interferometry with 10 pm accuracy. *Rev. Sci. Instrum. , 71* (7), 2669-2676.

Li, H., Kawashima, K., Tadano, K., Ganguly, S., & Nakano, S. (2011). Achieving Haptic Perception in Forceps' Manipulator Using Pneumatic Artificial Muscle. *IEEE/ASME Transactions on Mechatronics* (99), 1-12.

Litynski, G. S. (1999). Profiles is laparoscopy: Mouret, Dubois and Perissat: the laparoscopic breakthrough in Europe. *JSLS , 3* (2), 163-167.

Liu, H., Noonan, D., Althoefer, K., & Seneviratne, L. (2008). Rolling Mechanical Imaging: A Novel Approach for Soft Tissue Modelling and Identification during Minimally Invasive Surgery. *IEEE International Conference on Robotics and Automation*, (pp. 845 - 850). Pasadena,CA.

Liu, H., Noonan, D., Challacombe, B., Dasgupta, P., Seneviratne, L., & Althoefer, K. (2010). Rolling mechanical imaging for tissue abnormality localization during minimally invasive surgery. *IEEE Trans Biomed Eng , 57* (2), 404-414.

Liu, H., Noonan, D., Challacombe, B., Dasgupta, P., Seneviratne, L., & Althoefer, K. (2010). Rolling mechanical imaging for tissue abnormality localization during minimally invasive surgery. *IEEE Trans Biomed Eng , 57* (2), 404-414.

Lundborg, G., Rosen, B., Lindstrom, K., & Lindberg, S. (1998). Artificial sensibility based on the use of piezoresistive sensors - Preliminary observations. *Journal of hand surgery: British and European , 23B* (5), 620-626.

Mantwil, F., Schulz, A., Hollstein, D., Kammal, M., Fay, A., & Jurgens, C. (2005). Robotic systems in total hip arthroplasty - is the time ripe for a new approach? *Int J Medical Robotics and Computer Assisted Surgery , 1* (4), 8-19.

McGlone, V. A., & Jordan, R. B. (2000). Kiwifruit and apricot firmness measurement by the non-contact laser air-puff method. *Postharvest Biology and Technology , 19* (1), 47-54.

Melkafertility website. (n.d.). Retrieved January 2012, from Selva's: Fertility, Obstetrics and Gynaecology Clinic, where life begins: http://www.melakafertility.com/laparoscopy.shtml

Michalik, M., Orłowski, M., Frask, A., Bobowicz, M., Adamczewska, M., & Lech, P. (2009). LESS (laparo-endoscopic single-site surgery) right hemicolectomy. *Videosurgery and other miniinvasive techniques , 4* (4), 164-167.

Mintz, Y., Talamini, M., & Cullen, J. (2008). Evolution of laparoscopic surgery: lessons for NOTES. *Gastrointest Endosc Clin North Am , 18* (2), 225-234.

Modlin, I. M., Kidd, M., & Lye, K. D. (2004). From the Lumen to the Laparoscope. *Arch Surg. , 139* (10), 1110-1126.

Moy, G., Wagner, C., & Fearing, R. (2000). A compliant Tactile Display for Teletaction. *IEEE International Conference on Robotics and Automation*, (pp. 3409-3415). San Francisco,CA.

Murphy, D. A., Miller, J. S., Langford, D. A., & Snyder, A. B. (2006). Endoscopic robotic mitral valve surgery. *J. Thorac. Cardiovasc. Surg. , 132* (4), 776-781.

Ng, K.-H., Ahmad, A., Nizam, M., & Abdullah, B. (2003). Magnetic resonance imaging: health effects and safety. *Proc. Int. Conf. Non-Ionizing Radiation at UNITEN (ICNIR2003) Electromagnetic Fields and our Health.*

Ng, W. S., Davies, B., Hibberd, R., & Timoney, A. (1993). Robotic surgery: A first-hand experience in transurethral resection of the Prostate. *IEEE Engineering in medicine and biology* , 120-125.

Noonan, D., Liu, H., Zweiri, Y., Althoefer, K., & Seneviratne, L. (2007). A dual function wheeled probe for tissue viscoelastic property identification for minimally invasive surgery. *Proc. IEEE Int. Conf. Robot. Autom.*, (pp. 2629-2634). Rome, Italy.

Okamura, A. (2004). Methods for haptic feedback in teleoperated robot-assisted surgery. *Industrial Robot: An International Journal 31:6, 499-508 , 31* (6), 499-508.

Okamura, A. (2004). Methods for haptic feedback in teleoperated robot-assisted surgery. *Industrial Robot: An International Journal 31:6, 499-508 , 31* (6), 499-508.

Ott, D. O. (1901). Illumination of the abdomen (ventroscopia). *J Akush Zhensk Boliez , 15*, 1045-1049.

Pearl, J. P., & Ponsky, J. L. (2008). Natural Orifice Translumenal Endoscopic Surgery: A Critical Review. *J Gastrointest Surg , 12*, 1293-1300.

Peirs, J., Clijnen, J., Reynaerts, D., Van Brussel, H., Herijgers, P., Corteville, B., et al. (2004). A micro optical force sensor for force feedback during minimally invasive robotic surgery. *Sens. Actuators A-Phys. , 115*, 447-455.

Peng, P., Sezen, A., Rajamani, R., & Erdman, A. (2009). Novel MEMS stiffness sensor for in-vivo tissue characterization measurement. *Engineering in Medicine and Biology Society*, (pp. 6640 - 6643). Mineapolis, MN.

Petter, E., Biehl, M., & Meyer, J.-U. (1996). Vibrotactile palpation instrument for use in minimal invasive surgery . *Proceedings of the 18th Annual International*

Conference of the IEEE Engineering in Medicine and Biology Society, (pp. 179 - 180). Amsterdam, The Netherlands.

Picod, G., Jambon, A. C., Vinatier, D., & Dubois, P. (2005). What can the operator actually feel when performing a laparoscopy? *Surg Wndosc , 19*, 95-100.

Pirisi, A. (2003). Telerobotics brings surgical skills to remote communities. *The Lancet , 361* (9371), 1794-1795.

Prevedello, D. M., Doglietto, F., Jane, J. A., Jagannathan, J., Han, J., & Laws, E. R. (2007). History of endoscopic skull base surgery: its evolution and current reality. *J Neurosurg , 107*, 206-213.

Puangmali, P., Althoefer, K., & Seneviratne, L. D. (2009). Novel Design of a 3-Axis Op-tical Fiber Force Sensor for Applications in Magnetic Resonance Environments. *Proc.IEEE Int. Conf. Robot. Autom*, (pp. 3682 - 3687). Kobe, Japan.

Puangmali, P., Althoefer, K., Seneviratne, L. D., Murphy, D., & Dasgupta, P. (2008). State-of-the-Art in Force and Tactile Sensing for Minimally Invasive Surgery. *IEEE Sensors Journal , 8* (4), 371-381.

Qasaimeh, M., Sokhanvar, S., Dargahi, J., & Kahrizi, M. (2009). PVDF-Based Microfabricated Tactile Sensor for Minimally Invasive Surgery . *Journal of Microelectromechanical Systems* , 195 - 207 .

Rausch, J., & Werthschuetzky, R. (2009). A Miniaturised Piezoresistive Multi-Component Force Sensor for Minimally Invasive Surgery. *SENSOR+TEST Conferences 2009, A3 - Mechanical Sensors I*, pp. 83 - 88. Nürnberg.

Reyes, D., Tang, B., & Cuschieri, A. (2006). Minimal access surgery (MAS)-related surgeon morbidity syndromes. *Surg Endosc , 20*, 1–13.

Rock, J. A., & Warshaw, J. R. (1994). The history and future of operative laparoscopy. *Am J Obstet Gynecol , 170* (1 Pt 1), 7-11.

Salle, D., Gosselin, F., Bidaud, P., & Gravez, P. (2001). Analysis of haptic feedback performance in telesurgery robotics systems. *Robot and Human Interactive Communication, 2001. Proceedings. 10th IEEE International Workshop on*, (pp. 618 - 623). Bordeaux, Paris.

Santamore, D., & Cleaver, T. (2004). The sounds of saturation. *J Clin Monit Comput , 19*, 89-92.

Satava, R. (2003). Robotics surgery: from past to future - apersonal journey. *Surg Clin Am* , 1491-1500.

Schostek, S., Schurr, M. O., & Buess, G. F. (2009). Review on aspect of artificial tactile feedback in laparoscopic surgery. *Medical Engineering & Physics , 31* (8), 887-898.

Schreiber, H. W., Steichen, F. M., & Kraas, E. (2001). Minimally Invasive Surgery and Videolaparoscopic Surgery. In K. Kremer, W. Platzer, H. W. Schreiber, & F. M. Steichen, *Minimally Invasive Abdominal Surgery: Surgical Anatomy, Indications, Techniques, Complications* (p. 2). New York: Thieme Stuttgart.

Scilingo, E., Bicchi, A., De Rossi, D., & Iacconi, P. (1998). Haptic display able to replicate the rheological behaviour of surgical tissues. *20th Annual International Conference of the IEEE Engineering in Medicine and Biology Society*, (pp. 1738-1741). Hong Kong Sar, China.

Selvarajan, A., & Asundi, A. (1995). Photonics, fiber optic sensors and their applications in smart structures. *J. Non-Destruct. Eval. , 15* (2), 41-56.

Shellock, F. (2002). Magnetic resonance safety update 2002: Implants and devices. *J. of Magnetic Resonance Imaging , 16*, 485-496.

Sim, H., Yip, S., & Cheng, C. (2006). Equipment and technology in surgical robotics. *World J Urol , 24*, 128-135.

Sjoerdsma, W., Herder, J. L., Horward, M. J., Jansen, A., Bannenberg, J. J., & Grimbergen, C. A. (1997). Force transmission of laparoscopic grasping instruments. *Minimally Invasive Therapy & Allied Technologies , 6* (4), 274-278.

Spaun, G., Goers, T., Pierce, R., Cassera, M., Scovil, S., & Swanstrom, L. (2010). Use of flexible endoscopes for NOTES: sterilization or high-level disinfection? *Surg Endosc , 24*, 1581–1588.

Tabaie, H. A., Reinbolt, J. A., Graper, W. P., Kelly, T. F., & Connor, M. A. (1999). "Endoscopic coronary artery bypass graft (ECABG) procedure with robotic assistance. *The Heart Surgery Forum , 2* (4), 310-317.

Tada, M., Sasaki, S., & Ogasawara, T. (2002). Development of an optical 2-axis force sensor usable in MRI environments. *Proceedings of IEEE Sensors* , 984-989.

Tavakoli, M., Aziminejad, A., Patel, R. V., & Moallem, M. (2006). Methods and mechanisms for contact feedback in a robot-assisted minimally invasive environment. *Surg Endosc , 20*, 1570–1579.

Tavakoli, M., Patel, R., & Moallem, M. (2005). Haptic Feedback and Sensory Substitution during Telemanipulated Suturing. *First Joint Eurohaptics Conference*

and Symposium on Haptic Interfaces for Virtual Environment and Teleoperator Systems, (pp. 543-544).

Tendick, F., & Cavusoglu, M. C. (1997). Human-machine interfaces for minimally invasive surgery. *19th International Conference - IEEE/EMBS* (pp. 2771-2776). Chicago, IL. USA: IEEE.

Tholey, G., Pillarisetti, A., Green, W., & Desai, J. (2004). Design, development, and testing of an automated laparoscopic grasper with 3-D force measurement capability. *Proc. Int. Symp. Medical Simulation* , 38-48.

Tirabassi, M., Wadie, G., Tashjian, D., & Moriarty, K. (2007). Improving tactile sensation in minimally invasive pediatric surgery. *J Laparoendosc Adv Surg Tech A , 17*, 501-503.

Treat, M. R. (1995). A surgeon's perspective on the difficulties of laparosopic surgery. Cambridge, MA: MIT Press.

Ulmer, B. C. (2010). Best practices for minimally invasive procedures. *AORN J. , 91* (5), 558-575.

Uranues, S., Maechler, H., Bergmann, P., Huber, S., Hoebarth, G., Pfeifer, B., et al. (2002). Early experience with telemani[ulative abdominal and cardiac surgery with Zzeus Robotic system. *Euro. Surg. , 34* (3), 190-193.

Van den Dobbelsteen, J., Schooleman, A., & Dankelman, J. (2007). Friction dynamics of trocars. *Surg Endosc , 21*, 1338–1343.

Verger-Kuhnke, A. B., Reuter, M. A., & Beccaria, M. L. (2007). The life of Philipp Bonzzini (1773-1809) an idealist of the endoscopy [in Spanish]. *Actas Urol Esp. , 31* (5), 437-444.

Wellman, P. S., & Howe, R. (1997). Modelling probe and tissue interaction for tumour feature extraction. *ASME Summer Bioengineering Conference*. Sun River, Oregon.

Westebring-Van der Putten, E., Goossens, R., Jakimowicz, J., & Dankelman, J. (2008). Haptics in minimally invasive surgery - a review. *Minimally Invasive Therapy , 17* (1), 3-16.

Wilson, E. B. (2009). The evolution of robotic general surgery. *Scand J Surg. , 98* (2), 125-129.

Yao, H.-Y., & Hayward, V. (2005). A tactile enhancement instrument for minimally Invasive surgery. *Comput Aided Surg , 10*, 233-239.

Zbyszewski, D., Althoefer, K., Liu, H., Seneviratne, L., Challacombe, B., & Dasgupta, P. (2009). A comparative study between an improved novel air cushion sensor and a wheeled probe for minimally invasive surgery. *27th World Congress of Endourology & SWL WCE*. Munich, Germany.

Zbyszewski, D., Bhaumik, A., Althoefer, K., & Seneviratne, L. (2008). Tactile sensing using a novel air cushion sensor: A feasibility study. *International Conference on Intelligent Robots and Systems, 2008 IEEE*, (pp. 41-46). Nice, France.

Zbyszewski, D., Challacombe, B., Liu, H., Seneviratne, L., Dasgupta, P., Murphy, D., et al. (2009). Air-cushion force-sensitive probe for soft tissue investigation during minimally invasive surgery. *J Endourol. , 23* (9), 1421-1424.

Zbyszewski, D., Liu, H., Puangmali, P., Althoefer, K., Nunes, C. S., Seneviratne, L. D., et al. (2008). Wheel/Tissue Force Interaction: A New Concept for Soft Tissue Diagnosis during MIS. *30th Annual International IEEE EMBS Conference*, (pp. 5556-5559). Vancouver, British Columbia, Canada.

Zbyszewski, D., Polygerinos, P., Seneviratne, L., & Althoefer, K. (2009). A Novel MRI Compatible Air-Cushion Tactile Sensor for Minimally Invasive Surgery. *IEEE International Conference on Intelligent RObots and Systems (IROS)*, (pp. 2647 - 2652). St Louis, Missouri.

Zbyszewski, D., Polygerinos, P., Seneviratne, L., & Althoefer, K. (2009). A Novel MRI Compatible Air-Cushion Tactile Sensor for Minimally Invasive Surgery. *IEEE International Conference on Intelligent RObots and Systems*, (pp. 2647-2652). St Louis,Missouri, USA.

Zhao, D., Zhang, J., Yao, P., Jiang, X., & Chen, X. (2007). Photonic crystal Mach-Zehnder interferometer based on self-collimation. *Appl. Phys. Lett. , 90* (23), 231114/1-3.

Zhu, J. F. (2009). Which term is better: SILS, SPA, LESS, E-NOTES, or TUES? *Surg Endosc , 23*, 1164-1165.